Consideration of Factors that Affect Flood Levels in the Tana River Delta in Kenya

By
Kuria Kiringu

Thesis presented in fulfilment of the requirements for the degree of Master of Engineering (Research) in the Department of Civil Engineering at Stellenbosch University

Supervisor: Prof GR Basson

March 2015

DECLARATION

By submitting this thesis electronically, I declare that the entirety of the work contained therein is my own, original work, that I am the authorship owner thereof (unless to the extent explicitly otherwise stated) and that I have not previously in its entirety or in part submitted it for obtaining any qualification.

Date: .....

ABSTRACT

Tana River, the largest river in Kenya, is an important habit that supports numerous types of life, which creates an attractive environment. Occasionally loss of life and damage to property are experienced during floods. Upstream development of hydropower generation dams without consideration of downstream impacts is well documented in literature and the aftermaths are being well exhibited currently.

The aim of the thesis is to investigate and identify factors that affect the flood levels in the Tana River Delta by using a two dimensional model and eventually drawing up a velocity-water depth interaction hazard classification map.

Reviews of the literature clearly established that the floods in the delta are not generated by internal rainfall only but also operation of upstream dams accounting for 95% of the flood levels. Consequently, investigations of the impacts of dams have on flow regime were carried out.

Probabilistic analysis revealed that post dam seasonal patterns has not been impacted but the magnitude of flood peaks has generally declined due to the attenuation of small peaks. However, large/flash floods (10 year Annual Recurrence Interval (ARI) spill at the dams causing major flooding downstream.

Further probabilistic analysis on river discharges and sea water level was carried out to determine various ARI peaks. This incorporated climate change based on the 4th IPCC report. A two-dimensional hydrodynamic model was set up and calibrated with recorded discharges and theoretically derived parameters.

Impacts of extreme tidal levels were investigated on the water levels and other factors limiting flood propagation.

Finally, the model was used to simulate the 2, 50 and 100 year ARI inclusive of climate change floods and, based on Australian guidelines, flood lines and hazard maps were drawn.

The results show that high tides elevate water levels in the delta in combination with the bottleneck effect at the rechanneled canal. The road crossing through the delta has inadequate bridges to convey the floods.

The derived flood maps drawn (Figure 6-4) highlight that settlements in the lower delta are located within the 2 year ARI flood lines and that the extent of flooding is similar or less so in 50 and 100 year ARI flood peaks simulated.

The model predicted the velocity and water depths with sufficient accuracy and recommendations are made that the study area should be extended upstream, and more field data should be collected to aid in calibration and that land use should be incorporated in flood map classification. In conclusion, the thesis has identified the flood hotspots and factors governing floods. These findings could assist in decision making by various agencies proposing flood mitigation or advocating post dam flooding scenarios.

OPSOMMING

Die Tanarivier is die grootste rivier in Kenia en ’n belangrike habitat vir verskeie tipes diere en plante wat ‘n aantreklike omgewing skep.Verlies aan lewens en skade aan eiendom vind egter somtyds tydens oorstromings plaas. Die bou van damme vir die ontwikkeling van hidrokrag hoër op in die rivier sonder om die impak laer af in ag te neem, asook die gevolge daarvan, word dikwels in die lireratuur beskryf.

Die doel met hierdie tesis is om die faktore wat die vloedhoogtes in die Tanarivier beïnvloed met die gebruik van ’n twee-dimensionele hidrodinamiese model te ondersoek en te identifiseer en om dan ’n gevaarsonekaart te teken wat die interaksie tussen waterspoed en -diepte toon.

Die oorsig van die literatuur het getoon dat die oorstromings in die delta nie die gevolg is van reën in die binneland nie, maar dat die damme hoër op in die rivier verantwoordelik is vir 95% van die oorstromings. Dus is die impak van die damme op oorstromings ondersoek.

Waarskynlikheidsontleding het oor die algemeen getoon dat die na-dam seisoenale vloeipatrone nie beinvloed is nie, maar dat veral die kleiner vloedpieke in die algemeen afgeneem het as gevolg van vloedattenuasie deur die damme. Groter en frats oorstromings (>1:10 ARI) veroorsaak egter steeds dat die damme oorloop en lei tot ernstige oorstromings.

Die verdere waarskynlikheidsontleding van riviervloei en die seewatervlak is uitgevoer om die verskillende Jaarlikse Herhaling Periode (JHP) vlakke vas te stel. Dit het klimaatsverandering gegrond op die 4de IPCC verslag ingesluit. ’n Twee dimensionele hidrodinamiese model is opgestel en gekalibreer teen waargenome vloei en teoreties-afgeleide parameters is gekalibreer. Die impak van uiterste getyvlakke asook faktore wat die oorstromings beperk is ondersoek.

Die model is toe gebruik om die 2, 50 en 100 JHP vloedoorstromings te simuleer en vloedlyne en gevaarkaarte is volgens die Australiese riglyne geteken.

Die resultate toon dat hooggety die watervlak in die delta laat styg veral in kombinasie met die bottelnek effek van die nuwe kanaal. Daar is te min brûe op die pad wat die delta deurkruis, om die vloede se vloei deur te laat

Die kaarte wat geteken is toon dat daar nedersettings in die laer delta binne die 2 JHP jaar vloedarea is en dat die omvang van oorstromings dieselfde of laer is as die 50 en 100 JHP jaar vloedpieke wat gesimuleer is.

Die model kan gebruik word om die vloeispoed en waterdieptes redelik akkuraat te voorspel en die volgende aanbevelings word gemaak. Toestande hoër op teen die rivier moet ondersoek

word, meer data wat gedurende kalibrasie gebruik kan word moet versamel word en grondgebruik moet in die kaartklassifikasie ingesluit word. Ten slotte is die gevaarpunte vir oorstromings en die faktore wat oorstromings veroorsaak aangetoon. Hierdie bevindinge kan van nut wees as besluite geneem moet word veral wat betref die voorkoming van oorstromings nadat damme gebou is.

ACKNOWLEDGEMENTS

I would like to express my gratitude to the following persons:

- Prof. GR Basson, my supervisor for his guidance and support throughout my master's program;
- Ousmane Sawadago and Christiaan Visser, for assistance with Mike21C modelling;
- DHI for provision of MIKE 21c and MIKE 11softwares;
- Kiringu family for the support to see me through this.

TABLE OF CONTENTS

LIST OF FIGURES

LIST OF TABLES

ACRONYMS

1D	One Dimensional
2D	Two Dimensional
3D	Three Dimensional
AEP	Annual Exceedance probability
AMSL	Above Mean Sea Level
APDRC	Asia Pacific data Research Centre of the University of Hawaii
ARI	Annual Recurrence Interval
C	Chezy number
CC	Climate change
CD	Chart Datum
cv	Coefficient of variation
DEM	Digital Elevation Model
DHI	Danish Hydraulic Institute.
DTM	Digital Terrain model
EGM	Earth Gravitational Model
EV1	Extreme Value type 1 distribution
Fr	Froude number
g	Acceleration due to gravity, 9.81m2/s
GEV	General Extreme Value distribution
GIS	Geographical Information Systems
GOK	Government of Kenya
h	Stage above datum
HD	Hydrodynamic
HW	High Water
ITCZ	Inter-Tropical Convergence Zone

IUCN	International Union for Conservation of Nature
IPCC	Intergovernmental Panel on Climate Change
KENGEN	Kenya Electricity Generating Company
km	Kilometers
KMD	Kenya Meteorological Department.
KNBS	Kenya National Bureau of Statistics
LEVI	Log Gumbel (Log Extreme type 1) distribution
LIDAR	Light Detection and Ranging
LN	Log normal distribution
LP3	Log Pearson type 3 distribution
LW	Low Water
M	Reciprocal of Manning number
Max, Min	Maximum and Minimum respectively
MSL	Mean Sea Level
MODIS	Moderate-resolution Imaging Spectroradiometer
N	Normal distribution
n	Design life
N/A	Not available
NSW	New South Wales
PX	Probability of X exceedance
Q	Discharge (m3/s)
Q_2, Q_{50}, Q_{100}	2, 50, 100 year recurrence interval floods
R	Radius of curvature
RCP	Representative Concentration Pathways
RHS	Right Hand Side
STDEV	Standard deviation

T	Return period
USGS	United States Geological Survey
UTM	Universal Transverse Mercator
WL_2, WL_{50}, WL_{100}	2, 50, 100 year recurrence interval water level
WRMA	Water resources Management Authority
x, y	Coordinate system
y	Water depth
z	Cross sectional depth

1 INTRODUCTION

1.1 Background

Flooding in the Tana River delta is a recurrent problem. Floods with an annual recurrence interval of two year do cause major displacement of persons and loss of property. The delta, lying in an arid and semi-arid area is of national importance. In spite of limitations on hydrological data in the delta, this thesis attempts to overcome it by means of one and two dimensional numerical models.

1.2 Motivation

Deltaic habitats replenished by periodic floods are rich ecosystems with abundant flora and fauna. Large loads of sediment deposits, offer fertile agricultural land making them attractive to human settlements. In the world, the most densely populated zones are found along river mouths (Savenije H., 2012). With rapid population growth and expansion of economies, there has been a need for cheaper hydroelectricity power. In the past decade, large dams located upstream of such deltas have seriously affected the rivers' fluvial morphology and ecosystems. In particular, flow regimes have greatly been altered: increased base flows, reduced frequency and magnitude of floods have been observed (Basson, 2005).

With impacts of climate change becoming more evident, seasonal shifts, high magnitude and less frequent rainfalls have led to prolonged droughts followed by flash floods. Human settlements having encroached deeper into the delta floodplains, impacts of floods have been costly and more devastating.

Tana River catchment located in Kenya supporting approximately 17% of Kenyan population, has five upstream dams regulating 95% of its flows. Masinga Dam (0°52'46.23"S, 37°35'21.24"E), the first and largest in the series of Tana Dams was built as a hydroelectric water regulating reservoir. Despite its reservoir capacity, occasional flood release, overspills combined with normal hydroelectric generation causes major flooding in the downstream. In 1997, 1998, and 2013 there were floods causing major displacement, water borne diseases, destruction of livelihood and structures along the riverine flood plains RedCross (2007, 2008, 2013) and The World Bank (2007). It can be said that flooding is a perennial problem in the delta taking at least one month for water to subside.

A map showing the location of Tana delta with a pictorial illustration of 2008 flood encompassing a flood plain settlement is shown in Figure 1-1. Initially, complex distributary

river mouths were located further south east before it was manually redirected to create an artificial navigational canal in 1865 by Sultan of Witu (Wokabi, et al., 1976).

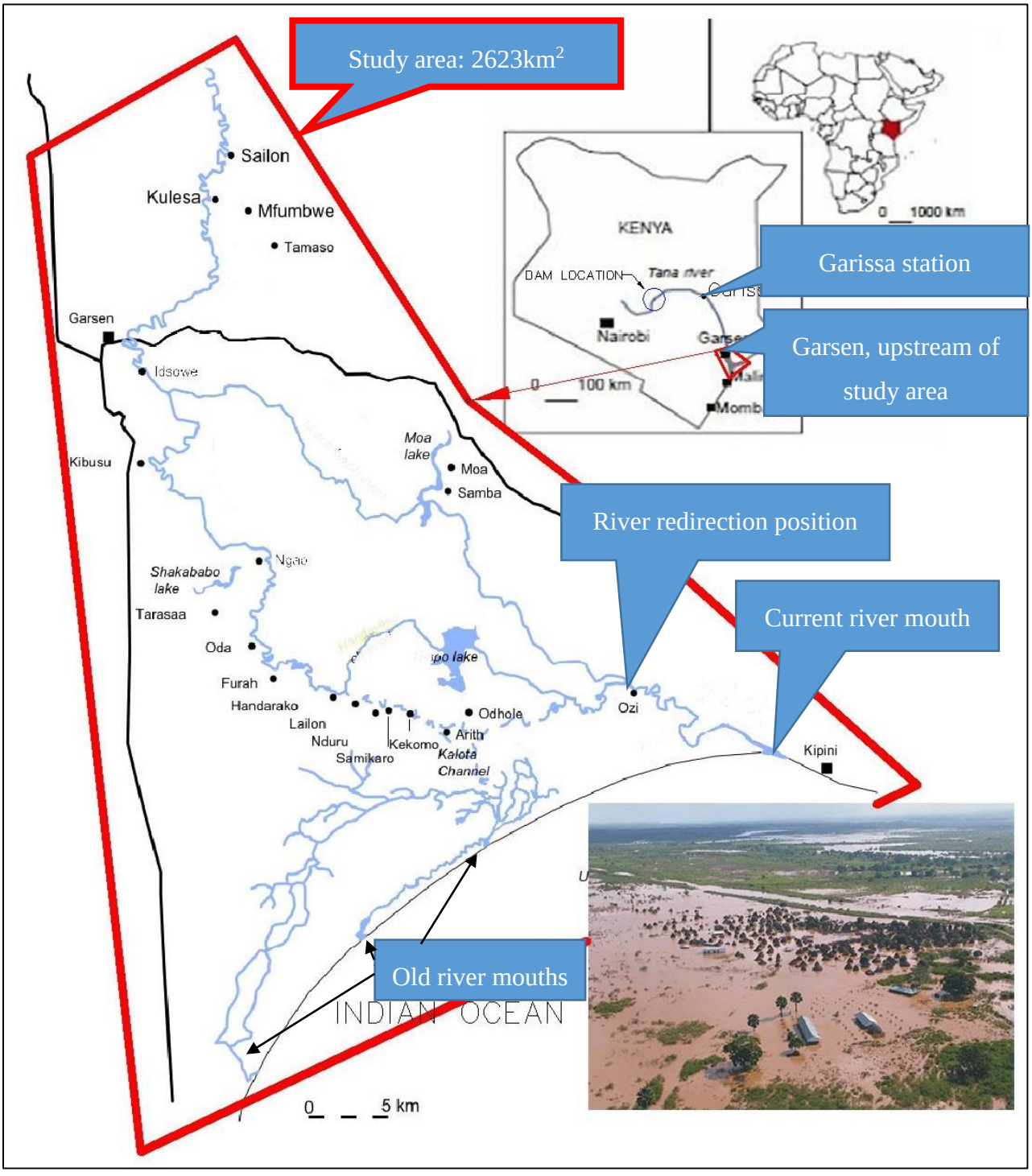

Figure 1-1: Map showing dam locations, Garrisa gauging station, Lower Tana Delta study area and pictorial representation of a sample flooded floodplain

In the delta various studies have been undertaken: environmental studies investigating pre- and post-dam construction effects (e.g. (Bunyasi, 2012) and (Leauthaud, et al., 2013). Oludhe (2011)

did studies on impacts of climate change on power production and Nakaegawa, et.al (2012) on environmental impacts on proposed dams and irrigation schemes A one-dimensional model quantifying the impact of dams on flooding has been undertaken (Maingi & Marsh , 2002). The study of delta flooding has been limited due to lack of data in the poorly gauged river.

In this thesis, the aim is to contribute to the better understanding of Lower Tana flood hydrodynamics using a two-dimensional hydrodynamic model on a medium-resolution digital elevation incorporating climate change. Eventually a flood hazard classification map generated, something that to the author's knowledge has not been undertaken before for the Tana River Delta.

1.3 Availability of data

It is considered that there is general lack of lower Tana River hydrological and topographical data or that there is difficulty in accessing it. Garissa[1] gauging station is the only station in the catchment with a long continuous flow record, but located 240km upstream of the study area as shown in Figure 1-1. For this study, river flow records were obtained from (WRMA, 2014), seawater levels from (APDRC, 2014) and bathymetry and river survey data obtained from fluvial and hydrological study undertaken by ASP (ASP, 2007).

1.4 Objectives

The main aim of this thesis is to investigate factors influencing flooding in lower Tana delta by means of a two dimensional hydrodynamic model and from conclusions drawn, generate a flood hazard map for the study area.

To successfully study the flood hydrodynamics, the following specific objectives were defined:

- Assessment of dam influences on flow regimes at Garissa station gauge.
- Estimation of 2, 50 and 100 year annual recurrence interval floods at Garissa station.
- Estimation of extreme high astronomical tides in the ocean near the river mouth incorporating future sea water level rise.
- Routing of floods from Garissa gauging station to upstream of study area at Garsen by means of a 1D model.
- 2D numerical model assessment of the lower Tana River hydrodynamics.
- Generate flood hazard maps for the lower Tana delta.

[1] Garissa station is the only stations that records floods accurately while other stations just measure the base flows.

1.5 Thesis methodology and presentation structure

This thesis is structured and presented as follows:

I. An overview of relevant literature on: Tana River, sea level rise, numerical modelling, probabilistic analysis and hazard classification mapping (Chapter 2).

II. The necessary two dimensional model boundary conditions for the study area were investigated. These included:

- Carrying out of relevant post and pre-dam analysis investigating impacts of dams on the flow regime at Garissa gauging station flow data records as it is the only station with long term records but located far upstream of study area (240 km upstream) (Section 3.2.4 and in detail, results presented in Section 5.1).
- From these results making necessary assumption, relevant Flood peaks and dimensionless hydrographs were derived (Section 3.3).
- A one dimensional (1D) model was calibrated for routing the relevant flood peaks from Garissa gauging station to upstream of study at Garsen deriving the relevant upstream boundary input hydrographs for the 2D model (Section 4.2.1).
- Estimation of extreme sea water levels incorporating future sea level rise due to climate change based on IPCC[2] (2013) reports and APDRC[3] tidal data bank of University of Hawaii at the river mouth deriving the relevant 2D downstream boundary (Section 3.5).

III. For the purpose of a two-dimensional (2D) model, setting up suitable grid resolution, bathymetry and relevant model parameters based on preliminary simulations and model setup guidelines in the manuals (Section 4).

IV. From the final model setup, effects of extreme high astronomical tides and other parameters influencing floods were investigated (Section 5.2).

V. Based on conclusions made on factors influencing floods, carrying out a fully 2D hydrodynamic simulations determining maximum velocity and water depths at the peak of relevant floods and, presenting the results in Google maps was done (Section 5.3).

VI. Further flood hazard classification mapping was carried out deriving flood lines for the Lower Tana delta (Section 6).

2 Intergovernmental Panel on Climate Change

3 Asia Pacific data Research Centre

1.6 Limitations and assumptions

Numerical models are powerful prediction tools from which quick outputs can be obtained. However, accuracy of input data and assumptions made in setting up the model influence the accuracy of results. Therefore, models need to be calibrated and verified with field measurements.

Assumptions made are discussed under each relevant section in this thesis, but in particular, limitation on field data and other issues listed below had an inherent limitation on the reliability of model results:

- Only dry weather flows and mean annual precipitation / evaporation rates were available for the study area at Garsen. Thus, discharges used, were based on an upstream gauging station at Garissa (240 km upstream) as shown in Figure 1-1.Within the stretch, there are various hydrological processes that would have altered the flows e.g. evaporation, water abstraction, infiltration and ground water recharge ; an attempt has been made to minimize these errors.
- Limitation of available field data, made decoupling of 1D and 2D models more attractive to minimize the likelihood of truncation errors.
- Manning's coefficient calibrating the model was theoretically determined by a combination of factors: vegetation, nature of channel and Garsen base flows against published data (Chow, 1959) and (SANRAL, 2006) drainage manual. Manning's number is a sensitive parameter prone to errors and its influence on discharge is extreme.
- In floodplains, low resolutions DEM can cause significant errors in predictions of water levels; elevations used in this thesis were obtained from various sources including satellite data, Landsat and ground surveys, resulting in a 10m x10m grid cells.
- Full hydrodynamic simulations require huge computational resources and longer execution times. Due to limitation of resources, grid cell sizes were selected such as to keep the simulation periods within a reasonable period and storage size.

2 LITERATURE REVIEW

2.1 Description of Tana River

2.1.1 Geographic location

From the Aberdare ranges in Nyeri and Murang'a Counties, the Tana River flows in a southeasterly direction into Masinga Dam that forms a major administrative border between Embu, Tharaka, Meru, Machakos, and Kitui Counties. It flows in a North Easterly direction through the seven fork dams where major tributaries from Mt Kenya and Nyambeni hills join the river. At Mbalambala, it then turns in the South Easterly direction, flowing through Garissa town, Hola and Bura irrigation schemes[4] before draining into the Indian Ocean at Kipini. It stretches over 1010 km, with a catchment area of approximately 126,000 km^2 supporting a population of about 7 million approximately 17% of Kenyan populations according to the 2010 census (WRMA, 2014and KNBS, 2010).

Location of Tana River is as shown in Figure 1-1.

2.1.2 Lower Tana Delta

The Lower Tana River is a digitate type of delta, located approximately 60 km inland of the Indian Ocean. Two distributaries break away at Garsen to form a rich alluvial floodplain of shallow lakes and mangrove swamps as shown in Figure 3-1. Before redirection of the main river channel in the 1865 by Sultan of Witu to have a navigational canal, its exit was approximately 31 km south west of current mouth; Kipini (Wokabi, et al., 1976). The remnants of the old riverbed are dotted with extensive mangrove forest and patches of grassland and are often flooded during the rainy season (Ministry of Lands, 2012) .

The lower Tana Delta is Kenya's sixth Ramsar site with a large biodiversity of plants and animals; considered as an important habitat for bird's a habitat for the five endangered sea turtles species and red listed IUCN monkeys[6] (Anon., 2012). Crocodiles, zebras, antelopes, hippopotamus, prawns, fresh water fish and shrimps among others form part of the delta's animals.

Communities in the delta are dependent on the cyclic floods for rich agricultural land. Farmers have constructed shallow lagoons to irrigate flood plain rice fields making use of high water

[4] Approximately 5000 hectares of land is under irrigation, 90 km upstream of study area (NIB, 2014)

[6] Red Columbus monkey, Crested Mangabey monkey, and white collared monkey and Africa elephant

tides to replenish with fresh water. After harvests, pastoralists graze their animals as an economic activity on fields further away from agricultural land. Poor agricultural practices, salt intrusion, and declined extent and frequency of floods have led to further encroachment and straining of the delta. (Anon., 2012)

2.1.3 Hydrological characteristic

The catchment area is mainly divided into upper, middle and lower catchment. Upper catchment runs from the agricultural highlands to Garissa, middle from Garissa to Garsen and the delta from Garsen to sea (See Figure 3-1). The upper catchment receives an annual average rainfall of about 2400 mm, lower Tana 200 mm and within the delta 300 mm. It can be said that over 80% of catchment area is within an arid and semi-arid region. (WRMA, 2014).

The rainfall pattern is bimodal with two distinct rainfall patterns: long and short rain. April to June is considered as the long rainy season while November to December is considered as the short rainy season. As has been noted in the delta from previous studies:

- Annual average temperatures have increased.
- Average annual rainfall intensity has declined.
- The number of rainfall storms events has declined.
- High intensity short duration rainfall events have increased.
- No impacts on seasonal rainfall patterns can be discerned.

2.2 Sea level rise

For estimation of extreme sea water level, estimates from recorded data on astronomical and local effects are probabilistically analyzed and expected future sea level rise due to climate change also considered. The literature supporting this is presented in this section.

2.2.1 The effects of astronomical tides and storm surges

In the upper sections of the rivers, upstream of the station under consideration, water level variations are mainly governed by the precipitation received, while deltaic water levels are governed by interaction between river flows and sea water level variations due to astronomical tides, storm surges and barometric local effects.

Astronomical tides are the result of attractive forces of the moon and sun causing short periodic rises and falls of water levels in the sea dependent on the position of moon, earth and the sun. These tide variations are predictable for any future time with great accuracy.

Tana River delta experiences a semi- diurnal type of tide: two high water and two low waters during the 24 hours and 50 minutes cycle as illustrated in Figure 2-1. The two high water and low water levels show different elevations due to angle of declination between the moon and the sun with respect to the equator.

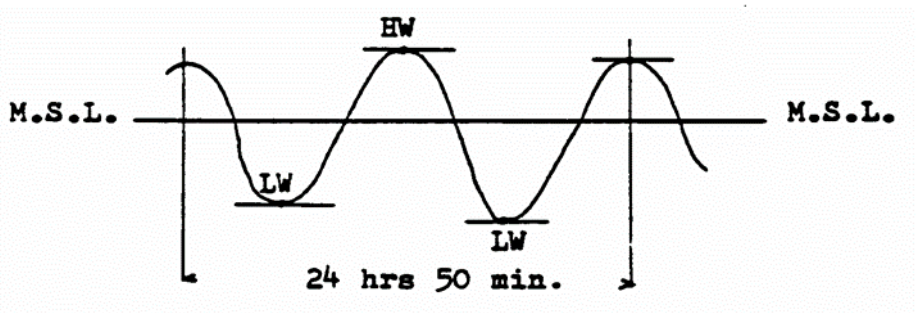

Figure 2-1: An illustration of semi-diurnal tide over a day span. Source: (David, et al., 2014).

Dependent on the position of the sun and moon with respect to the earth, there are tidal variation leading to spring and neap tides. Neap tides are experienced during the first and last quarters of the moon while spring tides occur at full moon and new moon as illustrated in Figure 2-2.

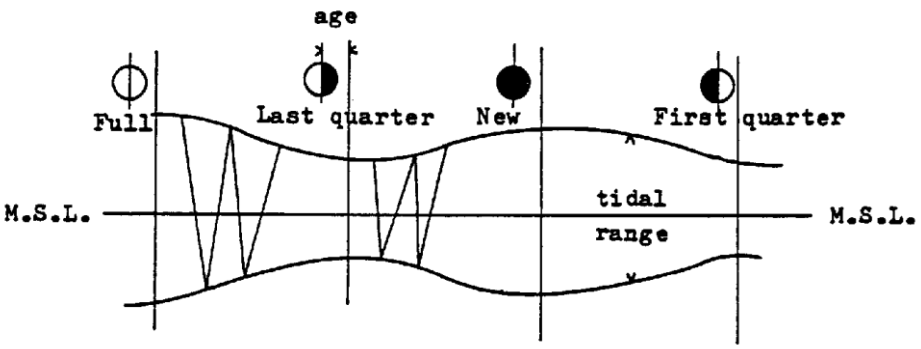

Figure 2-2: Tidal range due to spring and neap tides. Source: (Savenije H., 2012).

During spring tides[7], resonance and reflection amplify tides leading to higher than normal water levels as the tide propagates upstream of estuaries. If this rise coincides with upstream high water flows, major damming occurs leading to above normal water depths in the floodplains. Figure 2-3 illustrates this, indicating the high water envelope[8].

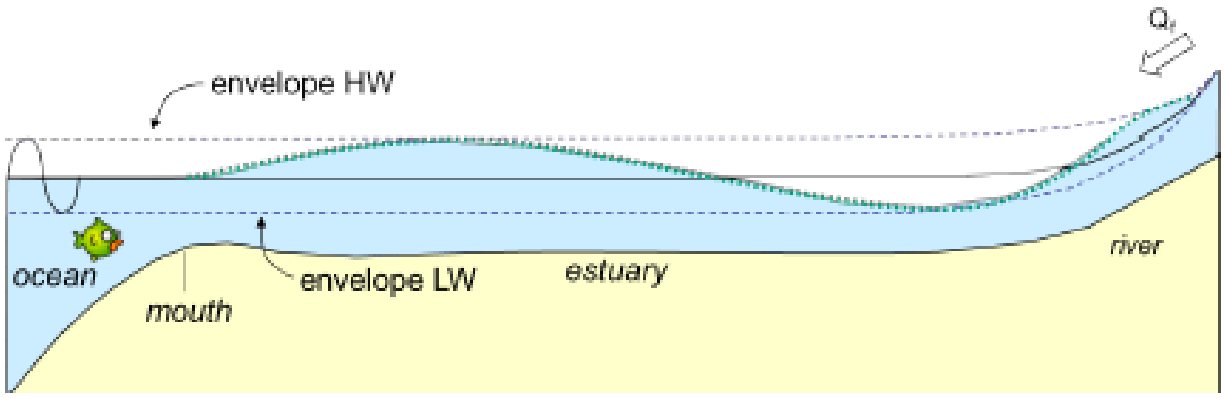

Figure 2-3: Longitudinal section showing a tidal wave causing water level rise in estuary. Source: (Savenije H., 2012)

Strong seaward winds blowing over a large fetch cause ‘drag’ on water surface, the friction between wind and the water surface causes a stress on the water surface making it assume a slope as shown in Figure 2-4. This rise in water level is super-imposed on astronomical tides, and their long-term predictability is probabilistic.

[7] Maximum or minimum water levels due to astronomical tides are experienced in any given period of the year.

[8] The level of the water will rise or drop due to high tide occurring in a spring tide.

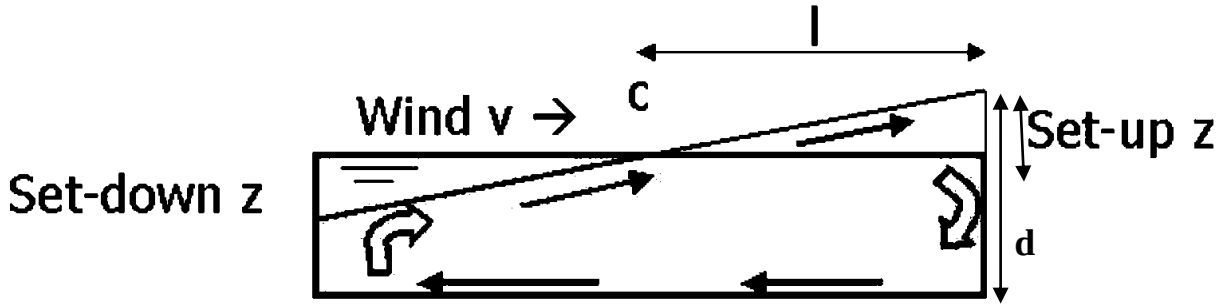

Figure 2-4: Set-up of water level due to wind effect in the sea. Source: (Savenije, 2013).

Where:

I	Distance from inshore point to station P on the shore (m),
v	wind velocity (m/s measured at 6 m above water surface),
d	water depth inclusive of setup (m) and
z	water setup $= 3.6 * 10^{-6} \frac{v^2}{gd} I$(m) if z $\ll$ d

Tsunamis and monsoon winds occasionally lead to above normal sea levels on East African coasts. Though the probability of these occurrences coinciding with spring tide is high[9], tsunami predictability is a science on its own, hence not covered further in this thesis.

2.2.2 The effects of climate change

The sea level rise due to climate change discussed in this thesis was based on 4th Assessment Report of the United Nations Intergovernmental Panel on Climate Change 2013[10]. During the period of 1993-2010, data from IPCC reports have shown great agreements between the predicted and recorded satellite altimeters sea level rise, thus giving good credibility to the projected values (Bosman, 2014). Figure 2-5 shows sample data comparison between the recorded and predicted values. (IPCC, 2013).

[9] Author's point of view

[10] "The main activity of the IPCC is to provide at regular intervals Assessment Reports of the state of knowledge on climate change. The latest being IPCC Fourth Assessment Report 2007 edition. Currently the Fifth Assessment report, to be released in phases from September 2013 to October 2014 is being prepared"

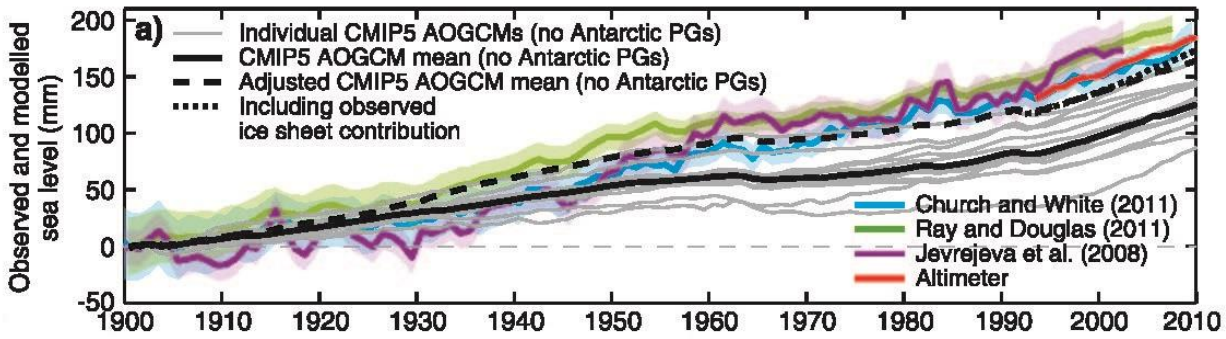

Figure 2-5: Comparison between the previous model projections and measured sea level values by the sea altimeters. Source: (IPCC, 2013)

IPCC predictions are based on many contributing factors: population growth, advancement in technologies, land uses, cement production, global warming, and energy production among others. Based on different consideration, four different scenarios or so called Representative Concentration Pathways (RCP) are possible: RCP 2.6, RCP 4.5, RCP 6.0 and RCP 8.5. (RCP, 2009). These projections are tabulated in Table 2.2-1 for a period up to 2100; high uncertainties inhibit extension beyond 2100.

Table 2.2-1 : Global mean sea level rise projections based on models for different scenarios. Source: (IPCC, 2013)

Scenarios	**2046-2065**	**2081-2100**
	Mean and likely range (m)	**Mean and likely range (m)**
RCP2.6	0.24 (0.17 to 0.32)	0.40 (0.26 to 0.55)
RCP4.5	0.26 (0.19 to 0.33)	0.47 (0.32 to 0.63)
RCP6.0	0.25 (0.18 to 0.32)	0.48 (0.33 to 0.63)
RCP8.5	0.30 (0.22 to 0.38)	0.63 (0.45 to 0.82)

Attributed to local effects, these global mean sea level rises differ with the regional sea level predictions. To correct the differences, spatial percentages deviations are used. Figure 2-6 shows these percentages.

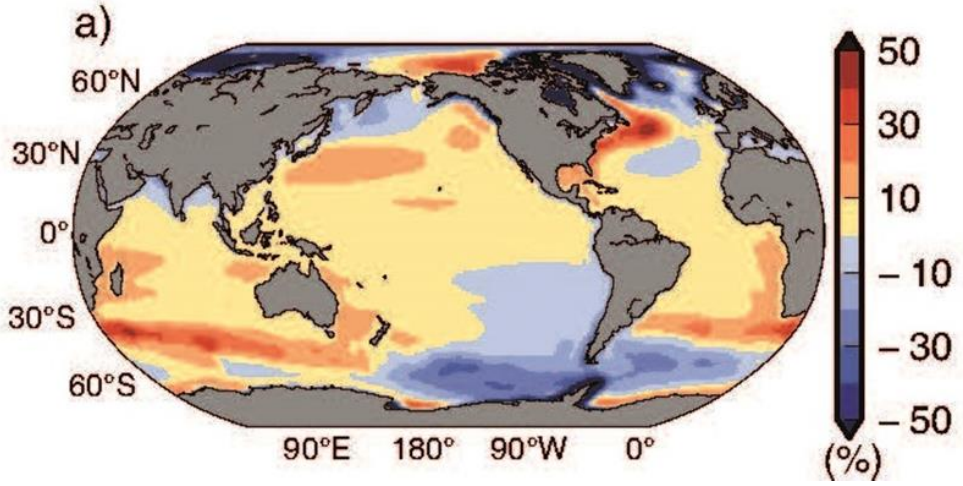

Figure 2-6: Mean regional percentage deviation from global mean sea level for all RCPs between 1986-2005 and 2081-2100. Source: (IPCC, 2013)

2.3 Numerical modelling

2.3.1 Criteria for model selection

Physical models have been a preferred choice of many studies, but their prohibitive cost and large lead times have led to the advent of analytical models as essential tools for physical process predications (Versteeg & Malalasekera, 2007). Based on observed data, dominant mechanisms are hypothesized and formulated into mathematical models that in most cases cannot be solved by simple analytical solutions. Computer algorithms are used in numerical models to solve these sets of differential equations. Sensitivity analyses are necessary to identify most influencing parameters before undertaking the actual analysis and representation of data for interpretation. Thus, understanding the theory behind each numerical model and its limitation is of essence as it is just a representation and can be erroneous if blindly followed (Savenije, 2009).

As a choice of which model to use, three types of hydrodynamic numerical models available: 1D, 2D and 3D. For quick solutions and ease of setup, 1D models are preferred but with reduced accuracy in complex channels and less output variables. On the other hand, 2D are a better representation of reality, but require more resources and time to simulate with improved accuracy and more variable outputs. 3D models are similar to 2D but far much complex and more outputs (El-Nasr, et al., 2005).

In this thesis, the hydrodynamics of Tana River are investigated; 1D was required for routing and 2D model for floodplain water depths and velocities calculations. Successfully implemented projects and studies, technical support, availability of license and robustness, made MIKE by DHI software packages preferred choice for the Tana study. A coupled module of 1D and 2D (MIKE FLOOD) was available from DHI but the limitation of available field data, made decoupling of each module separately more attractive to minimize the likelihood of truncation errors. (DHI, 2001).

DHI's 1D and 2D models (Mike 11 and Mike21C respectively) are discussed in more detail in the following subsequent sections: 2.3.2 and 2.3.3 .

2.3.2 One dimensional modelling by DHI MIKE 11 (DHI, 2013)

The MIKE 11 DHI package is a fully dynamic 1D-model tool using implicit finite differencing schemes to solve unsteady flows in channels. As described before, the relatively fewer data requirements and fast computational time makes it ideal for river studies and in particular, the routing of flood considered in this thesis (MIKE11 by DHI, 2013).

Subsequent discussions regarding MIKE 11 governing equations and model setup are limited to flood routing.

2.3.2.1 Governing equations

Continuity equation (2.3-1) and momentum equation (2.3-2) describe the storage function in routing. The continuity equation is discretized to yield equation (2.3-3), which is further substituted in the momentum equation to yield equation (2.3-4).

$$\frac{ds}{dt} = Q_i - Q_o \tag{2.3-1}$$

$$S = KQ_o^p - T_1 Q_o \tag{2.3-2}$$

$$\frac{S_{t+\Delta t} - S_t}{\Delta t} = Q_i - \frac{Q_{o,t+\Delta t} + Q_{o,t}}{2} \tag{2.3-3}$$

$$\frac{KQ_{o,t+\Delta t}^P - T_1 Q_{o,t+\Delta t} - (KQ_{o,t}^P - T_1 Q_{o,t})}{\Delta t} = Q_i - \frac{Q_{o,t+\Delta t} + Q_{o,t}}{2} \tag{2.3-4}$$

Where:

S	Basin storage
K, P	Constants
Q_o	Outflow at water way
Q_i	Inflow at water way
T_1	Duration of delay [Q (t) =Q (t+T_1]
Δt	Change in time.

Routing is applied on fully dynamic scheme that solves Saint Venant equation summarized in equations (2.3-5) and (2.3-6).

$$\frac{\partial Q}{\partial x} + \frac{\partial A}{\partial t} = q \tag{2.3-5}$$

$$\frac{\partial Q}{\partial x} + \frac{\partial \left(\propto \frac{Q^2}{A}\right)}{\partial x} + gA\frac{\partial h}{\partial x} + \frac{gQ|Q|}{C^2 AR} = 0 \tag{2.3-6}$$

Where:

A	Area of flow

h	Stage above datum
Q	Discharge
R	Hydraulic or resistance radius
$\propto$	Momentum distribution coefficient
q	Lateral inflow

Model application should be limited to flows that are parallel to the bottom, subcritical, negligible density variations and low bottom slope gradients[11].

2.3.2.2 Model editors

Mike 11 makes use of the simulation editor to control all the necessary inputs for complete model linking them together in one platform. These editors are shown in Figure 2-7 below.

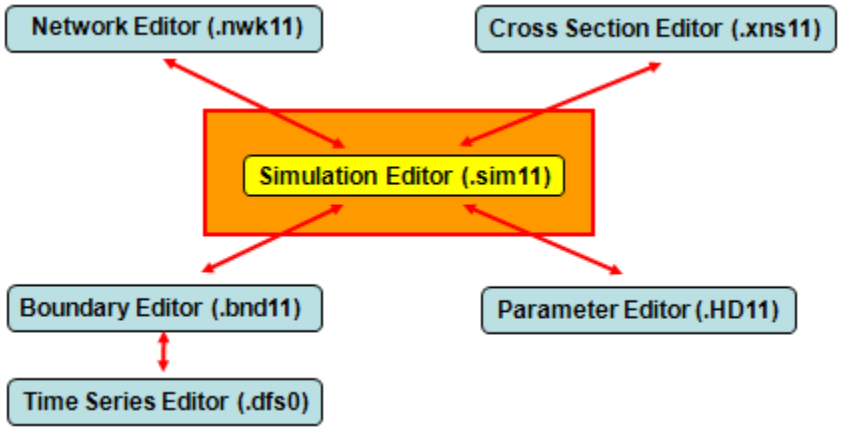

Figure 2-7:Illustration of MIKE 11 simulation editor and necessary input files. Source: (MIKE11, 2013)

Based on (MIKE11, 2013), a brief description of these is given below:

River Network Editor

This editor describes the river model area graphically / tabularly, showing all the connections, shapes and distances. All point's attributes can be accessed and edited on it.

[11] The cosine angle between the water depth and horizontal can be assumed to be 1

Cross Section Editor

The river network is defined by cross sectional data (x, z) coordinates derived typically from river surveys. In the editor, river Chainage and Manning number associated with the cross section are processed.

As guideline, number of cross sections should just be adequate to resolve all the water levels accurately describing the problem in hand.

Boundary Editor

Inflow hydrographs and water levels describe model boundary inputs. It is recommended boundaries should be placed further away from the point of interest and should describe the variations accurately.

Hydrodynamic editor

Definitions of global parameters are done in this editor. Model calibration (described under section 2.3.2) and routed hydrograph extraction are done in it.

Time steps

Recommended, courant number in order of 10-15 provides hydrodynamic accurate and stable time steps estimates.

2.3.3 Two dimensional modelling with DHI MIKE 21C

Complex 3D equations, requiring huge computational resources best describe flows in braided and meandered channels. To simplify the latter, MIKE 21C, a DHI module makes use of depth averaged St. Venant equations which when computed, results in water depths and velocities over a curvilinear/ rectilinear grid. In addition, its helical flow algorithm can solve secondary currents over bends making it a quasi-3D model (MIKE21C, 2013).

Other morphological study modules for sediment transportation, scour and deposition and bank erosion are present, but not considered in this thesis but future extension possible as hydrodynamics forms the building block of all the modules.

2.3.3.1 Saint Venant equation

This section is based on MIKE 21C scientific documentation manual (MIKE21C_s, 2012).

Equations used by the model are described through (2.3-7) , (2.3-8) and (2.3-9) simplified by the set of assumptions described below:

- Rigid lid approximation:

  Assumes rigidity and impermeability of water, thus stresses experienced are normal to the surface if ratio of $\frac{h}{R}$ and Froude number are small, hence negligible errors introduced.

- Shallow water approximation:

  Internal and wall frictions are neglected as errors introduced are equivalent to $\left(\frac{h}{R}\right)^2$ which is negligible.

- Hydrostatic water approximation:

  Vertical velocity gradients are neglected as the errors introduced are in the magnitude of $\left|\frac{h}{R}\right|$ which is negligible.

Due to these approximations, the model is only applicable to rivers with moderately curved wide channel beds with low Froude number, low gradient and shallow topographies.

$$\frac{\partial p}{\partial t}+\frac{\partial}{\partial s}+\left(\frac{p^2}{h}\right)+\frac{\partial}{\partial n}\left(\frac{pq}{h}\right)-2\frac{pq}{hR_n}+\frac{p^2-q^2}{hR_s}+gh\frac{\partial H}{\partial s}+\frac{g}{C^2}\frac{P\sqrt{P^2+q^2}}{h^2}=RHS \qquad (2.3\text{-}7)$$

$$\frac{\partial H}{\partial y}+\frac{\partial p}{\partial s}+\frac{\partial q}{\partial n}-\frac{q}{R_s}+\frac{p}{R_n} \qquad (2.3\text{-}8)$$

$$\frac{\partial p}{\partial t}+\frac{\partial}{\partial s}+\left(\frac{pq}{h}\right)+\frac{\partial}{\partial n}\left(\frac{q^2}{h}\right)+2\frac{pq}{hR_s}-\frac{p^2-q^2}{hR_n}+gh\frac{\partial H}{\partial n}+\frac{g}{C^2}\frac{q\sqrt{P^2+q^2}}{h^2}=RHS \qquad (2.3\text{-}9)$$

Where

p, q	Mass fluxes in the s- and n direction respectively
H	Water level (m)
g	Acceleration due to gravity
R_s, R_n	Radius of curvature of s- and n-line, respectively
h	Water depth (m)
s, n	coordinates in the curvilinear coordinate system
C	Chezy roughness coefficient
RHS	Right hand side of the force balance equation including terms for Coriolis force, atmospheric pressure and Reynolds stresses

To account for curvilinearity, equations (2.3-10) and (2.3-11) that assume R_s and R_n are large and slowly varying in the p and q directions respectively are used.

$$\frac{\partial}{\partial x}\left(E\frac{\partial P}{\partial x}\right)+\frac{\partial}{\partial y}\left(E\frac{\partial P}{\partial y}\right) = \frac{\partial}{\partial s}\left(E\frac{\partial P}{\partial s}\right)+\frac{\partial}{\partial n}\left(E\frac{\partial P}{\partial n}\right)-\frac{2E}{R_s}\frac{\partial q}{\partial s}-\frac{\partial E}{\partial s}\frac{q}{R_s}-\frac{2E}{R_n}\frac{\partial q}{\partial n}-\frac{\partial E}{\partial s}\frac{q}{R_n} \qquad (2.3\text{-}10)$$

$$\frac{\partial}{\partial x}\left(E\frac{\partial Q}{\partial x}\right)+\frac{\partial}{\partial y}\left(E\frac{\partial Q}{\partial y}\right) = \frac{\partial}{\partial s}\left(E\frac{\partial q}{\partial s}\right)+\frac{\partial}{\partial n}\left(E\frac{\partial q}{\partial n}\right)-\frac{2E}{R_s}\frac{\partial p}{\partial s}-\frac{\partial E}{\partial s}\frac{p}{R_s}-\frac{2E}{R_n}\frac{\partial p}{\partial n}-\frac{\partial E}{\partial s}\frac{p}{R_n} \qquad (2.3\text{-}11)$$

Where

$$E=\frac{\text{Turbulent}}{\text{Eddy viscosity}}\ (m^2/s)$$

2.3.3.2 Model inputs

Describing the model space, boundary conditions, calibration and time steps (interval and range) forms the basis of a good hydrodynamic model. In addition, other secondary parameters need to be specified, namely:

- Sources and sink
- Eddy viscosity

- Flooding and drying depth
- HD integration

Overviews of these and other related parameters are discussed further in subsequent sections:

Bathymetry

Describing the model space is the most important task in modelling; some of the steps in the bathymetry setup are listed below:

- What's the extent of working space?
- What features must be included?
- What's the location of boundaries?
- What's the size of grid cells?

As explained before, Mike 21C makes use of curvilinear grids generated by the purposely-built MIKE 21C grid generator. To create curvilinear bathymetry the following input data are required: land elevations mostly supplied in the form of GIS or in XYZ format, riverbanks boundary positions in (X, Y) and photos showing the extent of the model.

In the grid generator, polylines are drawn/imported, number of grids cells specified, orthogonalised and elevations imported to the specific grid points. The output files obtained are DEM/ bathymetry and 2D grid maps with coordinates of the four cell corners.

Time steps

The time steps are mainly influenced by the grid cell sizes and model complexity; small irregular grid cells take longer for model convergence. For accurate results within reasonable durations, a balance between the grid cell sizes and time steps need be struck keeping in mind that, smaller time steps do not necessarily guarantee accurate results if based on wrong bathymetry grid cell size, but greatly improve model stability.

As a guideline, the Courant number given by equation (2.3-12) should not be more than one.

$$C_R = c\frac{Cr\Delta t}{\Delta x} \tag{2.3-12}$$

Where:

c	celerity ($\sqrt{gy}$)
Δt, Δx	Time step and grid spacing respectively

Bed resistance and calibration

Manning / Chezy resistance numbers are the main parameter used to calibrate the model against observed data. The model makes use of equation (2.3-13) to calculate bed resistance with the input of roughness as constant values or in gridded map showing the variations.

Due to the sensitivity of the (Chow, 1959) Manning value (n), Chezy number is much preferred but a modified MIKE 21 Manning number M[12] is used.

$$\frac{g.u.|u|}{C^2} \qquad (2.3\text{-}13)$$

Where:

g	acceleration due to gravity
u	velocity
C	Chezy number

Eddy viscosity

The eddy viscosity in the model needs to be defined; flux based viscosity formulation (Smargorisnky) offers the best solutions but introduces instabilities in the computations due to constant water depth assumption. Consequently, the more stable velocity-based formulation is preferred.

It has been found that in most river studies, viscosity has little effect on the solution. Thus, it has been recommended to be left as a model default in river studies (MIKE21C, 2013).

Flooding and drying

This parameter controls the areas (grid points) that are included and excluded in the model computations during simulations. If small ranges are used, redundant grid cells are included in computation escalating computational time and inherent instabilities.

In deltas, flooding depths in ranges of 0.2-0.4m and drying depths of 0.1-0.2m have been found to be appropriate and a difference of 0.1m between the drying and flooding depth is recommended.

[12] Manning number M $=\frac{1}{n}$ $m^{1/3}/s$ and $C=M.h^{1/6}$ $(m^{1/2}/s)$

2.4 Probabilistic analysis

Probabilistic analyses are applied to gauged catchments with adequate record lengths to predict future flood magnitude. Use of directly measured flow makes this method preferred for large catchments as adjustments for storage in floodplains are catered for. The fundamental assumption that data is gauging error free can be misleading if the discharges are not well verified.

Probabilistic predictions on historical recorded events are susceptible to catchment changes and hence examination is necessary. Of major concern, is that the effects of climate change are not conclusively exhibited on short historical record. Hence, based on IPCC models, an increase of 10% for period up to 2025 and 20% henceforth are suggested on peak flows (Chadwick, et al., 2013) and (SANRAL, 2006).

The use of return period (T), annual recurrence interval (ARI) and annual exceedance probability (AEP) interchangeably has brought about confusion and will therefore be explained. The average duration over which a flood tends to repeat its self is the return period and in any given year, equation (2.4-1) gives the probability of exceedance. AEP/ARI describes the probability of flood occurrence (with certain T) once or a number of times over a certain design period calculated using equation (2.4-2). To demonstrate this, a summary of the probability of experiencing a certain flood once or more times over a period of 70 years is shown in Table 2.4-1. (IWE, 2014)

$$P = \frac{1}{T} \tag{2.4-1}$$

$$P_X = \frac{n!}{X!\,(n-X)!} P^X \left(1 - \frac{1}{T}\right)^{n-X} \tag{2.4-2}$$

Where

X	No of exceedances
n	Design life

HD integration

This defines how the model will compute solutions. Various schemes are available:

- Fully dynamic:

  The specified time step is used for both continuity and momentum equation.

- Scaled dynamic:

  Uses scaled HD time of general time step specified.

- Quasi steady:

  Different time steps for both continuity and momentum equations are used. Its use is recommended for steady flows with gradual boundary condition variations

- Steady:

  Stored pre-calculated solutions are used.

Table 2.4-1: Chances of encountering a given flood on one occasion or twice over a certain design life. Adopted from (IWE, 2014) and (NSW, 2005).

Return period	**Probability of occurrence in any given year**	**Likelihood of encountering a certain flood over a span of 70 years**	
		At least on one occasion	At least on two occasions
Q_{10}	10.0%	99.9%	99.3%
Q_{50}	2.0%	75.3%	40.8%
Q_{100}	1.0%	50.3%	15.6%

In this thesis, in order not to overestimate flood peaks, the use of annual series over partial series was preferred; annual series makes use of maximum peak per year for the records under consideration.

Probabilistic methods were preferred to avoid bias and inaccuracy associated with graphical methods. The guidelines in the SANRAL (2006) drainage manual were used to calculate the peaks and are summarized in three steps below:

I. Determination of data parameters: median, mean, standard of deviation and skewness of raw and log transformed data.
II. Selection of return period and frequency distribution method to use. Namely: Normal distribution, Extreme value type1, General extreme value, Lognormal, Log-Gumbel and Log-Pearson type III.

ASP (2007) and Maingi & Marsh (2002) had found log-Pearson and General extreme value most suitable for Tana River, nevertheless all methods were tried out.

III. Graphical illustration of data dependent on selected plot position: Weibull or Cunane plotting positions.

2.5 Hazard classification mapping

Flood risk mapping is an integration between probability of flooding causing damage and expected probability of flooding. There is no universally accepted criterion of flood classification mapping, each method is subject to its own interpretation and the 'one fits all' approach, undermines the underlying variability (Thomas & Golaszewski, 2012).

With regard to this thesis, (NSW, 2005)[13] Floodplain Development manual guidelines[14] are adopted and a summary is given below.

The manual is based on a combination of the hydraulic and hazard categories briefly discussed.

Hydraulic categories:

Divided into 3 prone land areas

- Floodways:

  Areas that if blocked will cause significant water level increase.

- Flood storage:

  Areas that offer temporal storage during flood propagation.

- Flood fringe:

  Other inundated areas.

Hazard categories

Two main categories are recognized:

- High hazard:

  In these conditions, wading is unsafe, vehicular mobility restricted and damage to light structures experienced.

- Low hazard:

  In these conditions, mobility of able-bodied adults and automobiles is possible.

[13] New South Wales

[14] The manual was adopted for its wide use and global acceptability as the initial guidelines for flood studies. An example of adoption is City of Cape Town floodplain and river corridor management policy based on Australian guidelines (COCT, 2009).

Based on hydraulic factors only disregarding other influencing parameters listed below, Figure 2-8 shows map classification graph used.

- Usage of land
- Magnitude of flood
- Flood duration
- Rate of water rise
- Prior readiness
- Evacuation issues
- Water depth and velocity

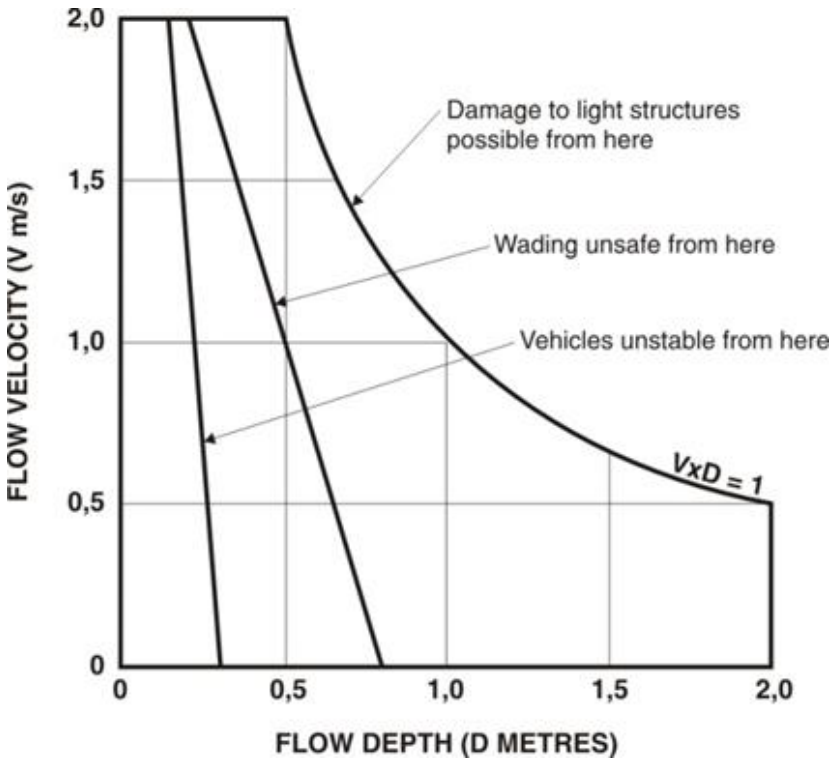

Figure 2-8: Flood hazard map classification based on velocity and depth relationship. Source: (NSW, 2005)

3 LOWER TANA RIVER FLOOD HYDROLOGY

3.1 Introduction

For the purpose of lower Tana 2D hydrodynamics modelling, upstream and downstream boundary inflows and water levels were required respectively. Tana 2D model upstream boundary is located at Garsen. Thus, flood hydrographs derived at Garissa are routed to Garsen using the 1D model under section 4.2.1. Tidal levels at the river mouths are defined as the 2D downstream boundary. These boundary values are determined in this section.

3.2 Catchment information

3.2.1 Study area

The study area is approximately 940 km from the upper catchment, running a length of approximately 60km to Indian Ocean and commanding a catchment size of 87500km^2 as shown in Figure 3-1. Table 3.2-1 shows basic catchment characteristics and in Appendix 2 there is an illustration of catchment elevation graph of the area.

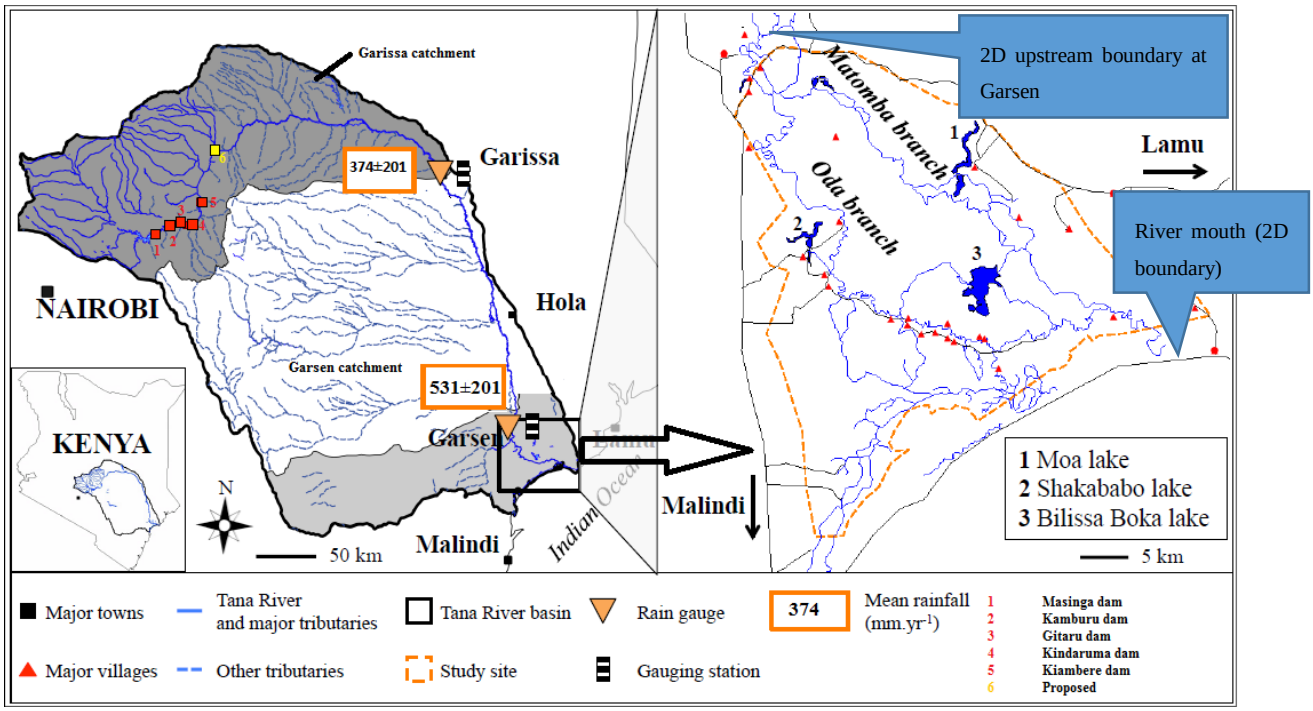

Figure 3-1: Study area general catchment information showing major basin characteristic, river channels, settlements and roads. Source: KMD, (Leauthaud, et al., 2013) and (WRMA, 2014)

Table 3.2-1: Catchment characteristic summary. Source: Google earth[15]and (WRMA, 2014)[16].

Catchment name	Upper Tana (Mt Kenya to Garissa)	Lower Tana (Garissa to Ocean)
Catchment area (km2)	33000	87500
Max elevation, AMSL (m)	2953	347
Min, AMSL (m)	261	0
Average slope	0.60%	0.20%
Longest water course (km)	375	620

3.2.2 Gauging stations

There are three major gauging stations in the lower catchment, namely Garissa, Hola and Garsen. Their particulars are listed in Table 3.2-2. However, Garissa is the only gauging station with the capability of measuring large peaks accurately and has a continuous record of data. Unfortunately, it is located ≈ 240 km (Google earth) upstream of the study area and is susceptible to upstream dam operations, abstraction works and hydrological processes, thus warranting further investigation. Such investigations are carried out in sections 3.2.3 and 3.2.4.

Table 3.2-2: Gauging station characteristics. Source: (WRMA).

Station name	Garissa (4G01)	Hola(4G04)	Garsen(4G02)
Location	lat: -0.45° long: 39.7°	lat: -1.5° long: 40.033°	lat: -2.275° long: 40.117°
Catchment area(km2)	33000	***	87500
Operation dates	1933 to current	1949 to 1998	1950 to 1998
Record dates	75	49	48
Gaps in record	8%	23%	41%
Peak recorded flow(m3/s)	3561	***	572
***** data not available**			

[15] Maximum and minimum elevation height and average slopes are obtained directly from Google earth elevation profile calculator

[16]WRMA is a Kenyan state corporation mandated with water resources management, thus data obtained from them is deemed accurate for research purposes. Daily flow records for all Kenyan basins are recorded and maintained by the corporation.

3.2.3 Precipitation, mean annual temperature and water losses.

Mean annual precipitation values are indicated in Figure 3-1 and summarized in Table 3.2-3 . High temperatures and low gradient cause reasonably high evaporation rates in the delta. Dagg, Woodhead, & Rijks (1970) observed 1400-1600 mm annual rates. Not quantitatively ascertained, to the knowledge of the author, these losses coupled with irrigation water abstraction works, cannot significantly alter the flood peaks; but they significantly influence the normal discharges, and duration of flooding. It is therefore not considered further in this thesis.

Leauthaud, et al. (2013) and Maingi & Marsh (2002) have ascertained low precipitation experienced in this region can only replenish the soil field capacity but not significantly contribute to the runoff as compared to upstream water inflows.

Table 3.2-3: Annual average precipitation summary. Source: Leauthaud, et al.(2013), Bunyasi (2012) and KMD.

Catchment	**Upstream**	**Garissa**	**Garsen**	**Delta**
Observation period	******	1962 to 2008	1972 to 1986	1962 to 2008
No of records years	******	46	14	46
Annual average (mm/yr.)	1622±587	374±201	531±201	1099±307
Temperatures (º C)	27	26-31	26-31	26-31

3.2.4 Pre-dam and Post-dam analysis

3.2.4.1 Dams

Five dams are operational with their characteristic shown in Table 3.2-4; six more have been proposed to maximize the available water head.

Table 3.2-4: Summary of Tana River seven fork dams' characteristics. Source: KENGEN

Reservoir	**Completion date**	**Reservoir capacity(km^3)**	**Installed capacity(MW)**
Kindaruma	1968	N/A	72
Kamburu	1974	1.23	100
Gitaru	1978	N/A	225
Masinga	1981	15.6	40
Kiambere	1988	5.35	168

Before completion of Masinga Dam in 1981, the previous dams were comparably small and their operation was geared towards maximum power production with low attenuation and

storage (KenGen, 2014)[17] and (Oludhe, 2011). Demonstrated in Figure 3-2, mean annual average inflows, and discharges[18] for a 24 years' record are plotted. Over this period, 80% of the time power production regulated the discharges, consequently, 1981 was taken as the datum for pre-dam and post-dam analysis.

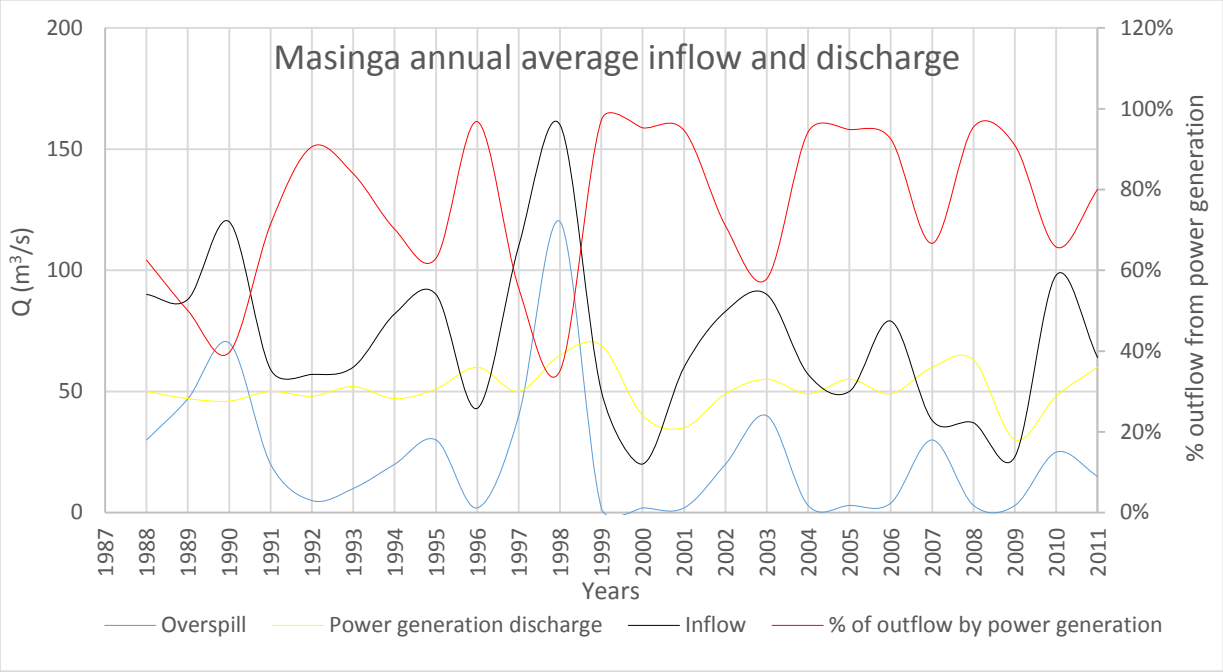

Figure 3-2: Annual average inflows and discharges from overspills and power generation at Masinga Dam. Source: KenGen(2014)

3.2.4.2 Analysis

To show changes over the post and pre-dam periods, average cumulative monthly flows were plotted for the entire two separate periods, Figure 3-3. Further probabilistic analyses as discussed under section 2.4 were carried out to ascertain the changes in magnitude and raw data parameters.

One of the objective of this thesis was to investigate effects of dams' construction on flow regime. The results are discussed in detail, under results in section 5.1. For the purpose of the next section, Masinga and Kiambere Dams did not significantly affect the peak flows in the second season (November to December), as shown in Figure 3-3. In the second season, short

[17] Kenya Electricity Generation Company (KENGEN) is mandated to produce electricity and manage hydroelectric dams on behalf of Kenyan government.

[18] A 24 years' record was used for the inflow and outflow, water levels data was only available for 12 years. For the recorded period, 80 % of the time the flow was controlled by power generation discharge into the other smaller dams. Only in bigger floods did the dams over spill.

duration high intensity rainfalls, likely to cause flash floods tend to occur. The six worst floods (above 2000 m^3/s) recorded at Garissa have been in this period. This tread can be explained due to seasonal shift of ITCZ[19] / monsoon winds. Combining data for both pre-dam and post dam was found necessary as the records for the post dam period were reduced to 30 years. Probabilistic approximation with such short data has the likelihood of erroneous impressions with regard to extreme floods peaks.

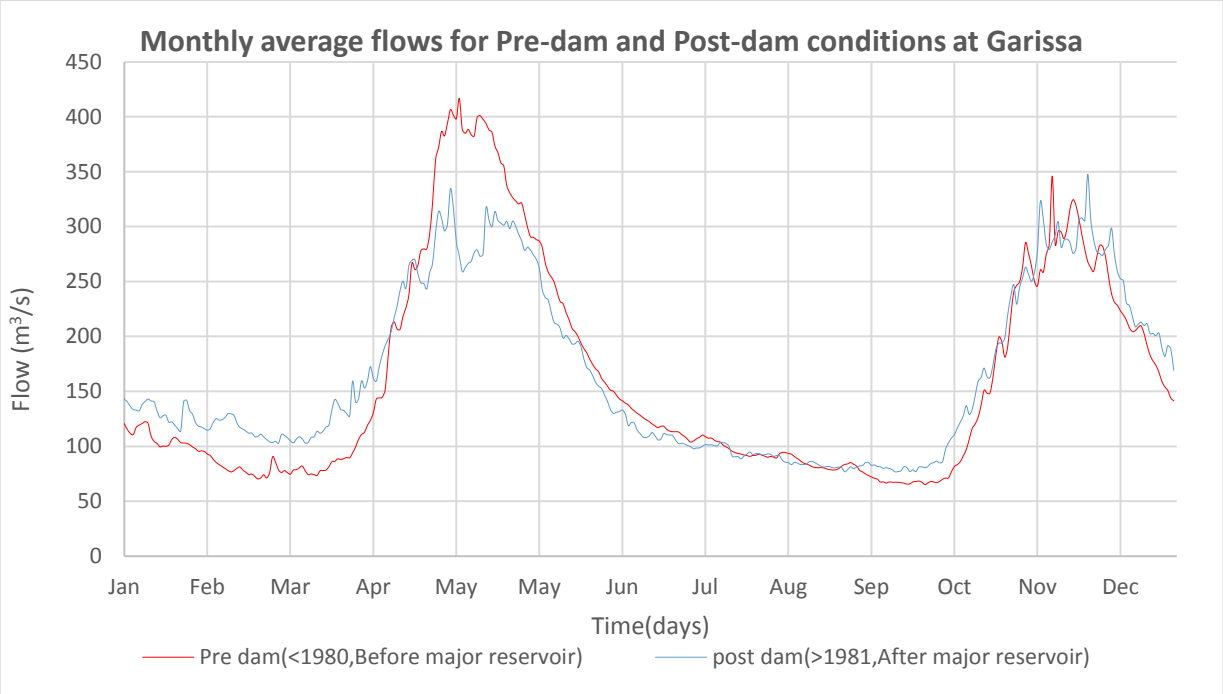

Figure 3-3: Average seasonal hydrograph for both Pre-dam and Post dam conditions at Garissa. Data source: (WRMA, 2014)

[19] Movement of Inter tropical convergence Zone / monsoon winds brings rain into East Africa, though the :'Short rains' is experienced in the second season, the winds blow mainly from the Indian Ocean bringing in excess moisture, causing high intensity short duration storms, hence maximum peaks have been recorded in this season.

3.3 Probabilistic flood analysis

From a 73 years record (1941-2013), annual maximum flood peaks at Garissa station were extracted and their values are shown in Figure 3-4.The largest recorded peak was in 1961 at 3561 m^3/s.

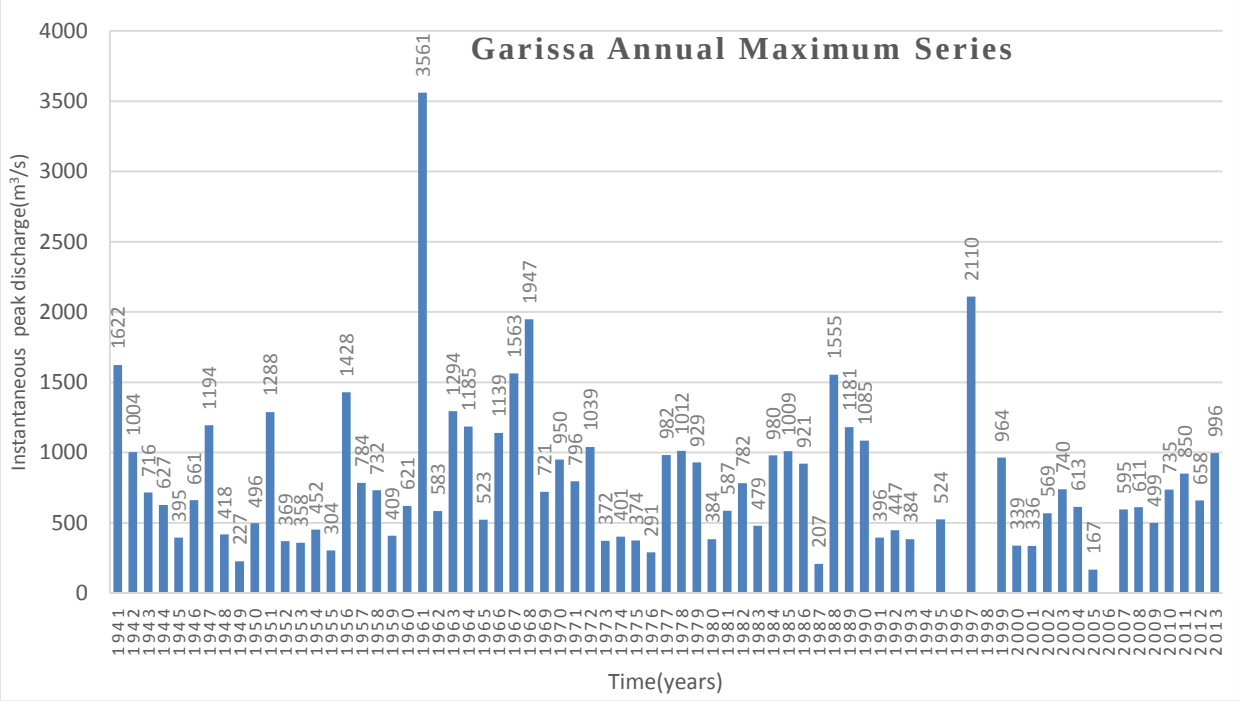

Figure 3-4: Historical recorded flood peaks at Garissa station. Source: (WRMA, 2014)

The record had eight percent missing data, with 1994, 1996, 1998 and 2006 records contributing most[20] . As a rule of thumb, on Gumbel distribution, river peaks with T≈ 1.5 lies on bank full levels (Savenije, 2013). Thus, other available flow records were analyzed using Gumbel distribution and a peak value of 830 m^3/s was used to replace the four missing years. This method of replacing with T=1.5 value has the advantage of not overestimating peaks as compared with when probabilistic estimations are done with gaps.

The general statistics of the data are presented in Table 3.3-1 and general Garissa gauging station statistics can be found under section 3.2.2 .

[20] Each had over 100 days gap in record

Table 3.3-1: Garissa station data general statistics. .

Variable	Normal data	Log10-transformed data
Mean (xmean)/Log (xmean)	819.325	2.841
Total time span (YT)	73	73
Missing data (NC)	0	0
Standard deviation (s)/(slog)	527.024	0.251
Coefficient of variation (cv)/(cvlog)	0.643	0.088
Skewness (g)/(glog)	2.354	0.044

General probabilistic hydrological analysis (Normal, Extreme Value type 1, General Extreme Value, Log-normal, log-Gumbel and log- Person type 3) distributions and graphical analysis (general purpose Cunene plotting position) were applied to the data. Figure 3-5 shows the resulting plot and it is summarized in Table 3.3-2 (SANRAL, 2006).

Table 3.3-2: Probabilistic flood peaks summary

Return Period	N/MM	EV1/MM	GEV/MM	LN/MM	LEV1/MM	LP3/MM
T, years	m^3/s	m^3/s	m^3/s	m^3/s	m^3/s	m^3/s
1.25	376	386	426	426	431	426
2	819	732	701	694	631	691
5	1263	1199	1127	1129	1052	1127
10	1495	1508	1447	1456	1476	1459
20	1686	1804	1787	1796	2044	1809
50	1902	2188	2280	2275	3113	2306
100	2045	2475	2693	2663	4267	2713
200	2177	2762	3147	3076	5843	3150
500	2336	3139	3815	3664	8844	3778
1000	2448	3425	4380	4142	12094	4294

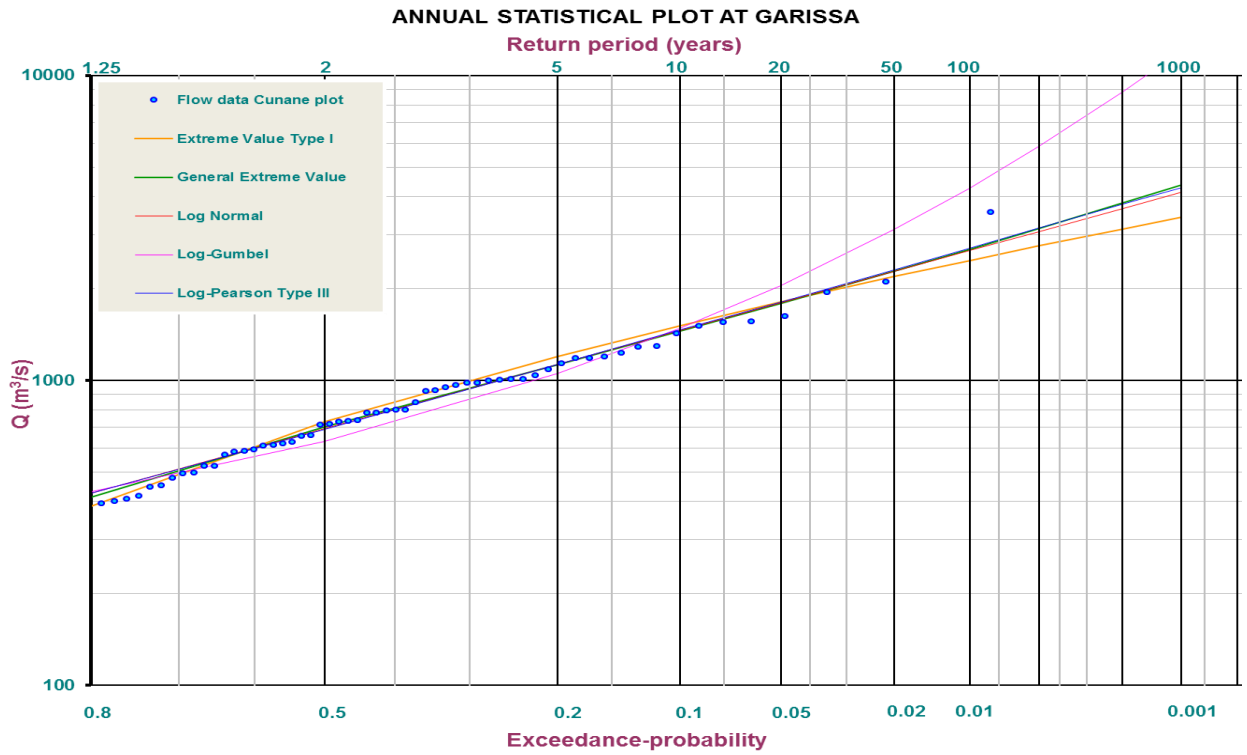

Figure 3-5: Annual maximum series graphical representation.

Of the six methods, log-Gumbel overestimated the observed peak floods while the other five underestimated but log Pearson type 3 less so. Thus, the author proposed the use Log Pearson type 3 and Log Gumbel. Figure 3-6 shows proposed fitted discharges.

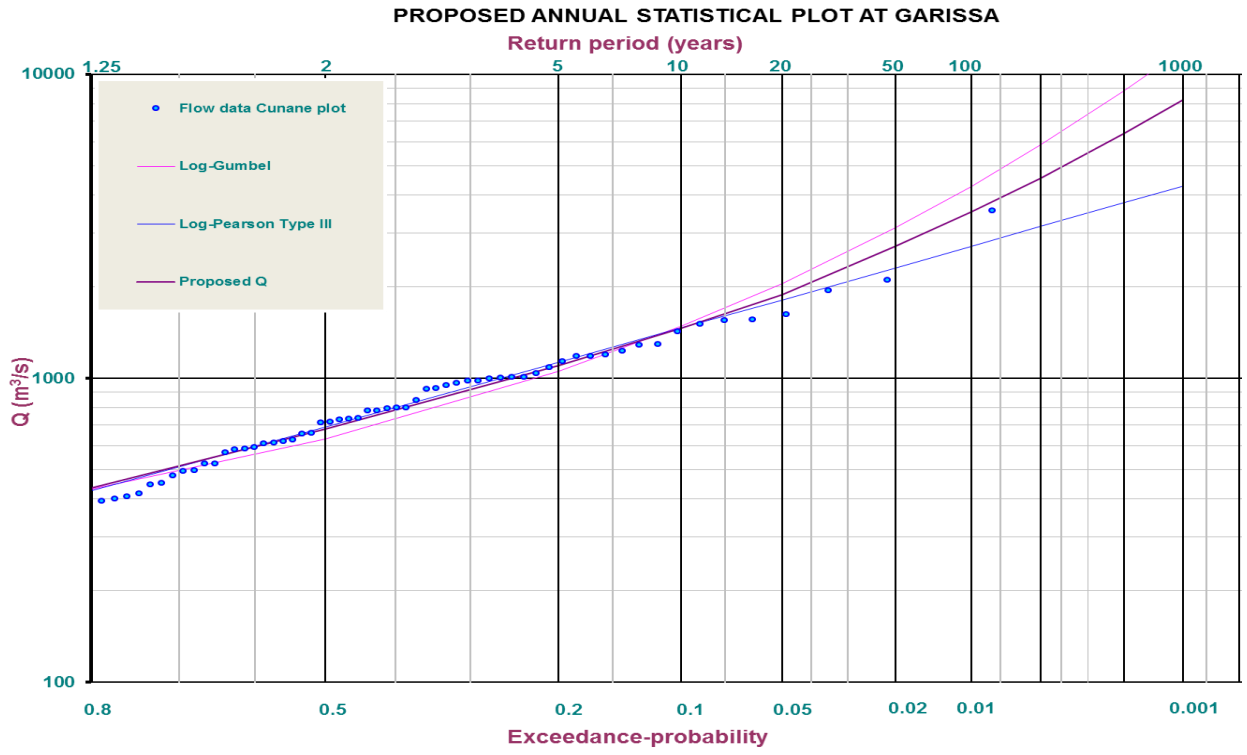

Figure 3-6: Proposed fitted annual maximum series graphical representation.

To account for inaccuracy in flow-gauging measurements, probabilistic fitting, ungauged runoffs and climate change, the proposed peaks were scaled up by a conservative value of 20%[21]. Table 3.3-3 shows the resulting values. It can be seen that, the largest flood recorded in Garissa (3561m^3/s) was approximately 1:100 year flood.

Table 3.3-3: Fitted and scaled probabilistic peak floods at Garissa

Return Period (Years)	1.25	2	5	10	20	50	100	200	500	1000
Proposed Q (m3/s)	436	680	1099	1457	1879	2717	3523	4558	6395	8253
Scaled up Q (m3/s)	523	816	1319	1748	2254	3260	4227	5470	7674	9904

These values multiplied with dimensionless hydrographs developed under section 3.4 below were routed from Garissa to Garsen in 1D model to generate upstream boundary hydrographs for the 2D model.

[21] The value was obtained from studying different case studies see section 2.3.3.2.

3.4 Flood hydrograph shape

To avoid deceptive flooding, a proper hydrograph was established. Six major floods (average return period of 1:10) were analyzed and the resulting hydrograph is shown in Figure 3-7 with the average hydrograph dotted. The second season (October to November), established as critical flooding period under section 3.2.4 ; a dimensionless hydrograph was developed for this period from the average hydrograph. Figure 3-8 shows the dimensionless hydrograph with its ordinates tabulated Appendix 6.

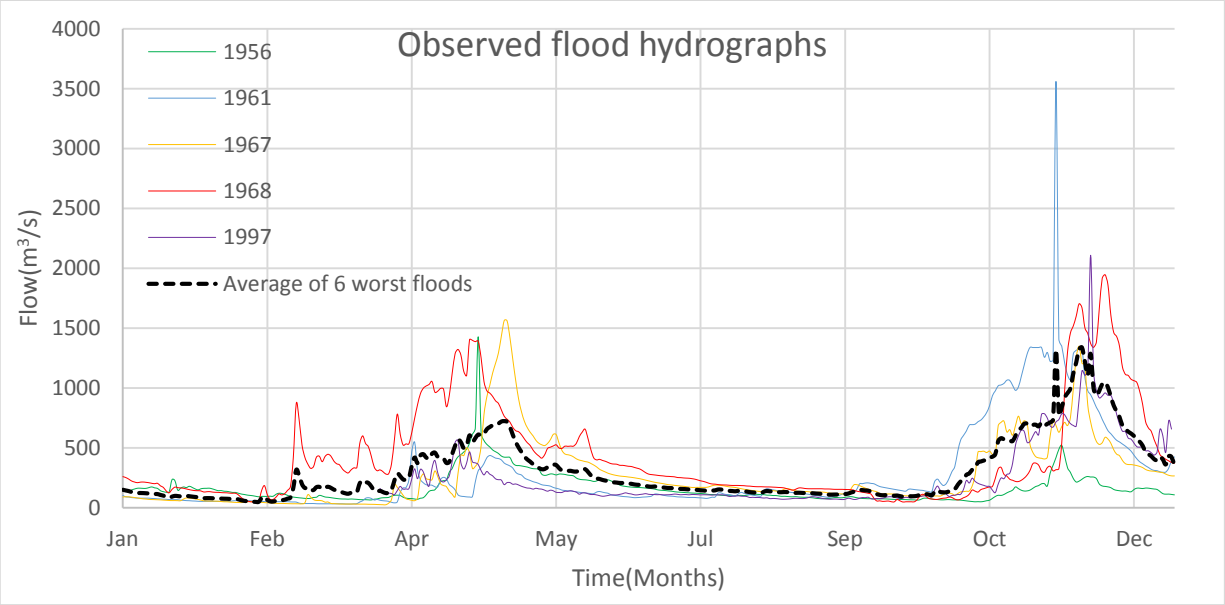

Figure 3-7: Observed major floods (ARI 1:10) hydrographs with average flood (dotted) at Garissa

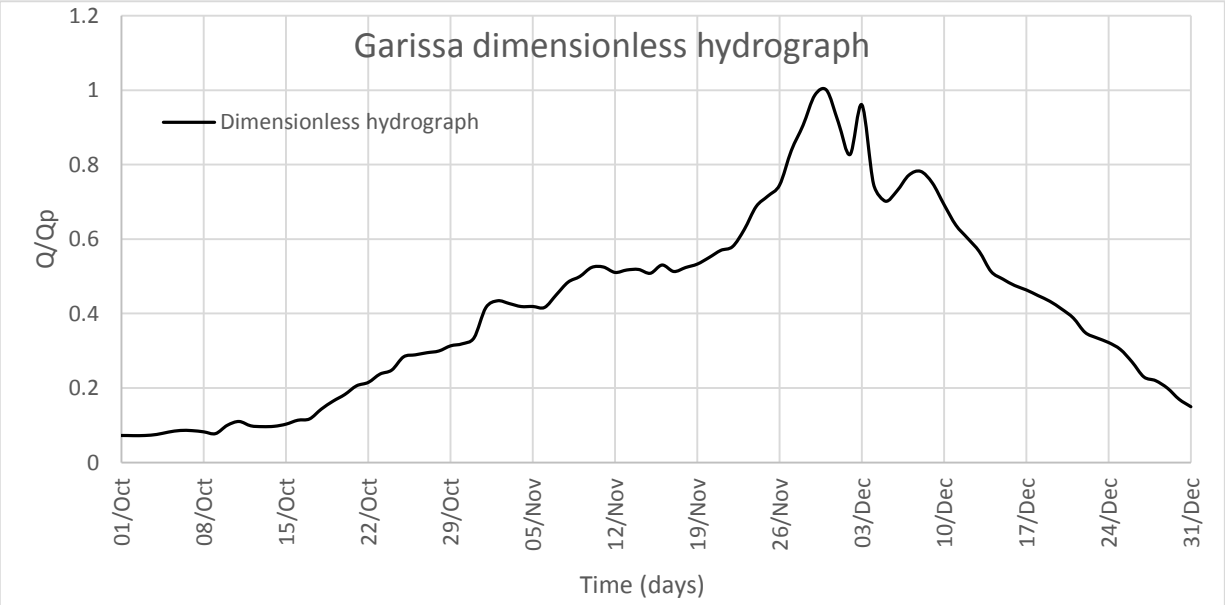

Figure 3-8: Garissa October to December dimensionless hydrograph

3.5 Extreme tidal levels

3.5.1 Sea tidal levels

The closest tidal level recordings were at Mombasa, located 180 km south east of river mouth (Google Earth).(see Figure 1-1). Twenty-seven years' record (1987-2013) were obtained through Live Access Server (LAS) of the Asia Pacific Data Research Centre (APDRC, 2014) of University of Hawaii data bank. Data from this database is ready to use and of research quality[22]. An hourly graphic representation of the data is presented in Figure 3-9.

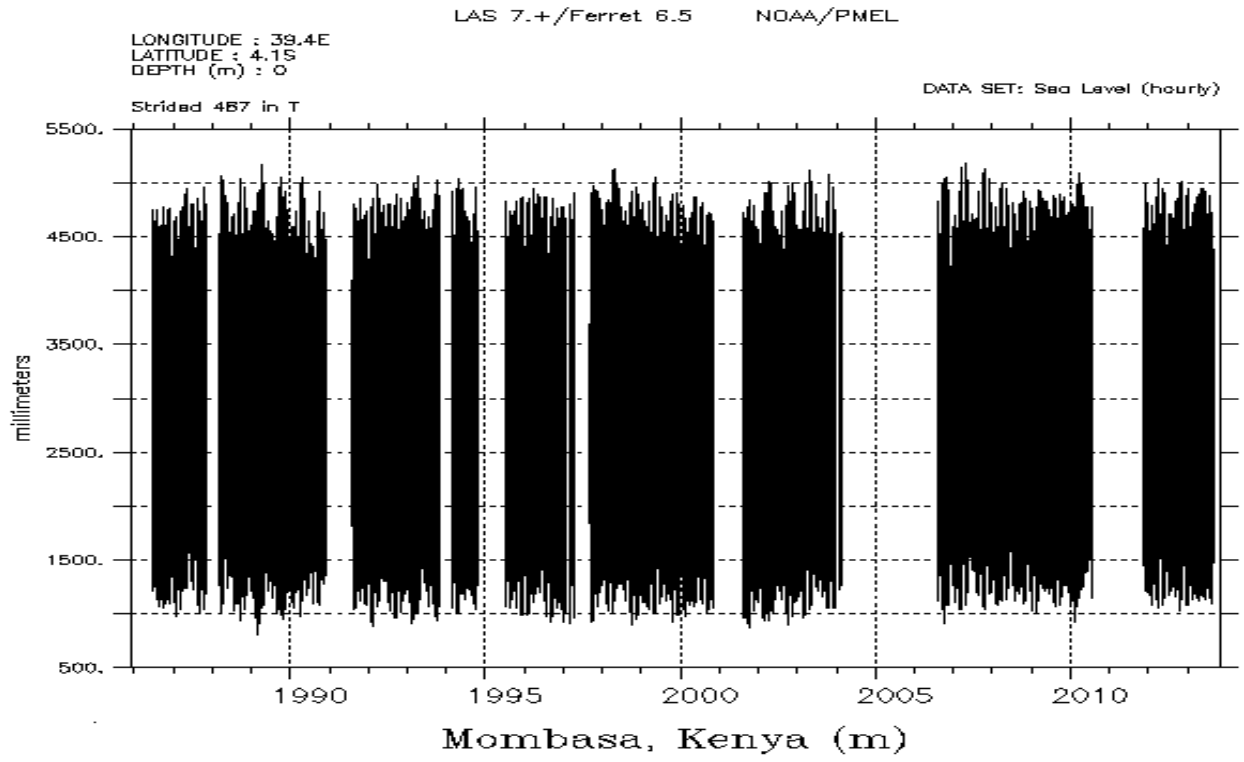

Figure 3-9: Hourly tidal levels recordings at Mombasa as obtained from (APDRC, 2014) referenced to the Chart datum. (-2.867m below geodetic mean sea level)

The data was 33% incomplete and there were no records for, 2004 and 2005. Years with gaps were excluded from further analysis reducing the record to 25 years. Table 3.5-1 shows extracts of annual maximum-recorded water levels at Mombasa.

[22] APDRC collects data from different stations around the globe, calibrates, references to RLR (Revised Local Reference), analyzes and releases it in hourly intervals in blocks of years within 1 to 5 years of collection. The recorded data is inclusive of tidal effects and short term sea level rise due to other factors i.e. barometric pressure, wind setup, storm surges etc.

Table 3.5-1: Maximum annual tidal level recordings at Mombasa.

Year	Max recorded level		Year	Max recorded level		Year	Max recorded level	
	m to CD	m to MSL (-2.867)		m to CD	m to MSL (-2.867)		m to CD	m to MSL (-2.867)
1987	4.890	2.023	1996	4.943	2.076	2005	#N/A	#N/A
1988	5.060	2.193	1997	4.909	2.042	2006	5.143	2.276
1989	5.170	2.303	1998	5.122	2.255	2007	5.176	2.309
1990	5.050	2.183	1999	5.129	2.262	2008	4.950	2.083
1991	5.050	2.183	2000	5.050	2.183	2009	5.091	2.224
1992	4.987	2.120	2001	5.013	2.146	2010	4.883	2.016
1993	5.067	2.200	2002	4.997	2.130	2011	5.032	2.165
1994	5.027	2.160	2003	5.111	2.244	2012	5.008	2.141
1995	5.037	2.170	2004	#N/A	#N/A	2013	4.951	2.084

3.5.2 Probabilistic tidal level analysis

The maximum tidal recordings referenced to chart datum were subjected to probabilistic analysis based on Gumbel type 1 probability distribution function (see Appendix 5). The best fit was extrapolated to extend to 100 year ARI and the resulting Gumbel graph is presented in Figure 3-10.

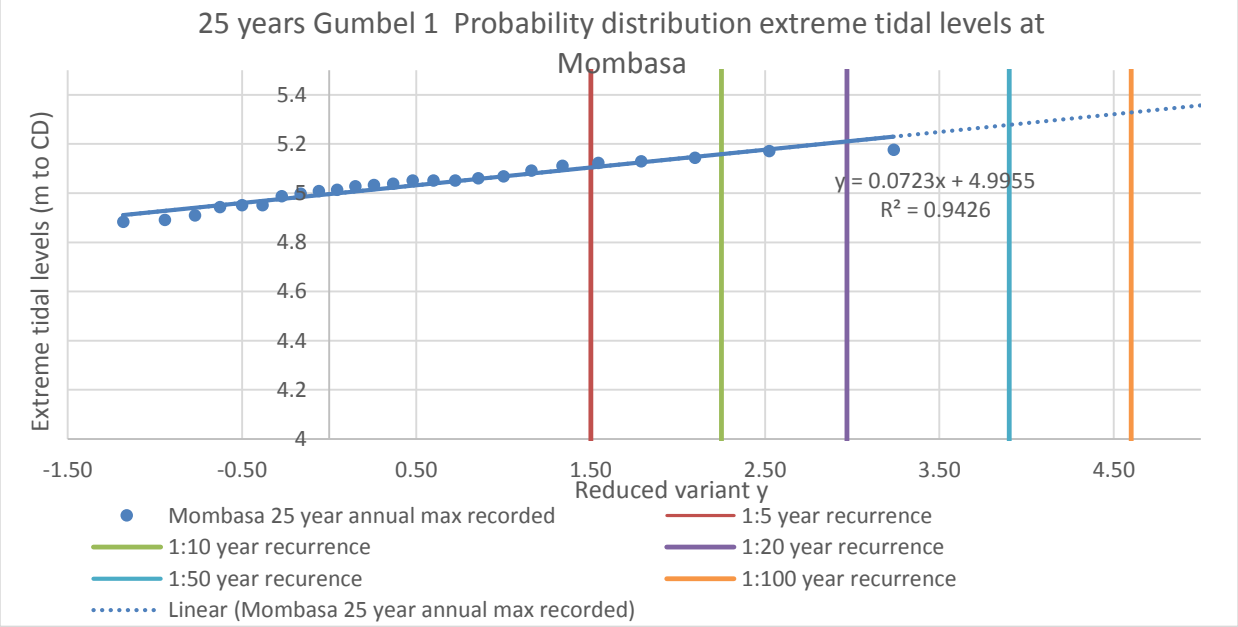

Figure 3-10: Extreme tidal levels at Mombasa inclusive of astronomical influences and short term influences, excluding rises due to climate change, natural and human induced land subsidence.

3.5.2.1 Extreme sea water Level rise at Lamu due to climate change

This section is based on International Panel on Climate Change report (see section 2.2.2) and estimated probabilistic extreme sea water levels analysis (see section 3.5.1). Estimated 2, 50, 100 year ARI extreme tidal level values were extracted from Figure 3-10 and added up to the global sea level rise due to climate change represented in Table 3.5-1. From Figure 2-6, the spatial regional percentage deviation from the global mean for the East African coast (EA) was estimated to be +10% above the global mean, thus an increase to the estimates. Table 3.5-2 shows the values and estimated extreme water levels referenced to chart datum and mean sea level (bolded). These estimates were used as the sea boundary water levels in setting up the 2D hydrodynamic model (section 4.2).

Table 3.5-2:Extreme sea water level inclusive of Sea level rise due to climate change at Mombasa for different ARI return periods and different climate change scenarios

ARI	Extreme tidal levels, based on Gumbel probability		IPCC scenarios RCP:	Predicted extreme sea water levels for East African coast taking into account changes due to climatic conditions								
	m to CD	m to MSL -2.867		2040			2060			2100		
				Sea level rise (m)		**Sea level**	Sea level rise (m)		**Sea level**	Sea level rise (m)		**Sea level**
				Global mean	EA coast	**m to MSL**	Global mean	EA coast	**m to MSL**	Global mean	EA coast	**m to MSL**
1:2 **year**	5.02	2.16	2.6	0.15	0.17	**2.32**	0.24	0.26	**2.42**	0.44	0.48	**2.64**
			4.5	0.18	0.20	**2.35**	0.26	0.29	**2.44**	0.53	0.58	**2.74**
			6	0.16	0.18	**2.33**	0.25	0.28	**2.43**	0.55	0.61	**2.76**
			8.5	0.19	0.21	**2.36**	0.30	0.33	**2.49**	0.74	0.81	**2.97**
1:50 **year**	5.28	2.41	2.6	0.15	0.17	**2.58**	0.24	0.26	**2.67**	0.44	0.48	**2.89**
			4.5	0.18	0.20	**2.61**	0.26	0.29	**2.70**	0.53	0.58	**2.99**
			6	0.16	0.18	**2.59**	0.25	0.28	**2.69**	0.55	0.61	**3.02**
			8.5	0.19	0.21	**2.62**	0.30	0.33	**2.74**	0.74	0.81	**3.22**
1:100 **year**	5.33	2.46	2.6	0.15	0.17	**2.63**	0.24	0.26	**2.73**	0.44	0.48	**2.95**
			4.5	0.18	0.20	**2.66**	0.26	0.29	**2.75**	0.53	0.58	**3.04**
			6	0.16	0.18	**2.64**	0.25	0.28	**2.74**	0.55	0.61	**3.07**
			8.5	0.19	0.21	**2.67**	0.30	0.33	**2.79**	0.74	0.81	**3.28**

4 HYDRODYNAMIC MODELLING

Simulating the Lower Tana River hydrodynamics with the 2D MIKE 21c model, at current ARI floods and future ARI floods were the main objective of this study. Table 3.5-1 gives a summary of the five-flood scenarios carried out with the upstream and downstream boundary condition combinations. The downstream boundaries were the extreme water levels predicted under section**Error! Reference source not found.**and upstream flows were obtained from routed floods in 1D MIKE 11 model done under section 4.2.1.2.

Table 3.5-1: Summary of five simulations scenarios investigated showing the upstream and downstream boundary conditions combinations.

Current scenario			Future scenarios inclusive of climate change		
NO	**Inflow**	**Sea level boundary**	**NO**	**Inflow**	**Sea level boundary**
I.	Q_2	Recorded water level			
II.	Q_{50}	Constant sea level (WL_{50})	IV.	Q_{50}	Constant sea level (WL_{50})
III.	Q_{100}	Constant sea level (WL_{100})	V.	Q_{100}	Constant sea level (WL_{100})

Mike 21C specifically developed for a river morphological study was used to investigate the flood scenarios. In section 2.3.2, more details of Mike 21C model setup, governing equations, criteria of software selection and limitations were discussed.

To fully describe the problem, the following tasks were completed in order of importance (.DHI, 2003):

I. Bathymetry setup:
   The model space to describe area under investigation with grid resolution affecting the model accuracy are discussed in section 4.1.

II. Boundary conditions creation:
   The model upstream and downstream inputs are discussed in section 4.2.

III. Model calibration :
   To account for assumptions and model limitations, calibration is done in section 4.3.
   In section 4.4, other minor model inputs are discussed and the final setup is presented.

4.1 Bathymetry setup

A suitable grid mesh for the model area was set up using the MIKE 21C grid generator and later elevations were imported into the orthogonalised curvilinear grid. The digital elevations heights were obtained from a survey carried out for a proposed development in the region (ASP, 2007).

The setting up of the model grid and methodology used to obtain the digital elevations is discussed further in subsequent sections.

4.1.1 Digital Elevation Model (DEM)

Elevation data acquisition was mainly from:

i. Ground survey(2007)
ii. 2000 NASA SRTM data
iii. Sonar river survey
iv. Major bridge and road surveys
v. Satellite images

These are further discussed through sections 4.1.1.1 to 4.1.1.4.

4.1.1.1 Survey

In 2007, ASP technologies undertook a survey of the delta using Trimble 5800 RTK GPS unit referenced relative to EGM96 geoidal model. As a check, it was referenced to survey of Kenya local datum[23] using concrete trigonometrical beacons. Within the surveyed area, the survey results correlated well with the benchmarks already established giving high confidence with the referencing (ASP, 2007).

In Feb 2002, on an 11 day mission NASA Shuttle Radar Topography Mission (SRTM), provided a 90m (three arc second) elevation of the study area. SRTM data is prone to inaccuracies in vegetated terrain as the shuttle C band RADAR[24] cannot penetrate canopies to the underlying terrain (NASA, 2000).This inaccuracy was confirmed as areas of little or no vegetation; the data from the two sources correlated well but had high inconsistency in densely vegetated areas.

---

[23] The survey of Kenya datum was established in 1892, much triangulation and re-triangulation has been done correlating the benchmarks to other references with high confidence. Currently it is referenced to 1960 Arc Datum, with zero set at point 2.79m above mean sea level. Clarke 1880 is the main ellipsoid reference for the UTM coordinates used.

[24] Makes use of radio waves that have fixed amplitude and frequency, thus depending on time the wave takes to be reflected back, speed , range, direction of objects , shape etc. can be determined.

Due to limitation of time and problems with accessibility, ground survey was only conducted in a small region of the study area, but there was an attempt to spread this survey out. Using satellite images, areas of low vegetation and not ground surveyed were identified and SRTM data was used to make the interpolation.

The ASP (2007) report does not mention how the elevations of densely vegetated terrain physically not surveyed were derived or the accuracies expected. However, the report has stated RADAR data was only intended to be used in area of little or no vegetation.

From these two data sources (SRTM and survey), contours at 1.0 m interval were generated for the study area.

4.1.1.2 River survey and Landsat Satellite images

Measured relative to MSL, riverbed survey was conducted using a sonar instrument attached to the Trimble 5899 RTK GPS kit. Meanders, inaccessibility and many distributaries of the lower Tana River delta inhibited the survey of the entire river channel. Consequently, un-surveyed channels were interpolated from neighboring channel beds. Due to limitation of survey equipment used, the lower bed depths of sections close to the river mouth where the Tana drained into the Indian Ocean, were approximated as -1.0 m. In order to derive a "terrain" model of the riverbed, processed bed levels were subjected to further interpolation using the neighbor interpolation method[25].

Delta Landsat[26] satellite images were acquired dated 2001, 2005 and 2006. Only 2001 images encompassed the whole project area. Riverbanks were reasonably delineated manually with preference being given to the latest date.

Figure 4-1 gives an overview of the resulting delineated interpolated and surveyed river.

[25] Neighboring interpolation has the disadvantage of creating sudden drop-offs in the model, not unrealistic but possibly sharper than reality, but has the advantage that it does not use data from other channels or from other meanders of the same channel

[26] Makes use of remote sensing providing moderate resolution satellite images of the world. The images can be downloaded free from USGS website (USGS, 2014) .

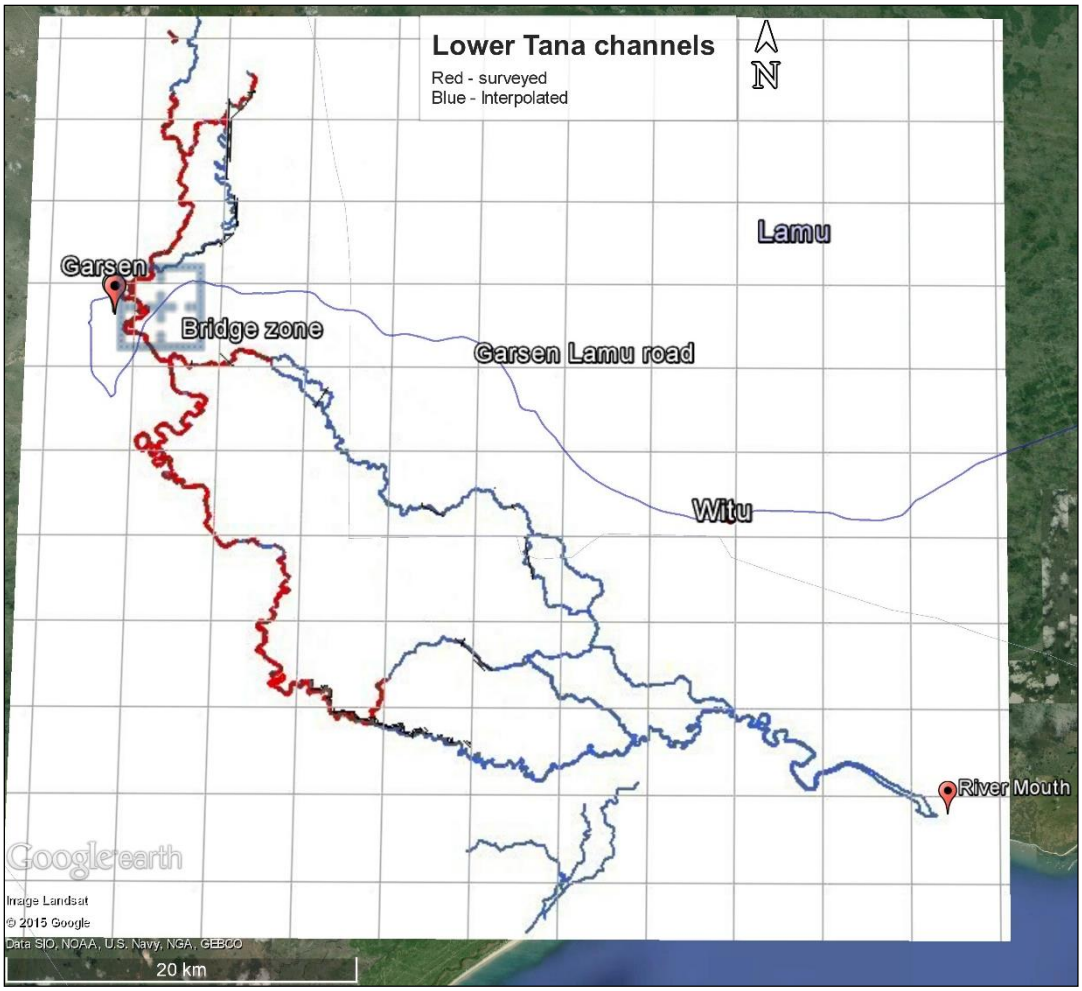

Figure 4-1: Lower Tana surveyed and interpolated channels. Source: (ASP, 2007)

4.1.1.3 Road and bridge surveys

Roads and major bridges that were likely to cause major damming of floodwaters, were surveyed. In particular, the Garsen –Lamu Road (see Figure 4-1) with its six bridges receiving major attention.

4.1.1.4 Digitized elevations

On a 10m grid, a digital terrain model was generated by interpolating the 1.0 m interval contour survey. Individual survey levels of river channels, roads and bridges were used to replace interpolated elevations in DTM. Further processing resulted in a 10m x 10m gridded surface of the entire area encompassing road elevations and riverbeds. The six bridge decks were not included in the model, however; the abutments and openings were.

Further processing was carried out to reduce the amount of data. Four main sections were established:

i. Regions within 500m of the riverbanks were re-gridded to 10mx10m.

ii. Bridges were maintained and 10mx10m gird with road elevation at other sections maintained at 50x50m grid

iii. Flood prone regions were re-gridded to 50mx50m

iv. No potential to flood regions were re-gridded to 250mx250m

The resulting processed DEM, supplied in UTM WGS84 is shown in Figure 4-2. For the purpose of this study, the DEM was converted to GIS to conserve model accuracy when re-interpolating. As a rule of thumb, if the objective is to improve the accuracy, any subsequent grid cannot be smaller than 10x10m grid.

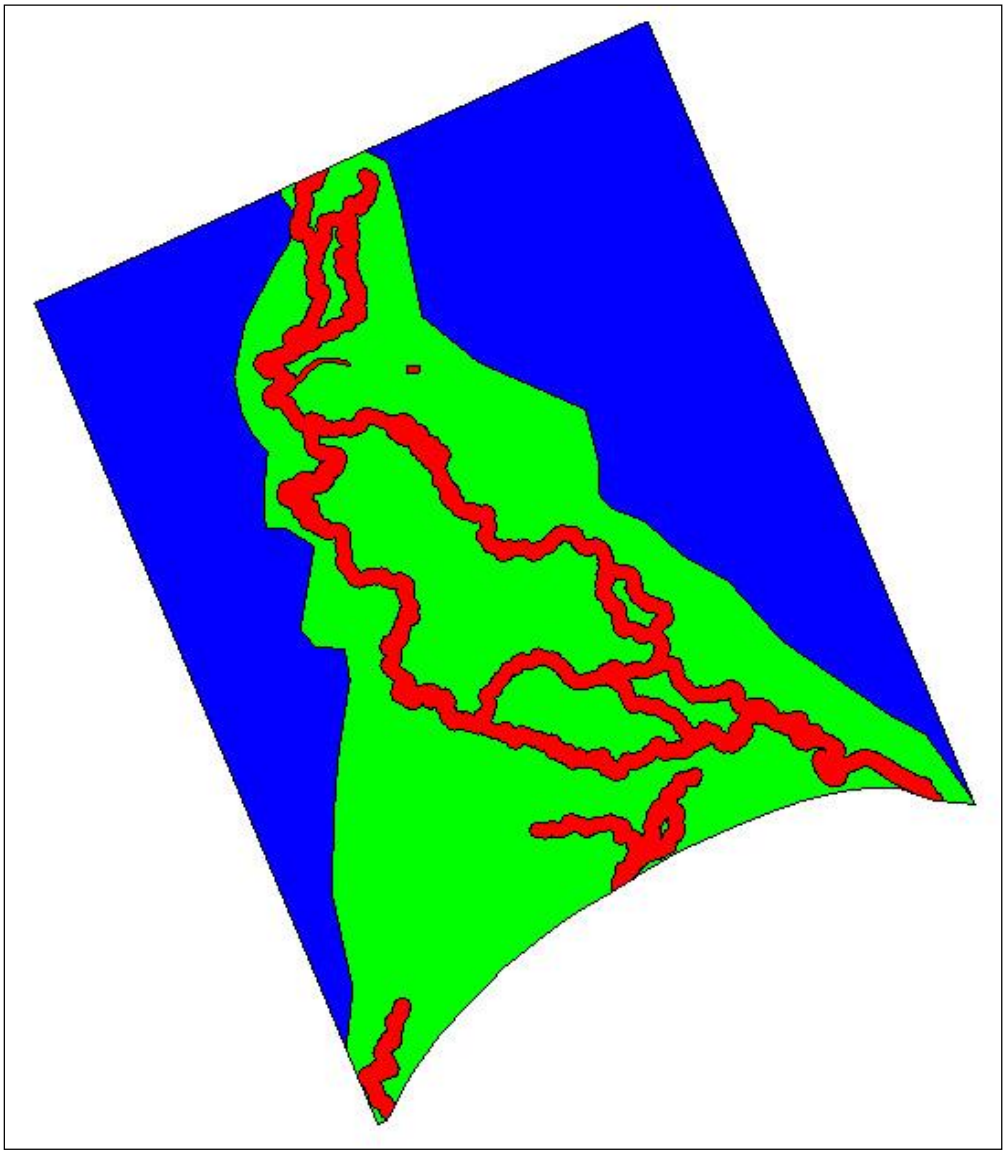

Figure 4-2: Processed DEM showing different grid sizes used. (Red=10mx10m, Green 50mx50m, Blue = 250mx250m). Source: (ASP, 2007)

4.1.2 2D model Grid setup

Before setting up the grid, the following considerations were taken into account:

- A grid/ bathymetry that describe water depths in the model area with the desired accuracy.
- Grid that give acceptable computation time.

A balance between these two has to be struck. Small resolution grids aligned to river flow give accurate results but at the expense of computational time[27]. On the other hand, a course grid with small time steps contradicts the purpose, however areas of high interest can be made to have higher resolution than the rest but care has to be taken not to introduce instabilities.

To check the quality of grid created, MIKE 21C user manual gives a few criterions that are summarized in Table 4.1-1. However, there are general guidelines and sound judgment is required.

Table 4.1-1: MIKE 21C grid quality guidelines check. Source: (DHI., 2014)

Criterion	Recommended values
Grid orthogonality	-0.05 to 0.05
Spatial spacing gradients in both x and y directions	No specific values, experience and good judgment are required, large spacing with highly variable boundary conditions cause instabilities
Grid aspect ratio	1 to 3 (flood plain dominated flow) and 3 to 8 (curvilinear grid aligned flow)
True land value	Above elevations that flow computations cannot occur and do not affect model stability

Before settling for the grid shape discussed further, several configurations and shapes of models were tried out. A rectangular grid with uniformly distributed grids aligned relative to general flow direction did not have instability issues and was therefore found to be most appropriate.

Several grid resolutions were tried out to check the effects they had on simulation time and accuracy. This was done after making checks for orthogonality, aspect ratio and updating the

[27] Computational time increases exponentially with increase of resolution of grids.

grid points with elevations in ArcGIS[28] and interpolating. The GIS method was preferred as it conserved the original data accuracy with much better interpolation engine as compared to MIKE generator. The model was tested using a constant upstream boundary inflow of 400m/s and tidal levels extracted from University of Hawaii Live Access Server (LAS) data bank for a similar seasonal period.

Table 4.1-2 summarizes different parameters of the model, grid resolutions and corresponding estimated simulations times.

Table 4.1-2: Summary of the different examined grid resolutions.

Grid Resolution	**1**	**2**	**3**	**4**
Flow used (1:1.5 ARI) (m/s)	400	400	400	400
Width of model area(m)	47889	47889	47889	47889
Length of model area(m)	63783	63783	63783	63783
Approximate grid length (m)	21	30	58	65
Approximate grid width (m)	10	30	37	37
No of cells in s-direction(j)	3000	2100	1100	981
No of cells in n-direction(k)	4820	1600	1300	1294
Aspect ratio	2	1	2	2
Orthogonality	(-0.01 to 0.002)	(-0.01 to 0.002)	(-0.01 to 0.001)	(-0.01 to 0.001)
Area		906-920	2127-2161	2426-2464
Time step (s)	1	5	8	10
CPU time for 96hr simulation (s)	N/A	96000	14400	10800
Anticipated run-time for 3 months simulation (days)	N/A	22.22	3.33	2.50

The velocity and flow depths, for each grid size tested were extracted at different locations selected randomly in the model as illustrated in Figure 4-3.

Figure 4-4 and Figure 4-5.show the resulting comparison of velocity and water depths at different cross sections.

[28] An application developed by ESRI developers for "data management, mapping and visualization and geo-processing of geographic information"

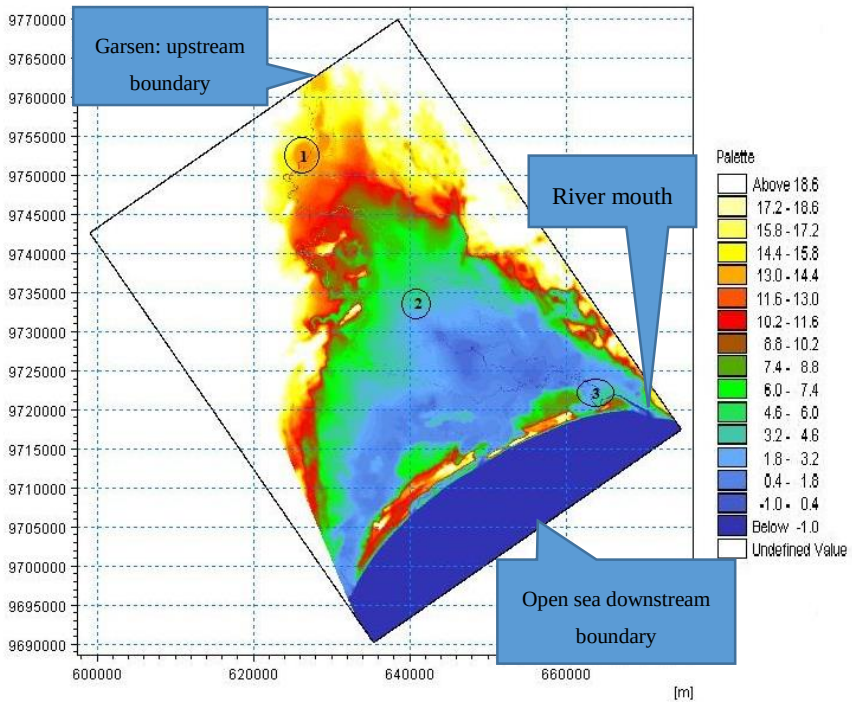

Figure 4-3: Model bathymetry illustrating different data extraction points.

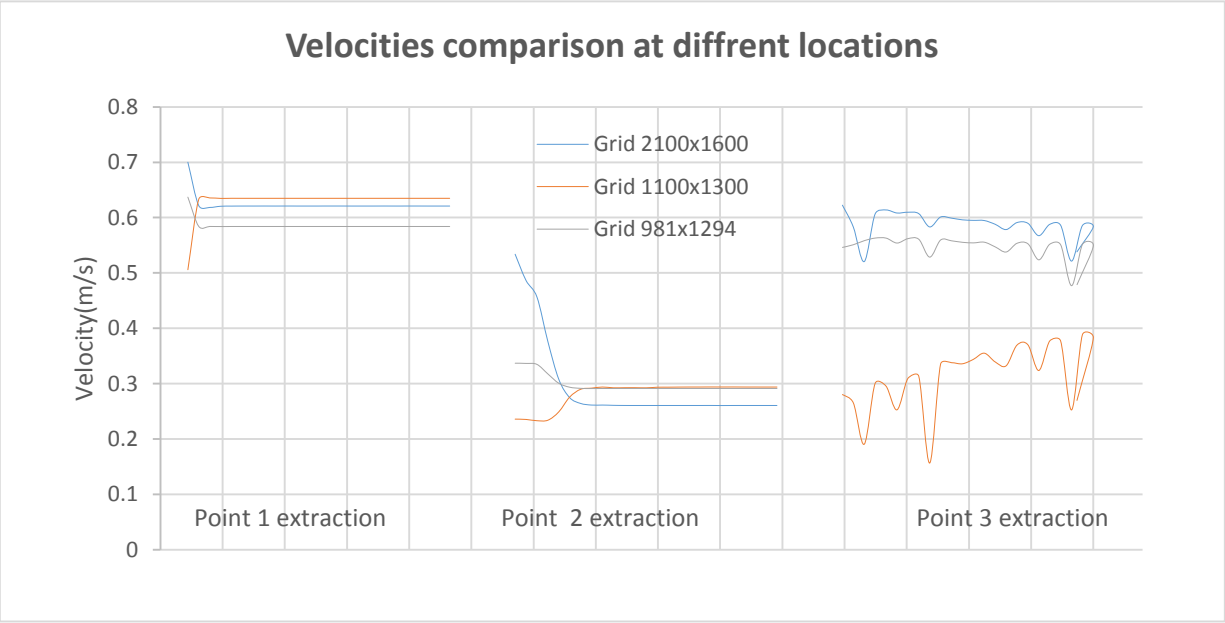

Figure 4-4: Grid resolutions influence on velocity at different locations examined at Lower Tana delta.

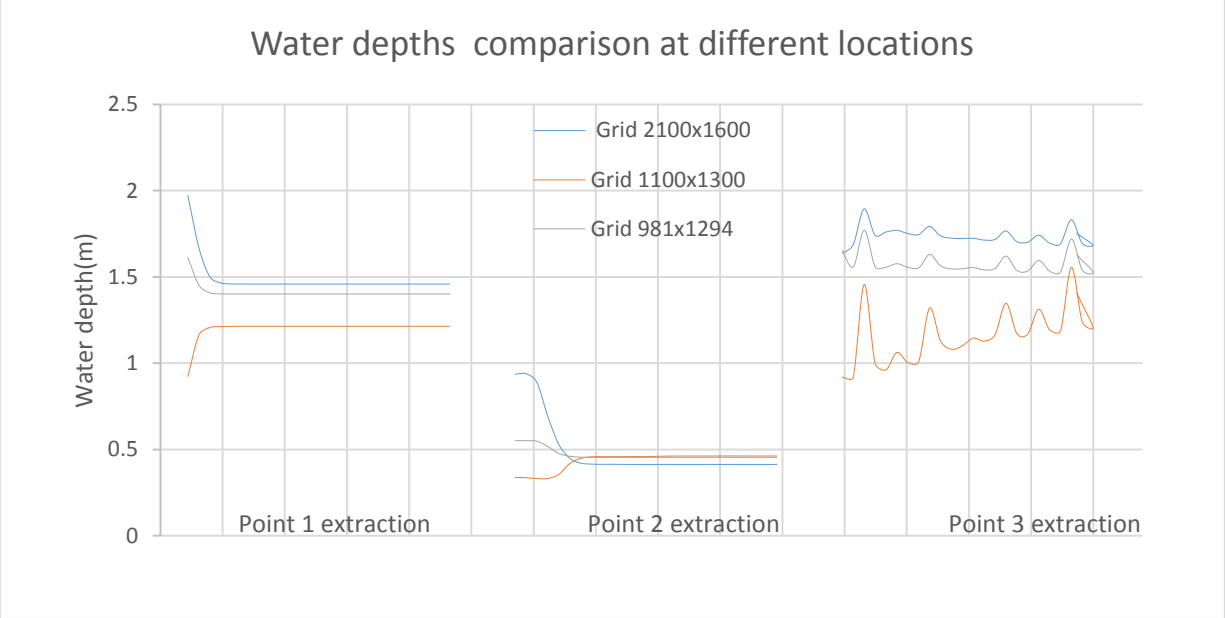

Figure 4-5: Grid resolutions influence on water depths at different location tested at lower Tana delta.

The results from the cross-sections tested correlated with each other as anticipated, an increase in model size grid resulted in loss of accuracy. It was observed there was simulation duration reduction as gird resolution became course from 23 to 4 and 3 normal earth days for 2100X1600, 1100x1300 and 981x1294 grid sizes respectively.

It was noted at position 3, the velocity and water depth was fluctuating due to sea water level variation and upstream water inflow interaction.

The water depths measured in meters, were extracted from the model to the third decimal point (mm), thus it was concluded that loss in accuracy was in terms of 10 cm in upper limit from the fine to course grid. However, the reduction in computational time was massive. Consequently, the final grid selected comprised of 981 cells in j[29] direction and 1294 cells in k[30] direction at sizes of 65m lengthwise and 37m in width.

Figure 4-3 represents the final grid resolution used in this thesis.

[29] Direction lengthwise, positive to water flow direction.

[30] Direction perpendicular to positive water flow direction.

4.2 Upstream and downstream boundaries for 2D model.

The 2D model was bounded by two boundaries; the upstream inflow boundary described by a hydrograph at Garsen routed on 1D model from Garissa and the sea water level boundary at the river mouth at the downstream described by either a tidal time series or an extreme predicted constant sea water level for the cases simulated. Figure 4-3 is a representation of the boundary locations. The analysis of upstream and downstream boundary values have been discussed in section 3; Tana River flood hydrology. This section summarizes the flood hydrology and gives the main MIKE 21C model input values.

4.2.1 Upstream Inflow boundary for 2D model

The 2D model upstream boundary was located at Garsen ≈ 240km downstream of Garissa (Google earth), thus necessitating routing of floods from Garissa with its more reliable flow data to Garsen at the upstream boundary of the 2D model. DHI's MIKE 11, one-dimensional model was used to carry out the flood routing; it was chosen for its speed, user friendliness, accuracy in calibrated model and flexibility. Under section 2.3.2, governing equations, model setup guidelines and assumptions are presented.

4.2.1.1 1D model (MIKE 11) model setup and calibration

The model was set up in accordance to MIKE 11-user guide (DHI, 2013), namely river network, cross sectional network, boundary data and hydrodynamics parameters (see section 2.3.2 for description). Cross sectional data were obtained from 1:50000 maps and Google Earth in the upper reaches and the 10 x 10m grid of local surveyed data as discussed in section 4.1.

The recorded flow data at Garissa of the year 1991 was used as the upstream boundary, its selections was based on it being a dry year and the fact that both the records at Garsen and Garissa station were available. Figure 4-6 shows all the available data set record at Garissa and Garsen.

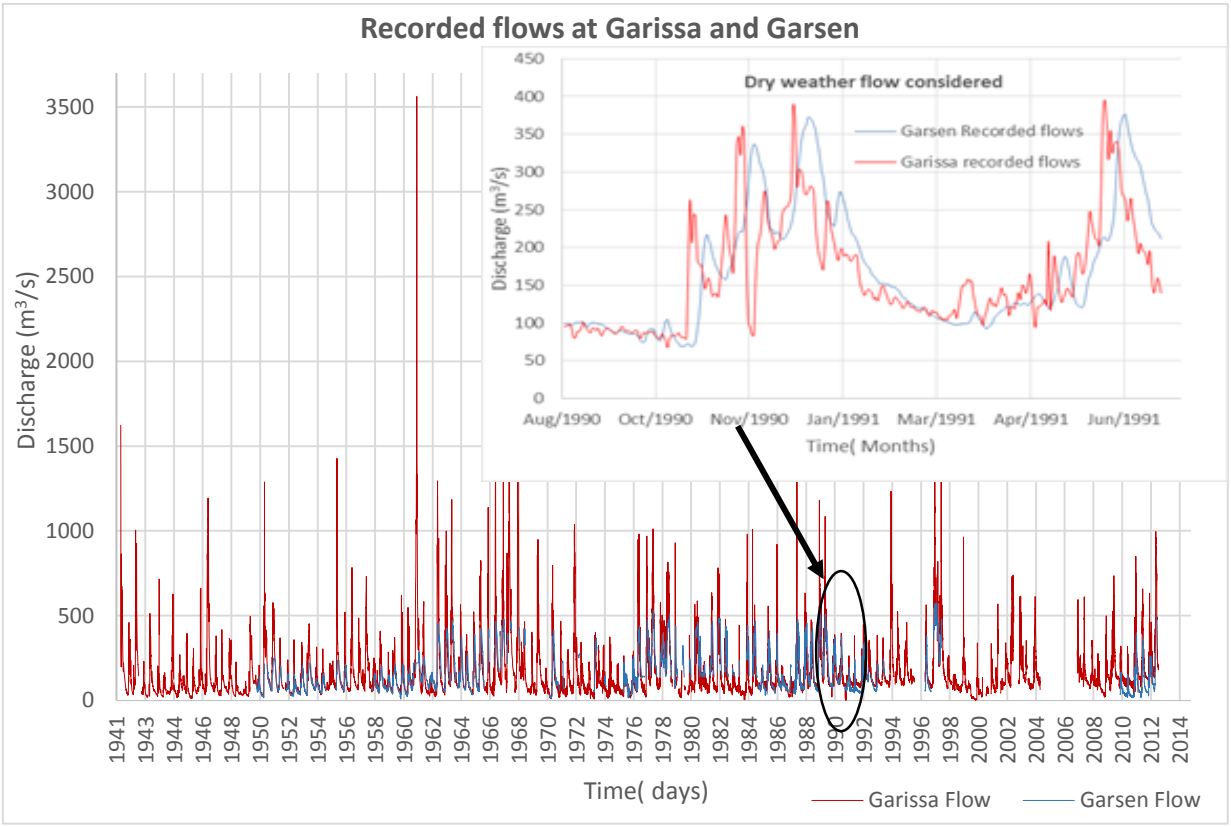

Figure 4-6: Daily recorded flows at Garissa and Garsen stations. Source: (WRMA, 2014)

The downstream boundary tidal water levels were obtained from the (APDRC, 2014) data bank in a text format. A sample graphical extract of the data referenced to chart datum (-2.867m below MSL) is shown in Figure 4-7.

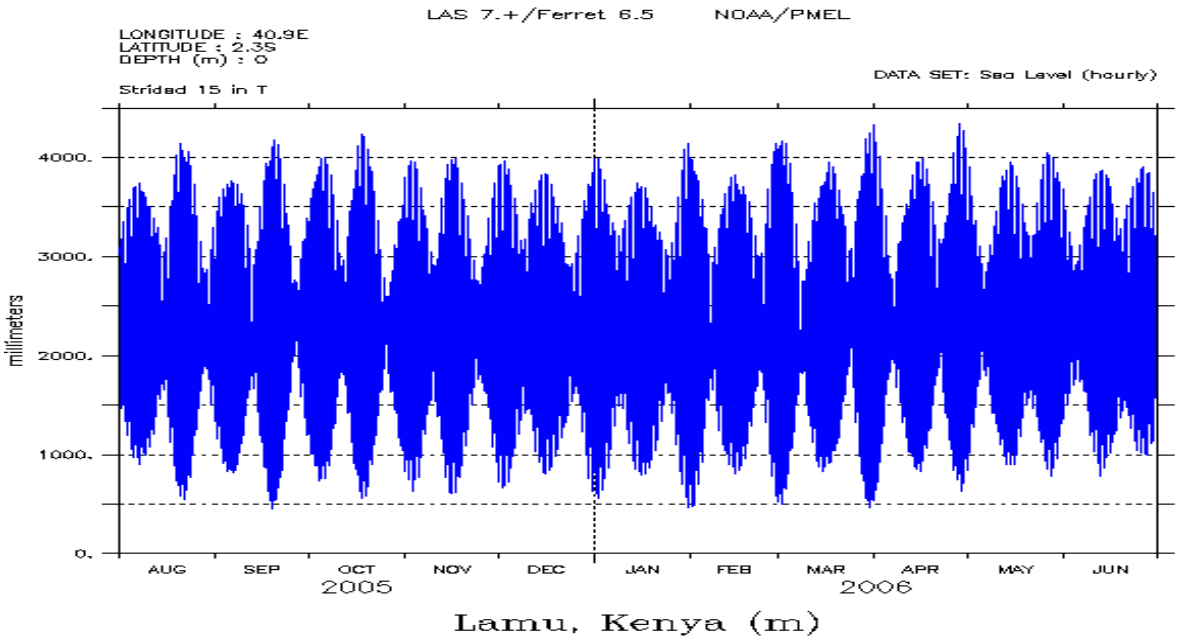

Figure 4-7: Hourly recorded tidal levels at Lamu referenced to the chart datum. (-2.867m below geodetic mean sea level) as obtained from (APDRC, 2014)

The MIKE 11 model was setup. Using the recorded flow at Garsen, altering the hydrodynamic parameters, the model was calibrated and a Manning hydraulic roughness of 0.04 for the main channel and 0.06 in the floodplains was found to be appropriate. Figure 4-8 shows the comparison between the simulated and recorded hydrographs at Garsen and the inflow hydrograph at Garissa. An R-squared value of 0.87 was found for the simulated and recorded hydrographs giving high confidence in the Manning value determined.It was observed that, it took approximately 8 to 10 days for the flow to propagate through the section.

As discussed under section 2.1.2, the meandering nature of the river, dense vegetation, and large trees justify the extremely high roughness values.

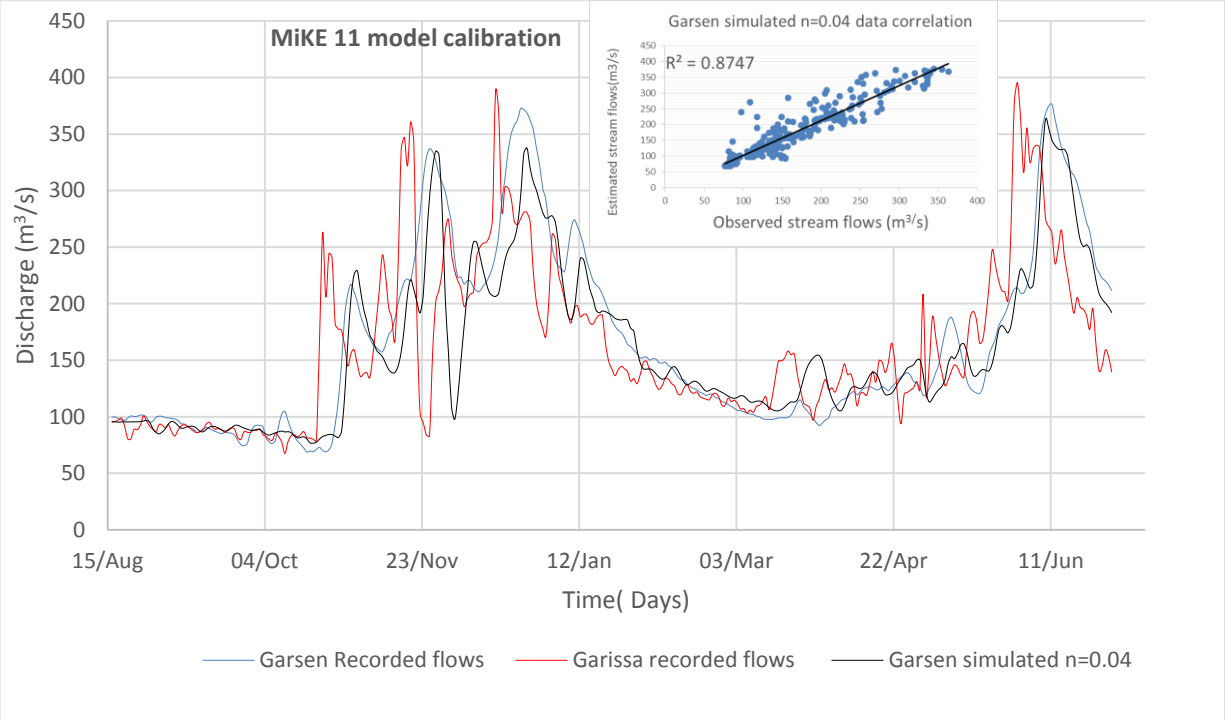

Figure 4-8: Lower Tana MIKE 11 calibration graph showing recorded hydrographs at Garissa and Garsen and simulated hydrograph at Garsen.

4.2.1.2 1D Flood routing from Garissa to Garsen

The calibrated 1D MIKE 11 model from Garissa to the river mouth was used to route floods from Garissa to Garsen. Under section 3.3, ARI flood peaks derived from the 73 years record at Garissa were used to derive MIKE 21C input hydrographs from dimensionless hydrographs derived under section 3.4 and ordinates presented in Appendix 6.

Table 4.2-1 represents the ARI flood peaks considered with Figure 4-9 representing the final analyzed and routed hydrographs for the various ARI flood peaks with ordinates represented in Appendix 6.

Table 4.2-1: Garissa probabilistic flood ARI flood peaks considered

Annual Recurrence Interval	1:2	1:50	1:100
Q (m^3/s)	680	2717	3523
Q (m^3/s)(Inclusive of climate change)	816	3260	4227

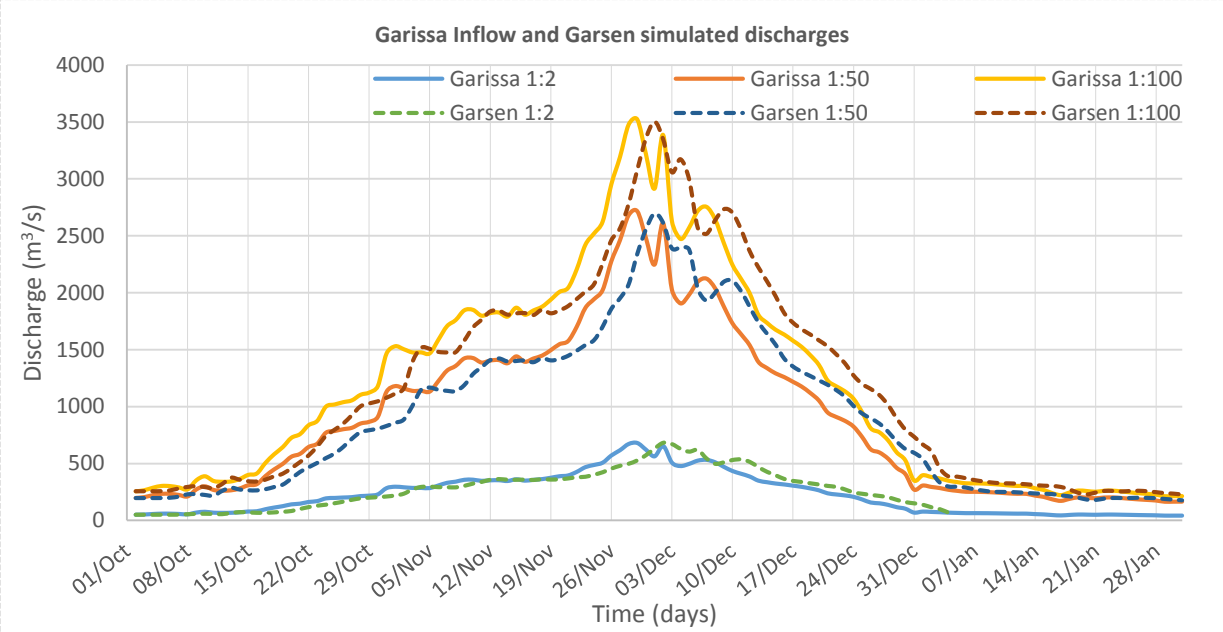

Figure 4-9_a: Garissa probabilisticly determined ARI derived inflow flood peaks hydrographs and calibrated routed Garsen ARI discharge hydrographs.

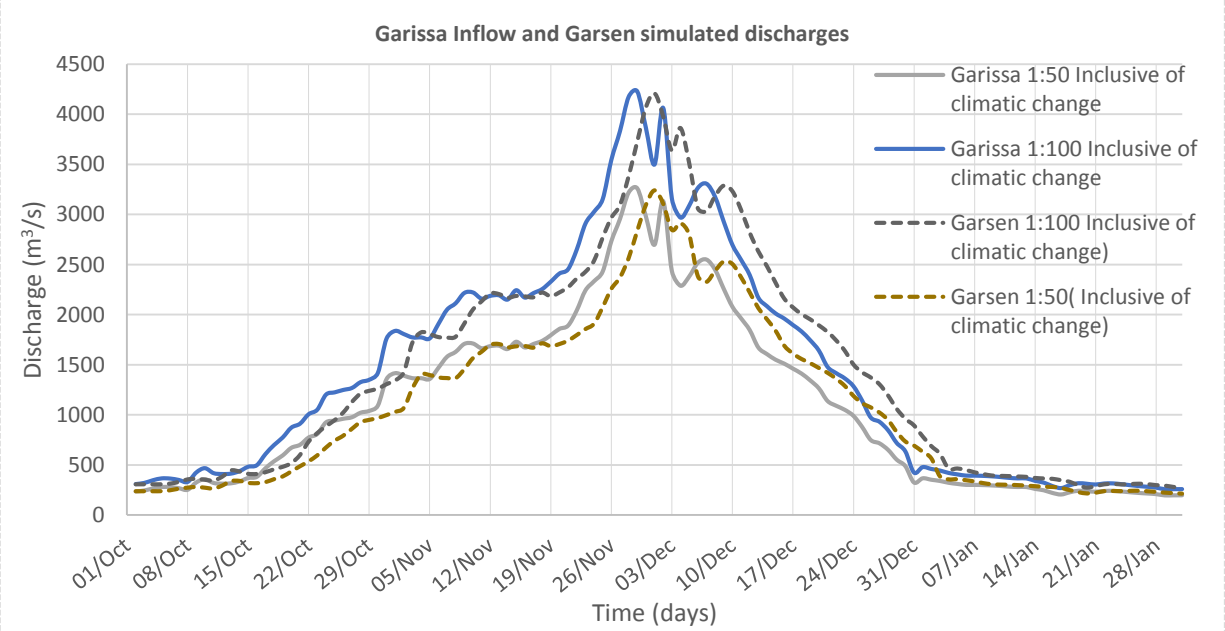

Figure 4-9_b: Garissa probabilisticly determined ARI derived inflow flood peaks hydrographs and calibrated routed Garsen ARI discharge hydrographs.

These routed hydrographs were used as upstream inflow boundary inputs for MIKE 21C.

4.2.2 Downstream sea water levels boundary for 2D model

The Indian Ocean was taken as the downstream open boundary described by water levels. Under section 3.5, from a 25 years record at Mombasa (190 km away from the river mouth), an extreme sea water level analysis was conducted based on Gumbel probability distribution and superimposed with sea level rise values due to climate change based on the 4th assessment report on climate change (IPCC, 2013). The recorded data took into account changes due to astronomical tides and local effects excluding surges due to tsunamis.

Despite the data obtained from the (APDRC, 2014) data bank being calibrated, ready to use and of research quality, there are high uncertainties and variability [31] in predicting future extreme sea water level rises incorporating climate change. The author thus assumed the conservative scenario IPCC RCP8.5 for this study. Table 4.2-2 represents the input sea water level with values used in bold.

In the simulation of current condition, average values of tidal levels of similar period were extracted from University of Hawaii data bank.

Table 4.2-2: Assumed extreme high sea levels for Tana River study

ARI	Extreme tidal levels, based on 19 years AMS using Gumbel probability		IPCC scenarios	Predicted extreme sea water levels for East African coast 2040, 2060 and 2100 taking into account changes due to climatic conditions								
	m to chart datum	m to MSL -2.867		2040			2060			2100		
				Sea level rise (m)		Sea level	Sea level rise (m)		Sea level	Sea level rise (m)		Sea level
				Global mean	EA coast	m to MSL	Global mean	EA coast	m to MSL	Global mean	EA coast	m to MSL
1:2 years	5.02	2.16		0.19	0.21	**2.36**	0.30	0.33	**2.49**	0.74	0.81	**2.97**
1:50 years	5.28	2.41	RCP 8.5	0.19	0.21	**2.62**	0.30	0.33	**2.74**	0.74	0.81	**3.22**
1:100 years	5.33	2.46	RCP 8.5	0.19	0.21	**2.67**	0.30	0.33	**2.79**	0.74	0.81	**3.28**

[31] Short duration data of less than 20 years can be greatly biased due to interannual and decadal variability

4.3 2D Model calibration

Roughness is best described by “Mike 21 Manning number” M which is a reciprocal of (Chow, 1959) Manning values (DHI., 2014).The only available stage discharges were just upstream of the study area thus comparison between simulated and observed discharges was not possible. Under section 4.2.1.1, using both simulated and recorded stage discharges, the MIKE 11 model was calibrated and Manning values of 0.04 and 0.06 for the main channel and floodplain respectively were found to be appropriate.

In the calibrated section, the river banks are covered with dense shrubs, trees and tall grass, while further away, scattered bushes with savannah grassland best describe the catchment. A pictorial illustration is attached in Appendix 3. More dense shrubs are present in Lower Tana, but it is similar to the upper Tana vegetation. Therefore, the author found a Manning M value of 25 in the main channel and 17 in the floodplains as appropriate. Figure 4-10 illustrates the roughness distribution.

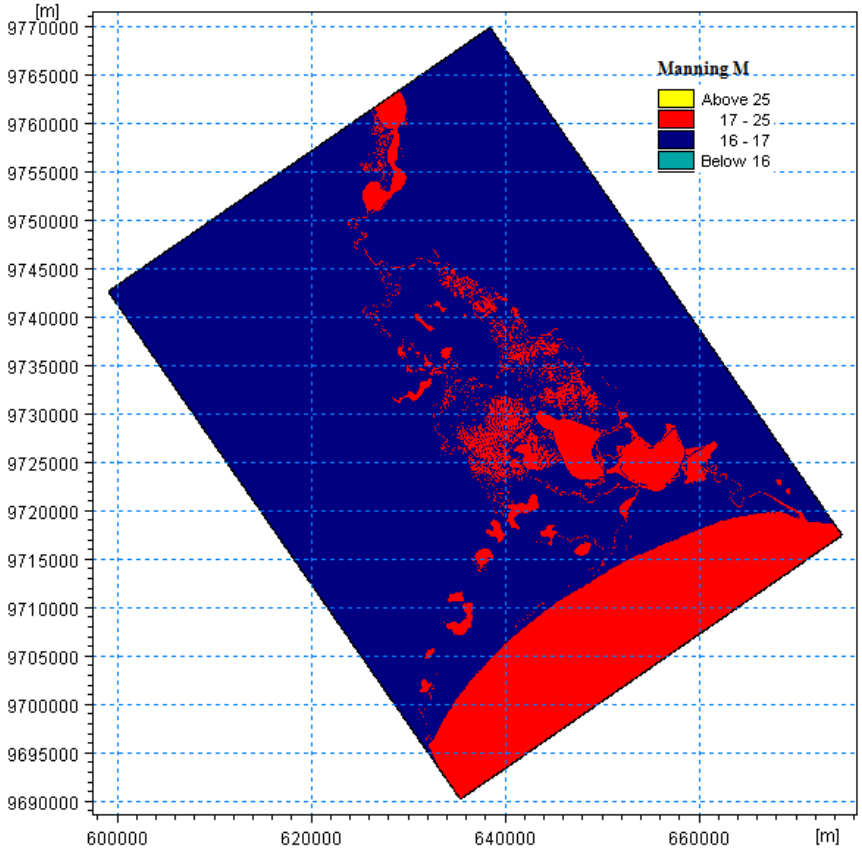

Figure 4-10: Lower Tana River delta roughness distribution.

4.4 Final 2D model set-up summary

The final model was set up as is described in the user manual, a summary of the values used and section under which it has been discussed is summarized in Table 4.4-1.

Table 4.4-1: Final 2D Model setup summary

Model parameter	**Discussed under section**	**Inputs**
Bathymetry and grid	4.1.2	1279 k cells and 979 j cells approximately 37 m width cells and 65m long grid cells in river direction
Simulation period	3.4	17th October to 31st December
Times steps	2.3.2	10 seconds
Boundary	3 and 4.2	**Current scenario 1.1:** Inflow hydrograph with $Q_{2\ peak}$=680 m^3/s and Sea level varying with peak at 2.16m MSL **Current scenario 1.2:** Inflow hydrograph with $Q_{50\ peak}$=2717 m^3/s and Sea level constant at 2.41m MSL **Current scenario 1.3:** Inflow hydrograph with $Q_{100\ peak}$=3523 m^3/s and Sea level constant at 2.46m MSL **Future scenario 2.1 inclusive of climate change:** Inflow hydrograph with $Q_{2\ peak}$=816 m^3/s and Sea level constant at 2.49m MSL **Future scenario 2.2 inclusive of climate change:** Inflow hydrograph with Q_{50}peak=3260 m3/s and Sea level constant at 2.74m MSL **Future scenario 2.3 inclusive of climate change:** Inflow hydrograph with Q_{100} peak=4227m3/s and Sea level constant at 3.28m MSL
Source and sink	2.3.2	None
Flood and drying	2.3.2.2	Drying depth=0.2 Flooding depth=0.3
Eddy viscosity	2.3.2	0.5 m^2/s

Resistance	4.3	Manning value M=17 to 25 in main channel M=25 to 30 in flood plains
HD integration	2.3.2	Full dynamic
Results		Results saved for whole model area in intervals of six hours

5 RESULTS AND DISCUSSIONS

5.1 Impacts of dams on flow regimes

Figure 5-1 shows a bar graph representing a comparison between the post dam and pre-dam discharges recorded at Garissa station for a period of 73 years.

It was found that small floods / flows in the long rainy season (April to June) have been reduced significantly. In May, a reduction of approximately 19% has been registered, while in June 9%. Flows in April did not register any significant reduction; 1% decline was noted. (See Table 5.1-1).

During the short rainy season (October to December), December flash floods have significantly increased by 11%.This can be explained by the draining of the dam in anticipation of floods and dam overspill. No significant changes have been registered in November flash floods (See Table 5.1-1).

The base flows have greatly been altered registering increased flows of up to 43% in the dry months of February and March.

Cunane plotting position of Log Pearson type III and Log-Gumbel[32] probabilistic estimates of Pre-dam and Post-dam are represented in Figure 5-2 and summarized in Table 5.1-2. Flows with return period of less than 1:2 registered no significant changes in both pre-dam and post-dam durations. 1:50 ARI floods declined from a predicted value of 3396 m^3/s to 2851m^3/s (-16%) in LEV1 and 2720m^3/s to 1841m^3/s (-32%) in LP3 probability distributions. The 1:100 ARI floods declined from a predicted value of 4721 m^3/s to 3855m^3/s (-18%) in LEV1 probability distribution[33].

The timing and seasonal flow patterns do not register significant change as indicated in Figure 3-3, though an average increase of 4 days lag time was noted. Thus, the dams can be said to attenuate the small floods reducing the downstream severity.

In the light of Tana hydrodynamics, construction of the five main dams and in particular Masinga (1981) and Kiambere Dams (1988), have greatly reduced the magnitude of floods and increased the dry weather flows. This is in agreement with general literature on large dams and

[32] Log Pearson type 3 was found to fit well up to return period of 1:20, and Log Gumbel fitted well in all distribution periods but tended to overestimate the flood. See section 3.3

[33] Log Pearson type 3 was not considered for flows with return period greater than 1:100 due to underestimation.

studies done on the Tana catchment. (Leauthaud, et al., 2013), (Maingi, et al , 2002) and (Hussein, et al., 2006).

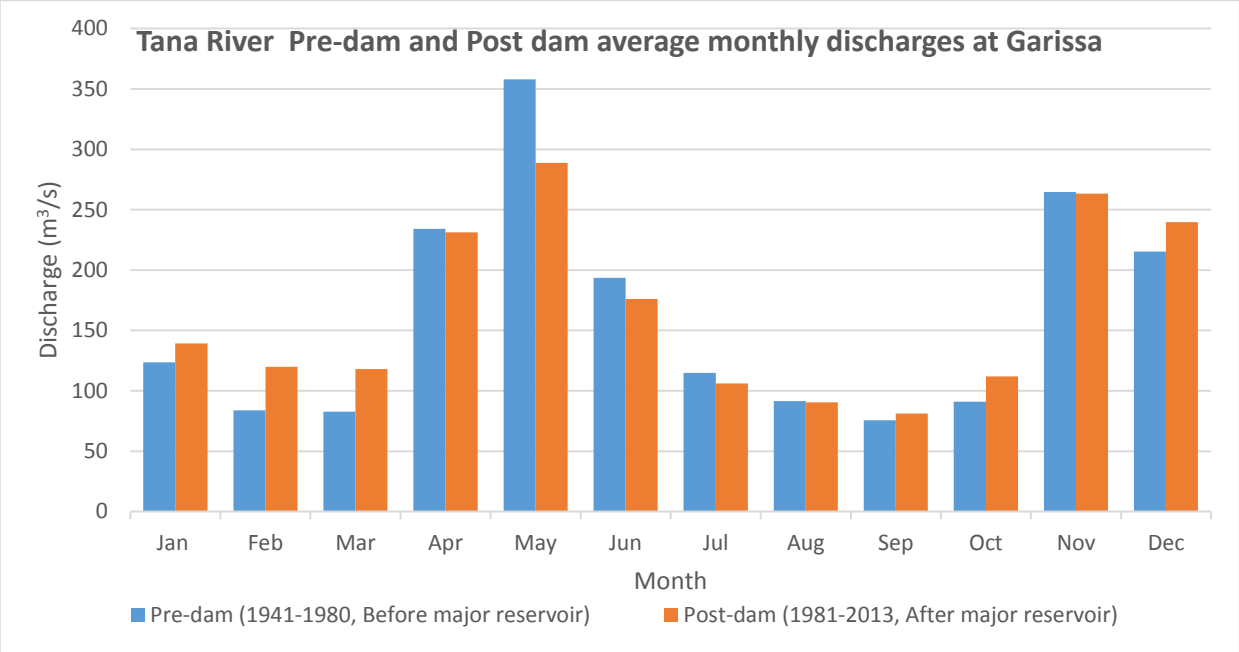

Figure 5-1: Bar graph showing monthly average flows for Tana River Pre-dam and post dam conditions for a period between 1942 to 2013 at Garissa.

Table 5.1-1: Monthly average, standard deviation and percentage changes of Tana River discharges at Garissa for Pre-dam and Post-dam analysis.

	Pre-dam (1941-1980, Before major reservoir)				**Post-dam (1981-2013, After major reservoir)**				
Month	Average (m^3/s)	Max (m^3/s)	Min (m^3/s)	STDEV (m^3/s)	Average (m^3/s)	Max (m^3/s)	Min (m^3/s)	STDEV (m^3/s)	% change
Jan	123	183	100	25	139	162	114	13	13%
Feb	84	103	70	10	120	142	106	9	43%
Mar	83	106	74	8	118	159	103	16	43%
Apr	234	394	111	89	231	314	153	50	-1%
May	358	417	287	42	289	334	259	19	-19%
Jun	194	281	138	43	176	242	119	36	-9%
Jul	115	135	104	9	106	122	98	6	-8%
Aug	92	101	82	4	90	103	83	5	-1%
Sep	76	85	67	6	81	85	77	2	7%
Oct	91	163	65	31	112	174	77	33	23%
Nov	265	346	181	44	263	323	189	37	0%
Dec	215	283	141	44	240	348	169	45	11%

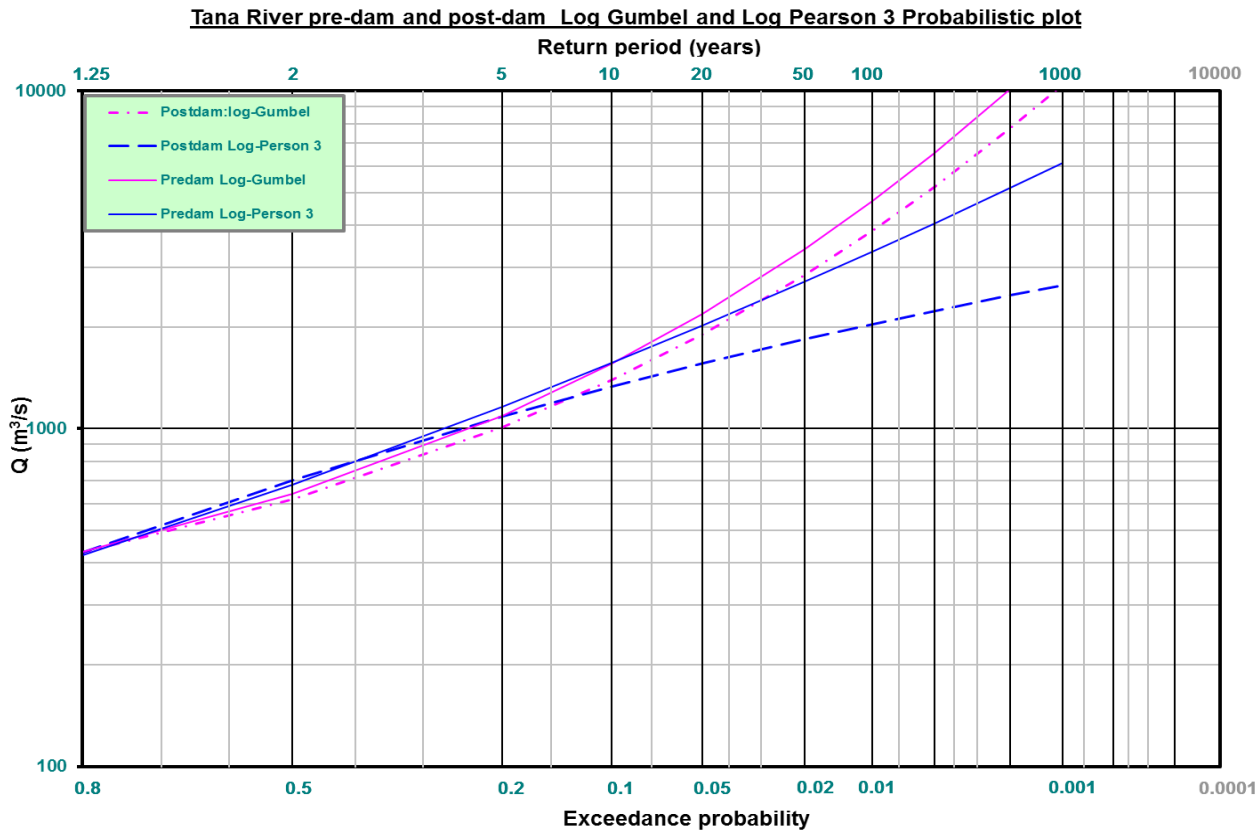

Figure 5-2: Tana River Log-Gumbel and Log-Pearson type 3 probabilistic plot for Pre-dam and Post dam analysis at Garissa recorded flows.

Table 5.1-2: Log-Gumbel and Log Pearson 3 Tana River probabilistic analysis summary for Pre-dam and Post-dam conditions at Garissa station.

Return Period T (Years)	Log-Gumbel			Log-Pearson 3		
	Pre-dam	Post-dam	% difference	Pre-dam	Post-dam	% difference
1.25	431	429	0%	423	431	2%
2.00	641	618	-4%	684	706	3%
5.00	1094	1009	-8%	1162	1088	-6%
10.00	1558	1396	-10%	1563	1334	-15%
20.00	2188	1905	-13%	2018	1561	-23%
50.00	3396	2851	-16%	2720	1841	-32%
100.00	4721	3855	-18%	3341	2041	-39%
200.00	6555	5209	-21%	4053	2234	-45%

5.2 Impacts of spring astronomical tide and rechanneling

During spring tides, high water tidal levels are at their highest. Concurrence of floods peaks and spring high water tide could lead to damming in the lower Tana River, which could cause excessive high river flood levels. Therefore, investigation of tide intrusion is of importance. Water level rise due to astronomical tides and storm surges has been discussed in detail in section 2.2.

The 1D Mike11 model was used to quantify the influence of tidal level on flood levels in the lower Tana River. A constant upstream boundary inflow of 400 m³/s at Garissa and a varying tidal level at the river mouth downstream boundary was used. A 5-day extract of the model run during a spring tide period is presented in Figure 5-3 below. From the latter 1D model simulation it can be deduced that tidal effects are propagated approximately 2 km inland of the Tana River mouth where its effect diminishes. This finding warranted a detailed investigation with the 2D model with similar boundary conditions since the 1D model did not account estuary shape effects.

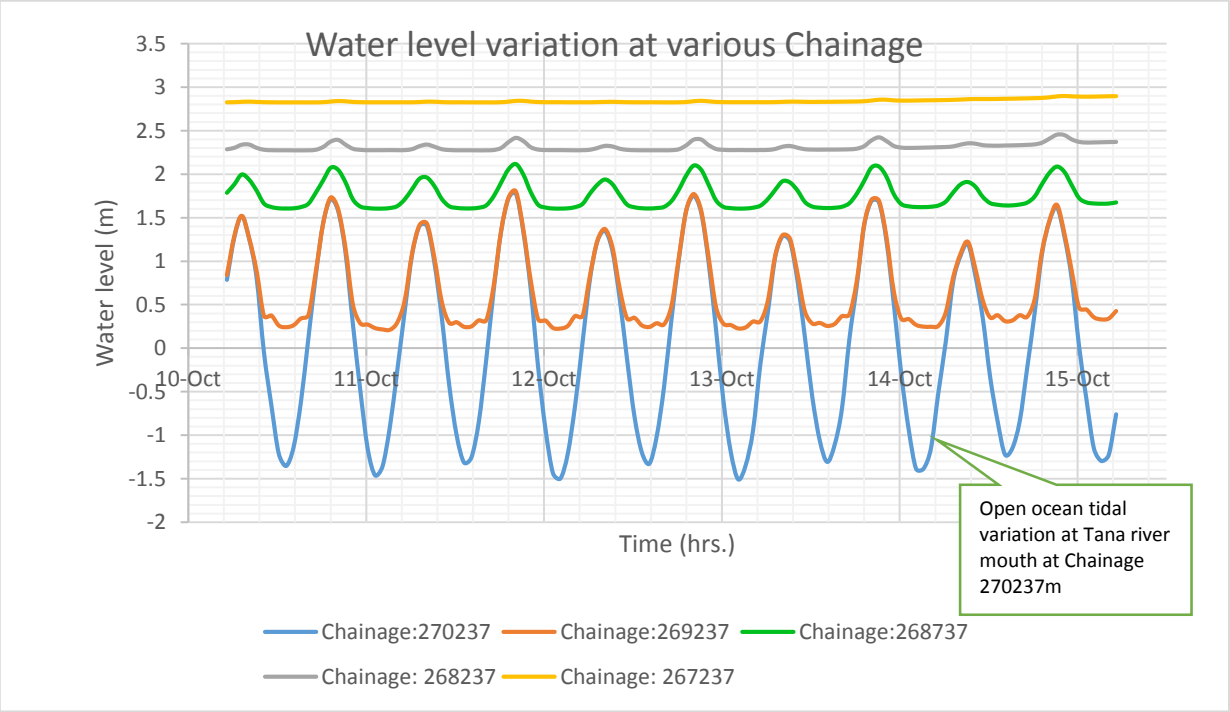

Figure 5-3: Water level variation at various Chainage due to tidal effects, for a five-day simulation.

During further investigation on a 2D model, upstream inflow of 400m^3/s (similar to that used for the 1D model) and varying water levels as recorded at Mombasa as downstream boundary were used. The simulations was carried out for a period of 12 days (The results were saved on an

hourly basis, thus inhibiting longer simulation durations as this would have required large memory saving space). Water levels were extracted at three positions as shown in Figure 5-4.

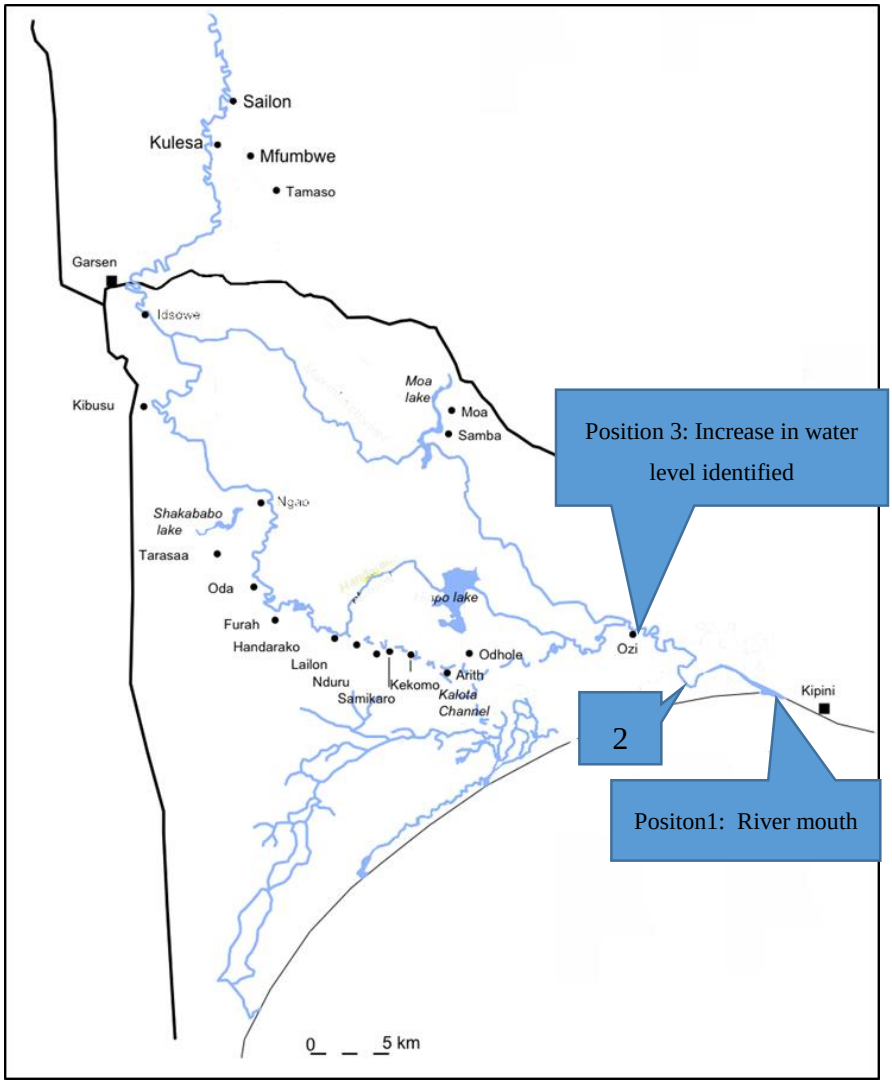

Figure 5-4:Positions where water levels were extracted to investigate tidal levels intrusion; positon 1≈ river mouth, 2 ≈ 6km inland and 3 ≈ 20 km.

From results represented in Figure 5-5, the model predicted that the tidal effect extends approximately 20km inland from the river mouth during spring tides. The intrusion length might not be entirely accurate , this can be attributed to approximation of the depth at the river mouth. A bottom depth of of -1.0 m below MSL was used in the river mouth (i.e. at the location where the river entered the sea (see section 4.1.1.2)).The meandering nature of the river, shallow lakes in the flood plains and the river flowing on an old smaller river channel, have an impact on intrusion lengths. The 2D model simulation demonstrated that upstream water flows tend to dominate the estuary water level and in particular during peak floods when the effects of tidal influence are minimised.This explains why the river mouth never closes even during low flows.

An increase in water level was noted at location 3 (refer Figure 5-4) despite using constant water inflow of 400m^3/s. Further investigation revealed that, this was occuring at the position where the river was rechanneled. Water depths variations at various time steps during a flood propagation are illustrated in Figure 5-6a and Figure 5-6b.It is apparent that there is a bottlle neck effect at the position before the river regains flow to the original channel.

The effects of tides can not be negleted,but interms of the regulation of flows, the bottleneck effect at the new smaller channel is more pronounced than the tide effects. None the less these effects are taken into account in major floods simulations.

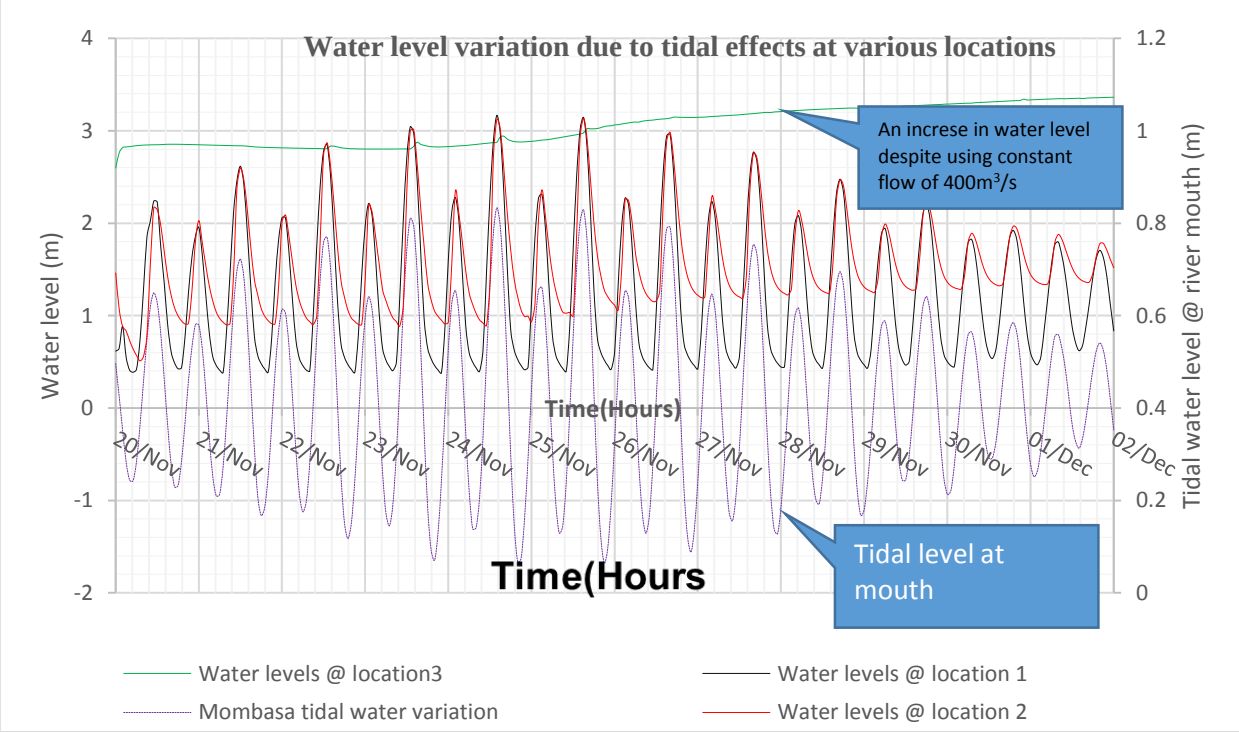

Figure 5-5: Hourly water level variation at various locations in the model for 12 days simulation.

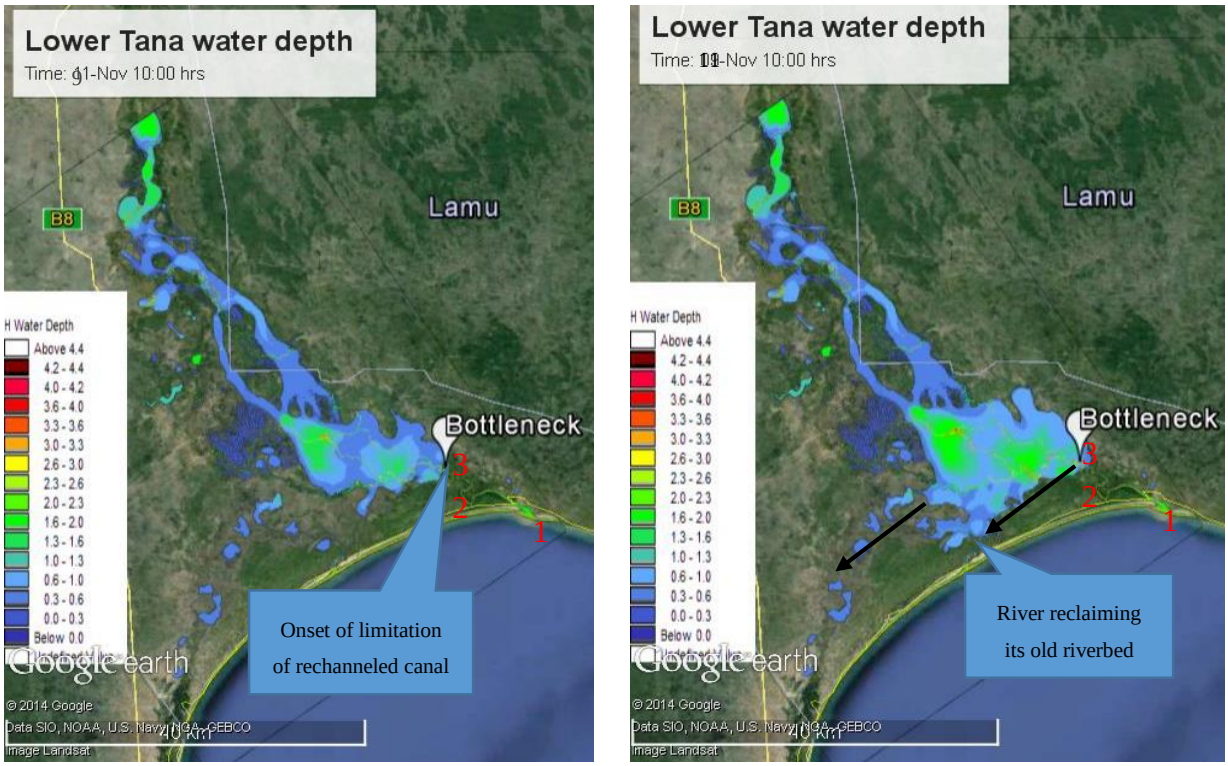

Figure 5-6a: Water depths at selected times showing bottleneck effect limiting flood propagation at rechanneled canal.

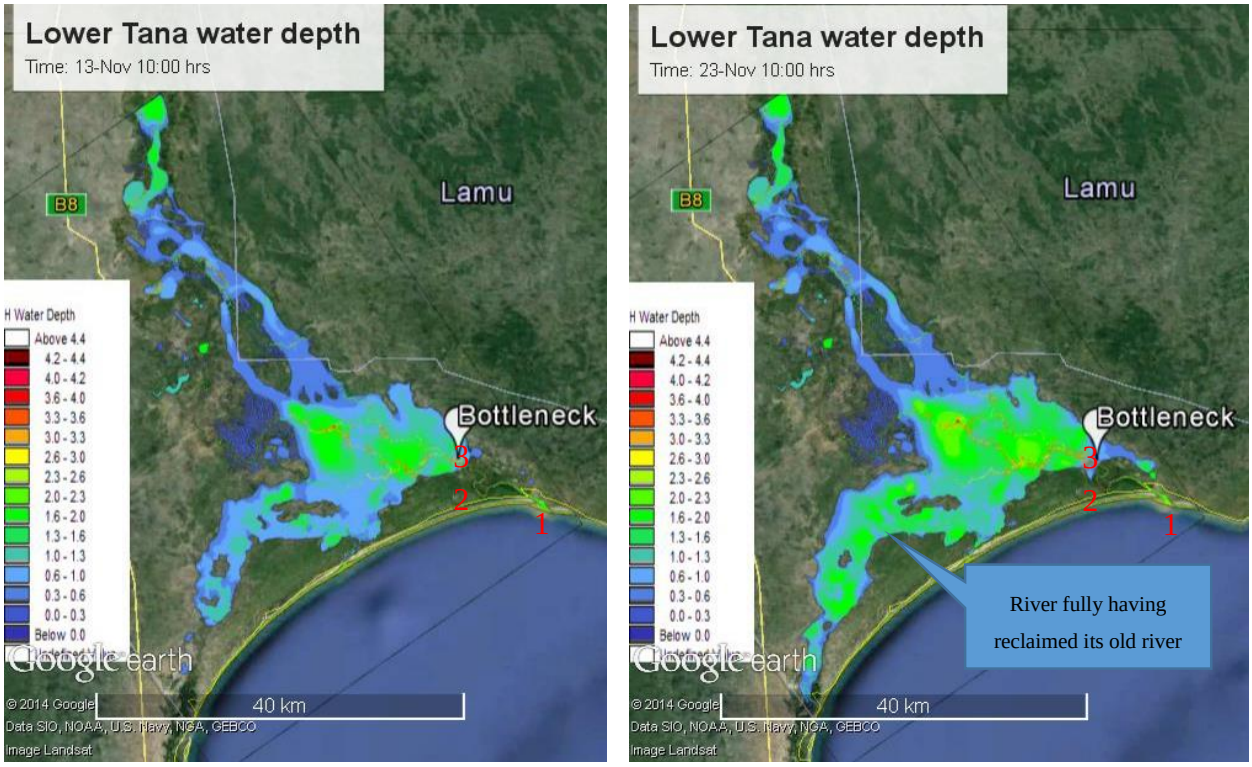

Figure 5-6b: Water depths at selected times showing bottleneck effect limiting flood propagation at rechanneled canal.

5.3 Extent of Flooding

The model water depths are shown in Figure 5-7 to Figure 5-12 and corresponding velocities in Figure 5-13 to Figure 5-18 on pages 66 to 68 for different floods, each for cases with and without climate change. At a glance, a summary extracts of water depths and velocities at three positions 2, 3 and 4 (see Figure 5-7) and percentage changes due to climate change is shown in Table 5.3-1.

During floods, near the main road at Garsen, the river breaks its main banks and spreads onto the floodplain in a southeasterly direction. It branches and spreads further before reclaiming its old channel broadening further in a southwesterly direction and opening up 3 more river mouths. It is evident that the sand dunes at the sea cause major damming effects making the water levels rise by up to 2 m high. This flow trend is equally true for small floods with annual recurrence interval of 1:2. The flow pattern can be explained, as ground levels on the eastern side are relatively lower than in the main channel to the west. The general flood direction movement is illustrated in Figure 5-8.

At current conditions, water depth of the Q_2 flood peaks are in the ranges of 0.6 m and 1.2 m excluding the lake depths. This significantly increases to 0.8 m and 2.6 m when climate change is included. There is not much difference in the Q_{50} and Q_{100} water depth. Their depth ranges are between 1.0 and 3.3 m. At the different locations sampled, an average of 5% increase is noted due to climate change (see Table 5.3-1). These water depths are experienced in areas adjacent to the shallow lakes and old riverbed marshlands. This observation is of importance, as major villages are located in these areas. It should be noted, RCP 2060 predictions on climate change were used for 1:2 ARI and 1:50 ARI while for 1:100 ARI, 2100 predictions was used.

Table 5.3-2 shows a summary of the flooded area in all scenarios and the relative percentages to the modelled area. The extent of flooded area does not significantly vary for 1:50 ARI to 1:100 ARI, registering a percentage change of 31 % to 34 %. 1:2 ARI flows have a flooded area of 592 km^2 (18 % of modelled area) and 592 km^2 (23 % of modelled area) inclusive of climate change. This observation is due to the sand dune on the sea front damming the floods and higher elevations in the east of the model area.

It is evident that the existing road cutting through the eastern side of the floodplain causes major damming. In section 4.1.1.3, it was noted that the road has one major bridge and six minor openings and they do not adequately convey the bigger floods.

The floodplain best described by gradual slope, shallow lakes, reclaimed agricultural land and re channeled streambeds, makes the velocity in the floodplain relatively low. Velocities of 0.07 to 0.1 m/s are mainly experienced in the lower part of the delta, while the upper regions experiencing higher values of 0.33 to 0.4 m/s. Q_2 floods experience velocities ranging between 0.03 to 0.07m/s for current and inclusive of climate change scenarios. Q_{50} and Q_{100} inclusive of climate change register the highest velocities in the order of 0.1 to 0.47 m/s.

The actual flooded area is relatively larger than what the model predicts. On the western boundary near the sea, marked as position 5 in Figure 5-7 , it is evident that the river floods further but it is limited by extent of modeled area. A call out in the Figure 5-7 illustrates this and the trend is equally true for all simulations. This observation can be confirmed on the ground as illustrated in pictorial representation in Appendix 7. In addition other hydrological processes that could impact on the extent of flooding are not taken into account e.g. groundwater and localized precipitation.

Table 5.3-1: Summary of water depths and velocities at selected positions and percentege change due to climate change

Scenario	**Current**	**+ Climate change**	**% change**	**Current**	**+ Climate change**	**% change**
	Depth(m)			**Velocity(m/s)**		
Q_2 @ positon 2	4.06	4.35	7%	0.366	0.377	3%
Q_{50} @ positon 2	5.72	5.91	3%	0.415	0.440	6%
Q_{100} @ positon 2	6.00	6.21	3%	0.426	0.465	8%
Q2 @ positon 3	1.89	1.98	5%	0.016	0.017	4%
Q50 @ positon 3	3.08	3.27	6%	0.039	0.041	6%
Q_{100} @ positon 3	3.36	3.56	6%	0.049	0.054	8%
Q_2 @ positon 4	1.46	1.55	6%	0.017	0.017	2%
Q_{50} @ positon 4	2.65	2.84	7%	0.039	0.041	5%
Q_{100} @ positon 4	2.93	3.13	7%	0.043	0.047	7%
		Average	5%		Average	6%

Table 5.3-2: Summary of simulated flooded area and percentage of area inundated

Annual recurrence interval	Area under flood (km^2)	% of area under flood relative to modeled delta area($2623km^2$)
1:2	570	21%
1:2 inclusive of climate change	592	23%
1:50	813	31%
1:50 inclusive of climate change	842	32%
1:100	856	33%
1:100 inclusive of climate change	889	34%

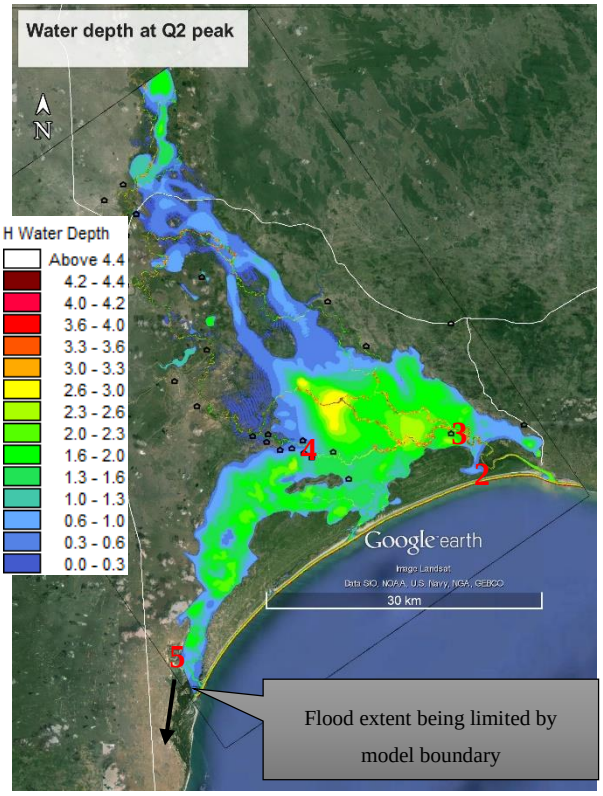

Figure 5-7:Lower Tana predicted Water depths at peak of Q_2 flood

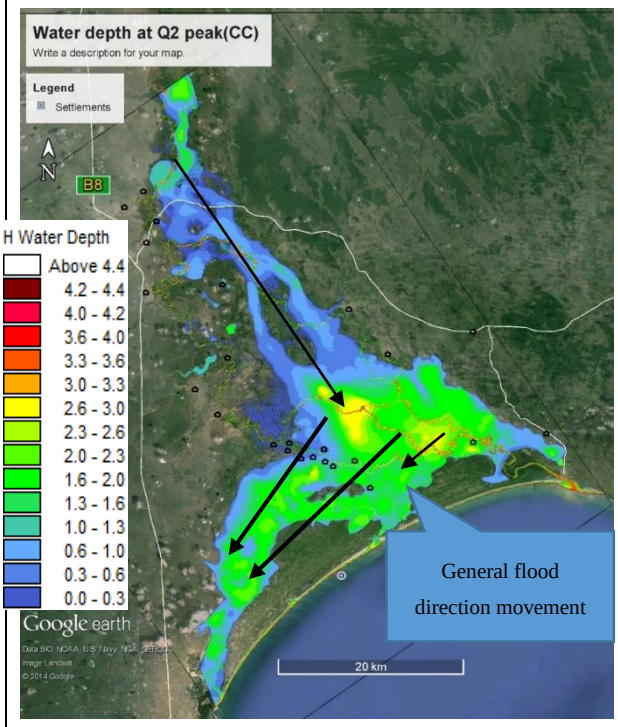

Figure 5-8:Lower Tana predicted Water depths at peak of Q_2 flood inclusive of climate change

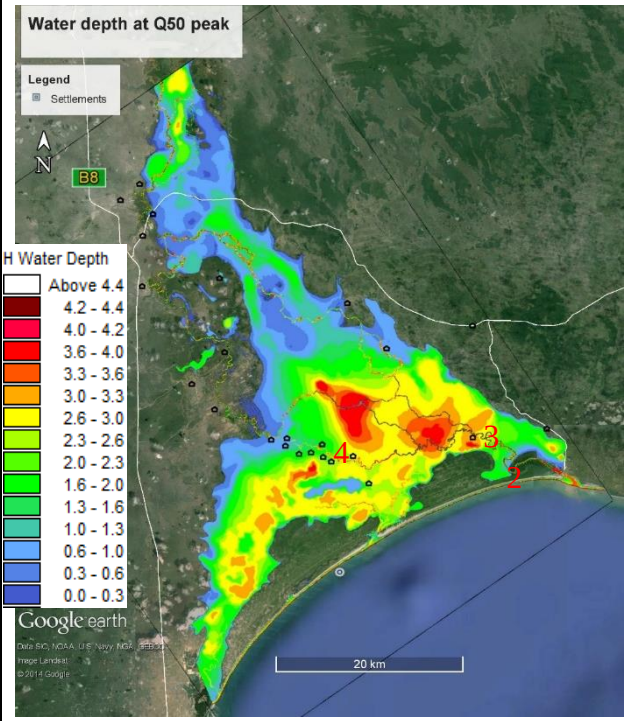

Figure 5-9: Lower Tana predicted Water depths at peak of Q_{50} flood

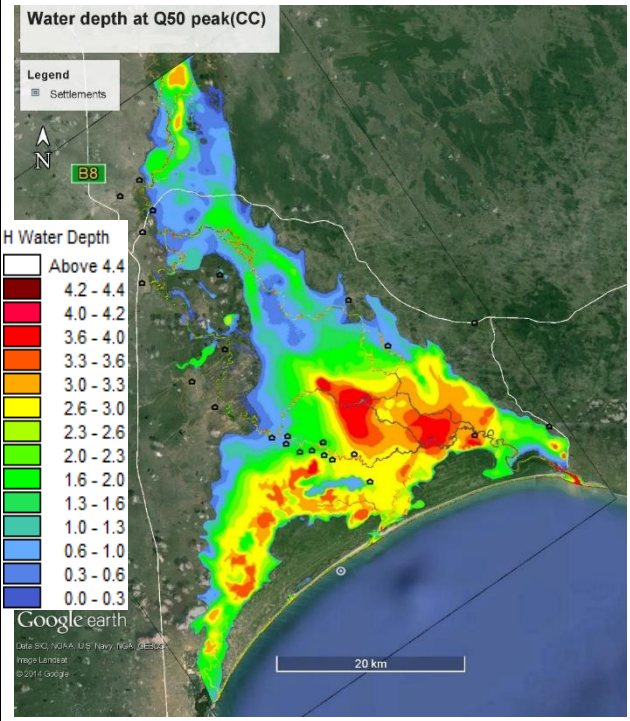

Figure 5-10: Lower Tana predicted Water depths at peak of Q_{50} flood inclusive of climate change

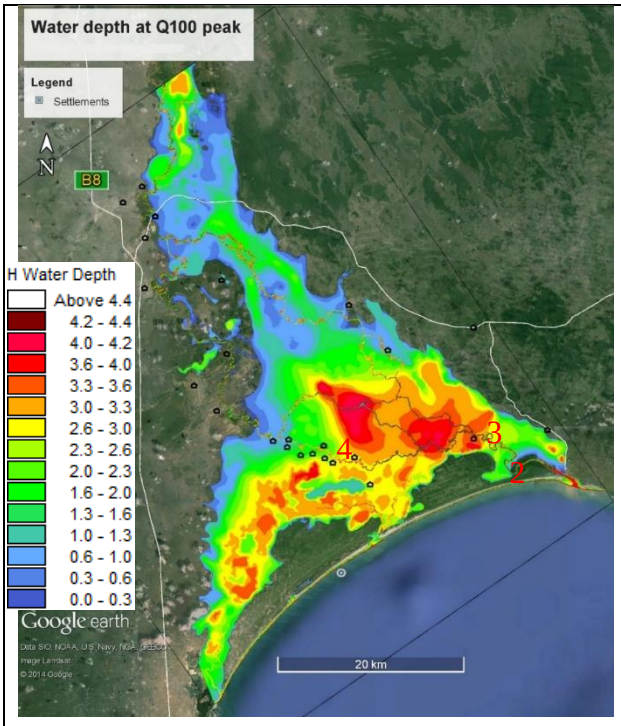

Figure 5-11:Lower Tana predicted Water depths at peak of Q_{100} flood

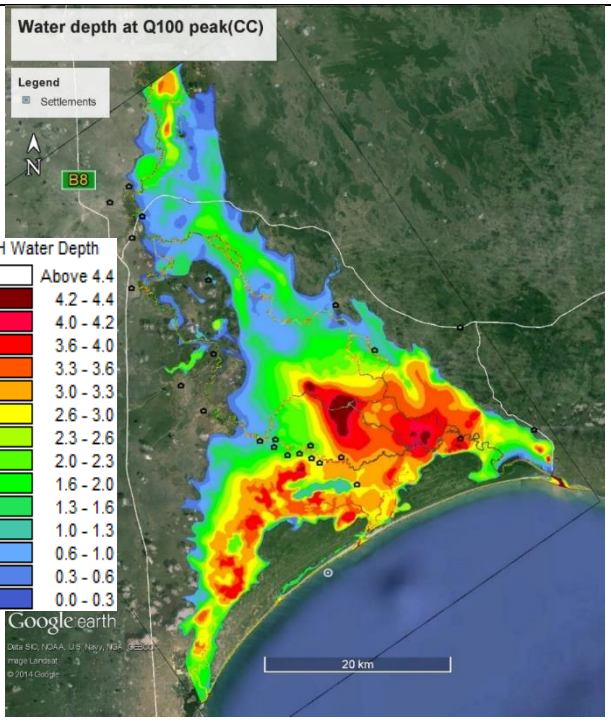

Figure 5-12: Lower Tana predicted Water depths at peak of Q_{100} flood inclusive of climate change

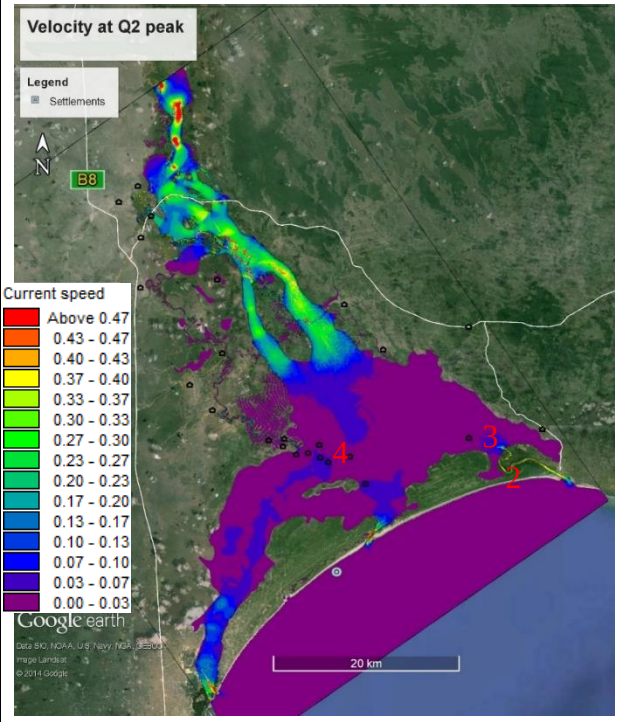

Figure 5-13:Lower Tana predicted velocities at peak of Q_2 flood

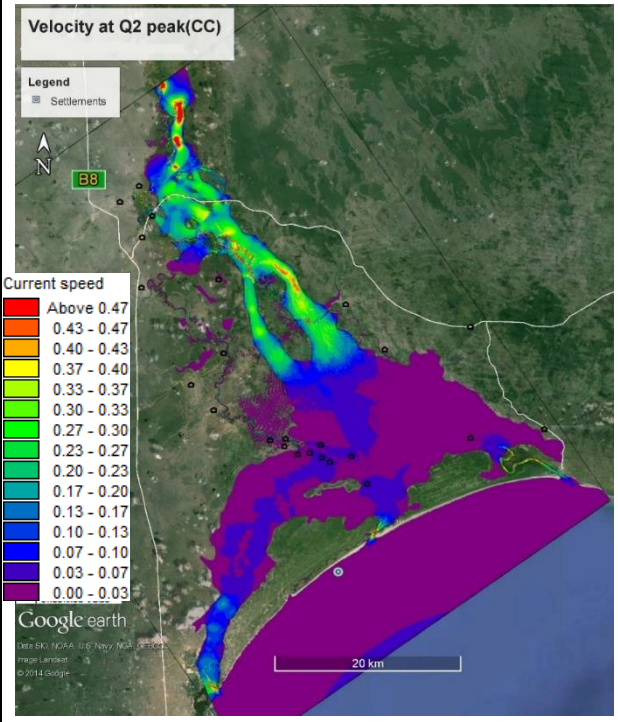

Figure 5-14: Lower Tana predicted velocities at peak of Q_2 flood inclusive of climate change

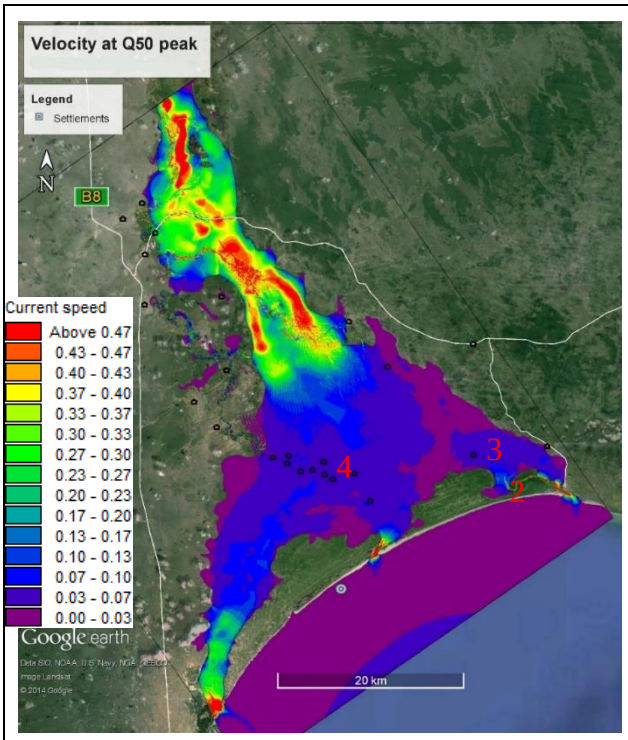

Figure 5-15:Lower Tana predicted velocities at peak of Q_{50} flood

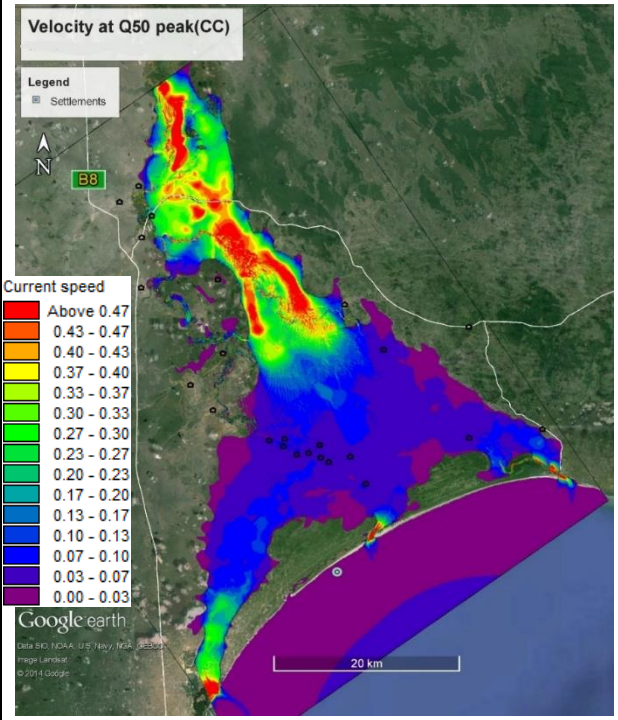

Figure 5-16: Lower Tana predicted velocities at peak of Q_{50} flood inclusive of climate change

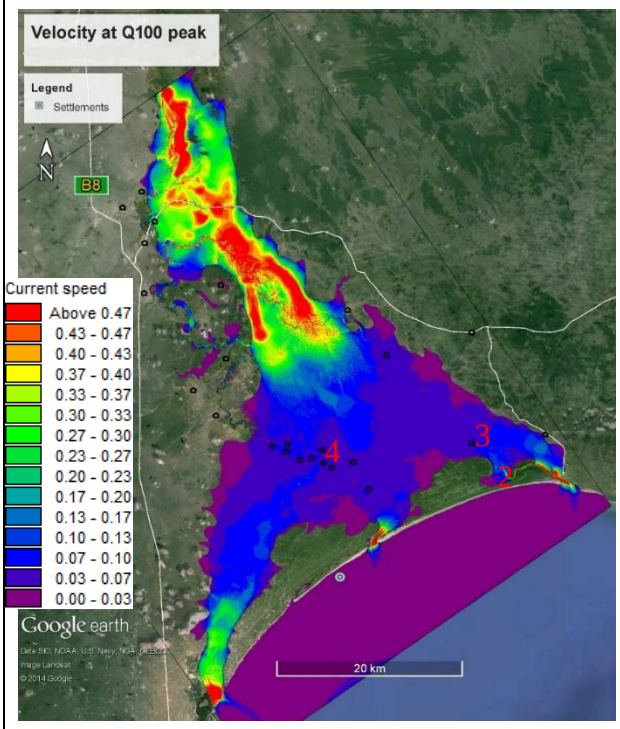

Figure 5-17:Lower Tana predicted velocities at peak of Q_{100} flood

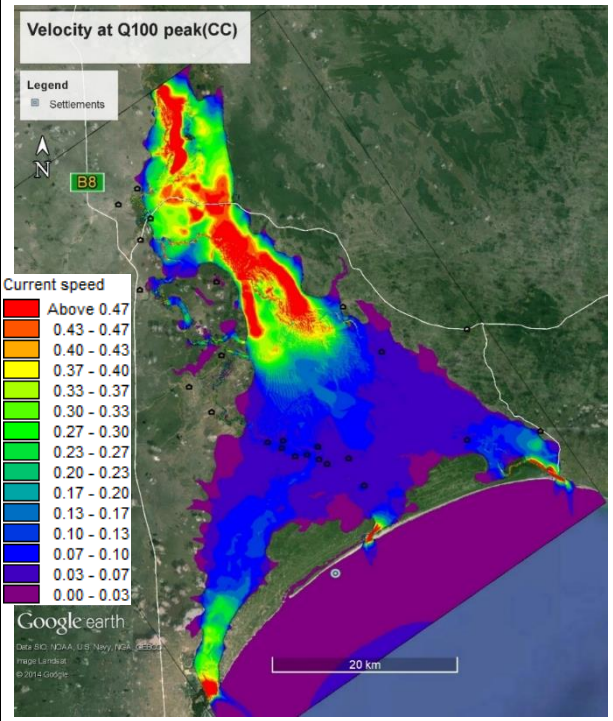

Figure 5-18: Lower Tana predicted velocities at peak of Q_{100} flood inclusive of climate change

6 FLOOD HAZARD CLASSIFICATION MAPPING

Based on velocity and water depths interactions at the peak of the floods, the modelled area was classified into four classes: safe, vehicles unstable, wading unsafe and damage to light structures as identified under section 2.5.

Inclusive of climate change, the Q_2, Q_{50} and Q_{100} floods hazard maps are shown through Figure 6-1, Figure 6-2 and Figure 6-3 respectively. It can be seen the Q_{50} and Q_{100} damage to light structures zone encompass most of the settlement. These settlements mainly include traditional houses supporting approximately a population size of 3000 to 8000 (KNBS, 2010). A detailed map of population distribution was not available limiting superimposition on the hazard maps.

Based on the classification used (Figure 2-8), the classification in the delta is mostly influenced by the water depths. Velocities apart from the main channel are low thus playing a minor role.

Figure 6-4 shows the Q_2, Q_{50} and Q_{100} flood lines. It was observed Q_{50} and Q_{100} flood lines do not significantly differ

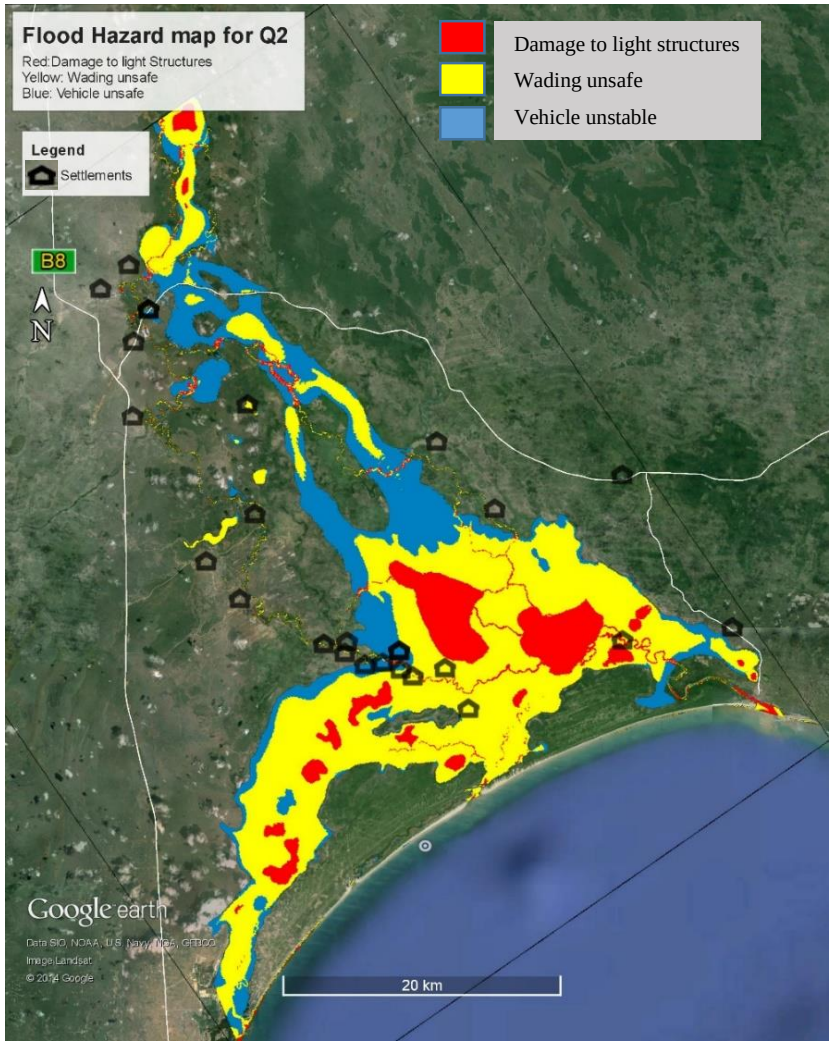

Figure 6-1: Flood hazard map for the Q_2 flood with climate change based on Australian guidelines

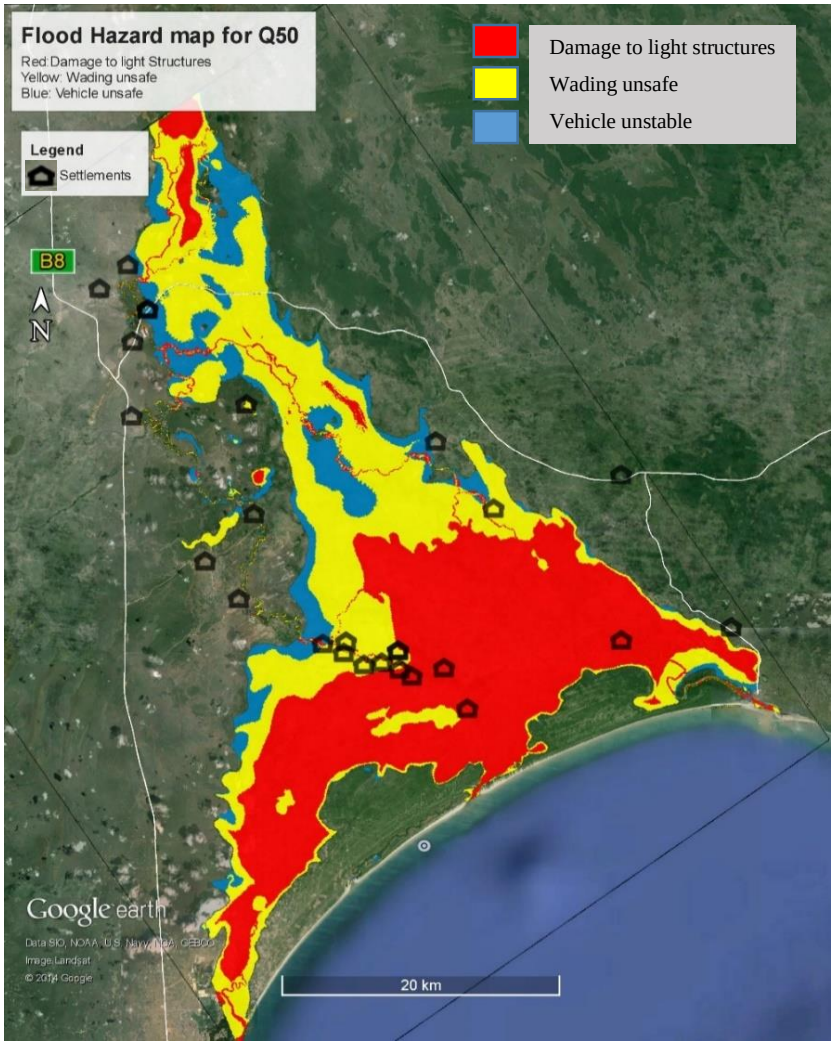

Figure 6-2: Flood hazard map for the Q_{50} flood with climate change based on Australian guidelines

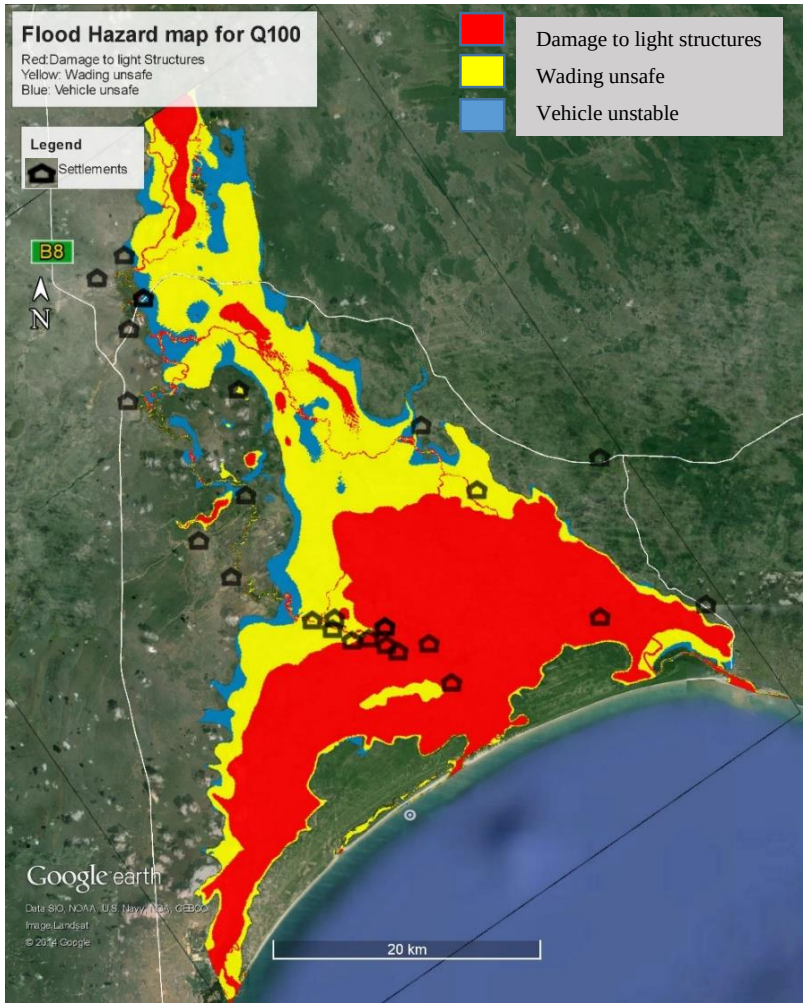

Figure 6-3: Flood hazard map for the Q_{100} flood with climate change based on Australian guidelines

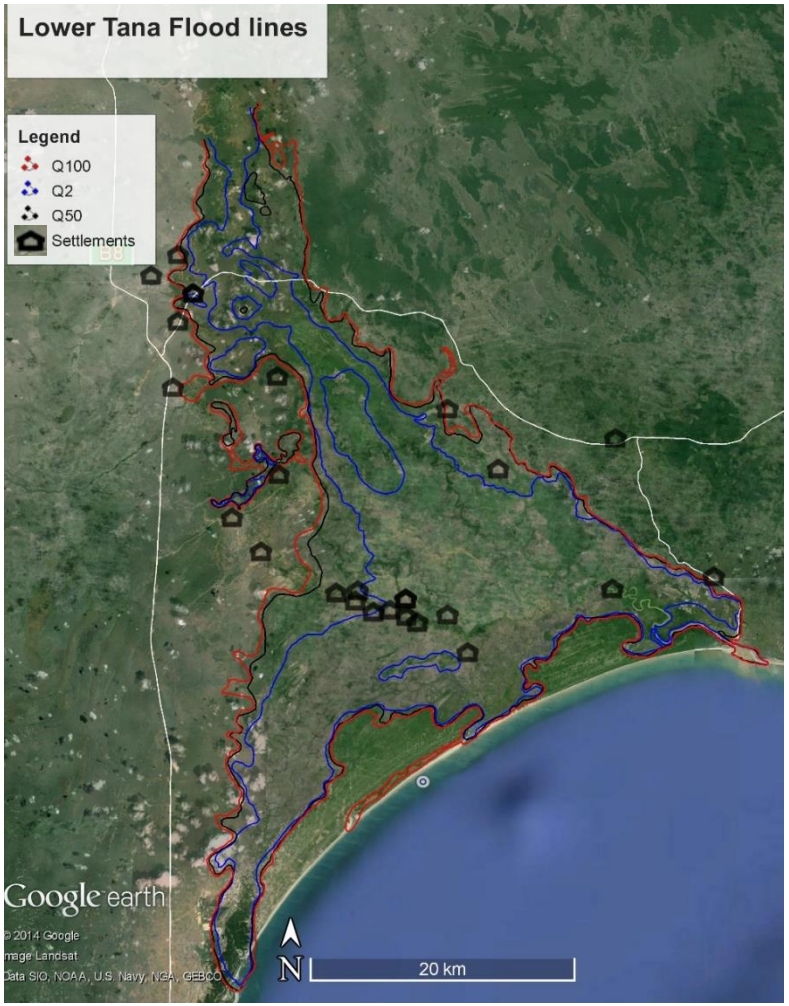

Figure 6-4: Lower Tana Flood lines for Q_2, Q_{50} and Q_{100} floods inclusive of climate change

7 CONCLUSION AND RECOMMENDATIONS

Hydrological probabilistic methods applied on the lower Tana River successfully determined various annual recurrence interval flood peaks, extreme sea water levels incorporating climate change and dam influences on flow regime. The calibrated one dimensional model routed the peaks to the study area where a two dimensional hydrodynamic model successfully investigated factors influencing flooding. Eventually 2, 50 and 100 year flood maps/flood lines were developed for the Tana River delta.

Storm events with return periods of two years, and upstream dam operation, cause flash floods on the upper catchment triggering excessive floods on the densely populated floodplain. Loss of life, damage to property and widespread displacement is experienced. Describing the hydrodynamics in a poorly gauged catchment is what this thesis tries to answer. This can be summarized as follows:

- The dams have had significant impacts on flow regime. The Masinga Dam (built in 1981) operation has increased the magnitude of discharges in the short rainy season of December but the magnitude of overall peak floods has reduced.
- Seasonal flow pattern timing has remained much the same after Masinga Dam construction.
- Mild gradient, sand dune on the sea side, high roughness on the floodplains and the bottleneck effect on the rechanneled river canal cause significant flooding upstream of this sections.
- Small lakes / lagoons at the delta act as temporary storage reducing the severity of small floods.
- Inadequate sizing of bridges and culverts limit the propagation of major floods causing major damming upstream of the road in the flood plain.
- High water levels due to spring tides have a damming effect on the water depths.
- The 2 year ARI flood line encompass most of the settlements with 50 and 100 year ARI flood line extent not significantly different from that of the 1:2 ARI.
- Villages in the floodplain lie within wading unsafe and damage to light structures hazard classification zones.
- Climate change due to sea level rise will not significantly alter the extent of flooding but will have a major influence on increasing the water depths and consequently increasing the extent of damage to light structures zone.

Numerical models in a poorly gauged floodplain with Manning number theoretically determined to calibrate the model influences the accuracy of predicted water depths. Despite this, the results were promising. To further improve Lower Tana hydrodynamics, the following are suggested:

- A coupled 1D and 2D dimensional model. Two-dimensional model scope extension from downstream boundary to Garissa and onwards a one-dimensional routing model to the dams, effectively determining lag time to implement effective flood warning system in the delta.
- Finer grid resolution and more detailed surveyed bathymetry subject to availability of resources to improve overall velocity and water depths prediction.
- The inclusion of land use and flood duration in flood mapping categories will make the hazard map more significant.
- Detailed survey of river mouth cross sections to effectively determine the effects of tides and storm charges.
- Additional field data within the delta should be acquired to calibrate the model and other hydrological processes should be included.

Delta ecosystems thrive on cyclic flooding and drying and mitigation of such is a contentious issue with numerous stakeholders. In this thesis, the flood hot spots and hydrodynamics controlling them have been identified. Information and lessons learned from this thesis will go in hand to involved stakeholders to make better-informed decisions.

REFERENCES

DHI, 2003. Mike 21 flow model hints and recommendations in applications with significant flooding and drying, Horsholm Denmark: Mike by DHI.

Anon., 2012. Ramsar News archives. [Online]
Available at: http://www.ramsar.org/cda/en/ramsar-news-archives-2012-kenya-tana/main/ramsar/1-26-45-520%5E25948_4000_0

APDRC, 2014. Asia Pacific Data Research Center. [Online]
Available at: http://apdrc.soest.hawaii.edu/las/v6/dataset
[Accessed 28 July 2014].

ASP, 2007. Tana River Delta-Assessment of flood hydrology, river hydraulics and fluvial morphology report, Stellenbosch: ASP Technology.

Basson, G. R., 2005. Hydropower Dams and Fluvial Morphological Impacts –An African Perspective. s.l., s.n., pp. 7-29.

Bosman, D., 2014. Estimation of the Extreme high sea water levels for seaward boundary conditions of Berg River flood line study, Stellenbosch: ASP Technology.

Bunyasi, M. M., 2012. Vulnerability of Hydro-Electric Energy Resources in Kenya Due to Climate Change: The Case of the seven Forks project. Journal of Agriculture and Environmental Sciences, pp. 36-49.

Chadwick, A., Morfett, J. & Borthwick, M., 2013. Hydraulics in Civil and Environmental Engineering. 5th ed. London and New York: CRC Press.

Chow, V. T., 1959. Open Channel hydraulics. New York: McGraw-Hill.

COCT, 2009. Floodplain and River Corridor Management Policy, Cape Town: s.n.

Dagg, M., Woodhead, T. & Rijks, D. A., 1970. Evaporation in East Africa. International Association of Scientific Hydrology, 15(1), pp. 61-67.

David, P. & Philip, W., 2014. Sea-Level Science: Understanding , surges, Tsunamis and Mean Sea-Level Changes. Cambridge: Cambridge University Press.

DHI., 2014. Grid Generator for MIKE 21C_User Guide, Horsholm Denmark: MIKE by DHI.

DHI, 2001. Water resources. [Online]
Available at: http://mikebydhi.com/Products/WaterResources.aspx
[Accessed 17 August 2014].

El-Nasr, A. A., Arnold, J. G., Feyen, J. & Berlamont, J., 2005. Modelling the hydrology of a catchment using a distributed and a semi-distributed model. Hydrological Processes, p. 19: 573–587..

Hussein, G. et al., 2006. National Disaster Hotspots Case Studies. Washington: The World Bank.

IPCC, 2013. Climate Change 2013: The Physical Science Basis. Contribution of Working Group I to the Fifth Assessment Report of the Intergovernmental, United Kingdom and New York: Cambridge University Press.

IWE, 2014. Lourens river flood study: Hydrology, Hydrodynamic modelling and Evaluation of Mitigation measures, Stellenbosch: s.n.

KenGen, 2014. Hydro power stations. [Online]
Available at: http://www.kengen.co.ke/index.php?page=business&subpage=hydro&id=6

KNBS, 2010. The 2009 Kenya Population and Housing, Nairobi, Kenya: GOK.

Leauthaud, C. et al., 2013. Characterizing floods in the poorly gauged wetlands of the Tana. Hydrology and Earth System Sciences, Volume 17, p. 3059–3075.

Maingi , J. K. & Marsh , S. E., 2002. Quantifying hydrologic impacts following dam construction along the Tana River, Kenya. Journal of Arid environments, pp. 53-79.

MIKE11 by DHI, 2013. A Modelling System for Rivers and Channels Reference Manual, Horsholm Denmark: DHI.

MIKE11, 2013. A Modelling System for rivers and Channels_ User Guide, Horsholm Denmark: MIKE by DHI.

MIKE21C_s, 2012. MIKE 21C Curvilinear Model Scientific Documentation, Horsholm Denmark: MIKE by DHI.

MIKE21C, 2013. MIKE 21C Curvilinear Model for River Morphology User Guide, Horsholm Denmark: MIKE by DHI.

Ministry of Lands, 2012. Tana River Delta Strategic Environmental Assessment Scoping Report, Nairobi: Government of Kenya.

Nakaegawa, T., Wachana, C. & Kakushin, T.-3. M. G., 2012. First impact assessment of hydrological cycle in the Tana River Basin, Kenya, under a changing climate in the late 21st Century. Hydrological Research Letters, Volume VI, pp. 29-34.

NASA, 2000. NASA. [Online]
Available at: http://www2.jpl.nasa.gov/srtm/
[Accessed 05 August 2014].

NIB, 2014. National Irrigation Board. [Online]
Available at: http://www.nib.or.ke/

NSW, 2005. Floodplain Development Manual; the management of flood liable land, Sydney, Australia: New South Wales Government.

Oludhe, C., 2011. Impacts of Climate Variability on Power Generation within the 7-Forks Dams in the Tana river Basin. The Kenya Meteorological Society, pp. 13-20.

RCP, 2009. RCP Database. [Online]
Available at: http://www.iiasa.ac.at/web-apps/tnt/RcpDb
[Accessed 30 July 2014].

RedCross, 2007, 2008, 2013. Fundamental Principles of the International Red Cross & Red Crescent Movement: Annual Report & accounts 2007, 2008, 2013, Nairobi: Kenya Red Cross.

SANRAL, (. S. A. N. R. A., 2006. Drainage Manual. 5th ed. Pretoria: The South African National Roads Agency Ltd.

Savenije H., H. G., 2012. Salinity and Tides in Alluvial Estuaries. 2nd ed. Delft, The Netherlands: Elsevier.

Savenije, H. H. G., 2009. HESS Opinions "The art of hydrology". Hydrology and Earth System Sciences, Issue 13, pp. 157-161.

Savenije, H. H. G., 2013. Hydrology of catchments, rivers and delta's. Delft: Delft University of Technology.

Thomas, C. R. & Golaszewski, R., 2012. Refinement of procedures for determining floodway extent. Batemans Bay, FMA.

USGS, 2014. USGS. [Online]
Available at: http://landsat.usgs.gov/

Versteeg, H. K. & Malalasekera, W., 2007. An Introduction to Computational Fluid Dynamics: The finite volume method. 2nd ed. London: Pearson Education Limited.

Wokabi, S. M., Sombroek, W. & Mbuvi, J., 1976. Preliminary evaluation of the soil condition of the Tana delta for irrigation development, Nairobi: Republic of Kenya.

WRMA, 2014. Tana Catchment status. [Online]
Available at: http://www.wrma.or.ke/index.php/wrma-regional-offices/tana/catchment-status.html

APPENDICES

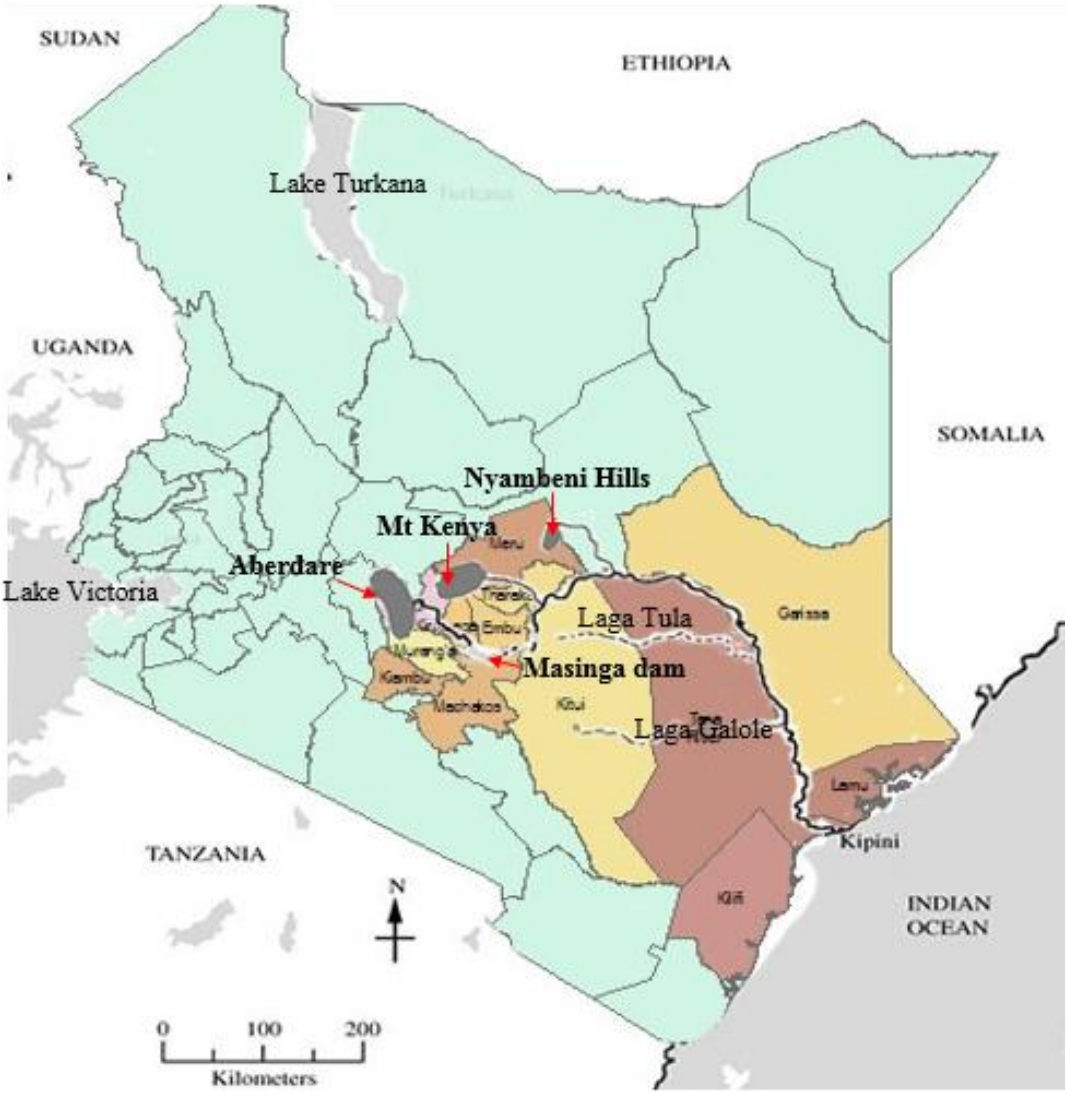

Appendix 1: Tana River political location, river source and boundaries. (Source: ESRI ArcGIS)

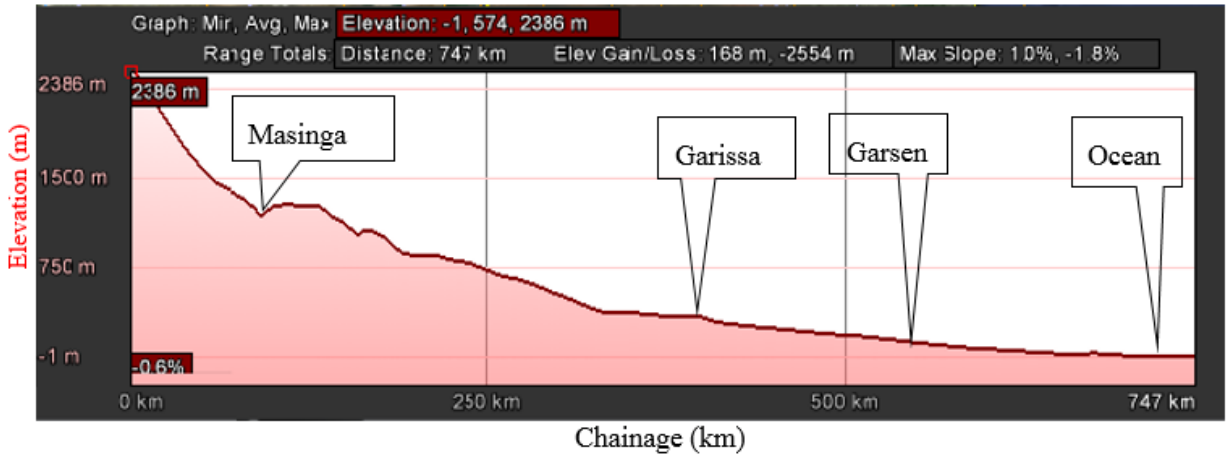

Appendix 2: Tana River catchment longitudinal profile. (Source: google earth).

Appendix 3: Vegetation characteristic of Tana River (Source: google earth, (Ministry of Lands, 2012) and C. S. Owen)

Appendix 4: Masinga dam inflow, discharge and storage analysis

Year	Hydro power generation (m^3/s)	Overflow (m^3/s)	Total discharge (m^3/s)	Inflow (m^3/s)	Water level (AMSL) (m)	% of outflow by power generation
1988	50	30	80	90		63%
1989	47	47	94	88		50%
1990	46	70	116	120		40%
1991	50	20	70	59		71%
1992	48	5	53	57		91%
1993	52	10	62	60		84%

1994	47	20	67	82		70%
1995	51	30	81	90		63%
1996	60	2	62	43		97%
1997	50	40	90	110		56%
1998	65	120	185	160		35%
1999	69	2	71	50		97%
2000	40	2	42	20	1051	95%
2001	35	2	37	60	1052	95%
2002	49	20	69	83	1054	71%
2003	55	40	95	90	1056	58%
2004	49	3	52	57	1053	94%
2005	55	3	58	50	1052	95%
2006	49	4	53	79	1050	92%
2007	60	30	90	38	1057	67%
2008	63	3	66	37	1050	95%
2009	30	3	33	23	1035	91%
2010	48	25	73	98	1054	66%
2011	60	15	75	64	1052	80%

Appendix 5: Gumbel type one extreme tidal levels analysis.

Rank (M)	**Max recorded level**	**P Probability of Exceedance**	**T Return period**	**Log T**	**q Probability of non-exceedance**	**y Reduced variant**
1	5.176	0.04	26.00	1.41	0.96	3.24
2	5.17	0.08	13.00	1.11	0.92	2.53
3	5.143	0.12	8.67	0.94	0.88	2.10
4	5.129	0.15	6.50	0.81	0.85	1.79
5	5.122	0.19	5.20	0.72	0.81	1.54
6	5.111	0.23	4.33	0.64	0.77	1.34
7	5.091	0.27	3.71	0.57	0.73	1.16
8	5.067	0.31	3.25	0.51	0.69	1.00

9	5.06	0.35	2.89	0.46	0.65	0.86
10	5.05	0.38	2.60	0.41	0.62	0.72
11	5.05	0.42	2.36	0.37	0.58	0.60
12	5.05	0.46	2.17	0.34	0.54	0.48
13	5.037	0.50	2.00	0.30	0.50	0.37
14	5.032	0.54	1.86	0.27	0.46	0.26
15	5.027	0.58	1.73	0.24	0.42	0.15
16	5.013	0.62	1.63	0.21	0.38	0.05
17	5.008	0.65	1.53	0.18	0.35	-0.06
18	4.997	0.69	1.44	0.16	0.31	-0.16
19	4.987	0.73	1.37	0.14	0.27	-0.27
20	4.951	0.77	1.30	0.11	0.23	-0.38
21	4.95	0.81	1.24	0.09	0.19	-0.50
22	4.943	0.85	1.18	0.07	0.15	-0.63
23	4.909	0.88	1.13	0.05	0.12	-0.77
24	4.89	0.92	1.08	0.03	0.08	-0.94
25	4.883	0.96	1.04	0.02	0.04	-1.18

Appendix 6: Dimensionless hydrograph ordinates, Garissa statically determined flows and corresponding routed Garsen flows.

Time	**Dimensionless hydrograph ordinates**	**Garissa 1:2**	**Garissa 1:2 Inclusive of climatic change**	**Garissa 1:50**	**Garissa 1:50 Inclusive of climatic change**	**Garissa 1:100**	**Garissa 1:100 Inclusive of climatic change**
02/Oct	0.073	50	59	198	237	257	308
03/Oct	0.076	51	62	205	246	266	320
04/Oct	0.082	56	67	223	267	289	346
05/Oct	0.086	59	70	234	281	304	365
06/Oct	0.086	58	70	233	280	302	363

07/Oct	0.083	56	67	224	269	291	349
08/Oct	0.078	53	63	211	254	274	329
09/Oct	0.100	68	82	272	327	353	424
10/Oct	0.110	75	90	300	360	389	467
11/Oct	0.099	67	81	268	322	348	417
12/Oct	0.097	66	79	262	315	340	408
13/Oct	0.097	66	80	265	318	343	412
14/Oct	0.103	70	84	280	337	364	436
15/Oct	0.114	77	93	309	371	401	481
16/Oct	0.117	80	96	319	382	413	496
17/Oct	0.144	98	117	390	468	506	607
18/Oct	0.165	112	135	448	538	581	698
19/Oct	0.183	124	149	497	596	644	773
20/Oct	0.206	140	168	560	672	726	872
21/Oct	0.215	146	176	585	702	759	911
22/Oct	0.238	162	194	646	775	838	1005
23/Oct	0.249	169	203	675	810	875	1051
24/Oct	0.284	193	232	771	926	1000	1200
25/Oct	0.289	197	236	786	943	1019	1223
26/Oct	0.295	201	241	802	962	1040	1248
27/Oct	0.300	204	245	814	977	1056	1267
28/Oct	0.313	213	256	852	1022	1104	1325
29/Oct	0.319	217	260	867	1040	1124	1349
30/Oct	0.335	228	273	911	1093	1181	1417
31/Oct	0.416	283	339	1130	1356	1466	1759

01/Nov	0.435	295	355	1181	1417	1531	1837
02/Nov	0.427	290	348	1160	1392	1505	1805
03/Nov	0.419	285	342	1139	1366	1476	1772
04/Nov	0.419	285	342	1139	1367	1477	1772
05/Nov	0.417	283	340	1132	1359	1468	1762
06/Nov	0.451	306	368	1225	1469	1588	1905
07/Nov	0.485	329	395	1316	1580	1707	2048
08/Nov	0.500	340	408	1358	1629	1761	2113
09/Nov	0.524	356	428	1424	1709	1846	2216
10/Nov	0.525	357	429	1427	1712	1850	2220
11/Nov	0.511	347	417	1387	1665	1799	2159
12/Nov	0.517	352	422	1405	1686	1822	2187
13/Nov	0.519	353	423	1409	1691	1827	2193
14/Nov	0.508	346	415	1381	1658	1791	2149
15/Nov	0.531	361	433	1442	1730	1869	2243
16/Nov	0.513	349	419	1394	1673	1808	2169
17/Nov	0.524	356	427	1423	1708	1845	2215
18/Nov	0.533	362	435	1448	1738	1878	2254
19/Nov	0.551	374	449	1496	1796	1940	2328
20/Nov	0.570	388	465	1549	1858	2008	2410
21/Nov	0.580	394	473	1576	1891	2044	2452
22/Nov	0.626	426	511	1702	2042	2206	2648
23/Nov	0.687	467	561	1868	2241	2422	2906
24/Nov	0.716	487	584	1945	2334	2521	3026
25/Nov	0.745	507	608	2025	2430	2626	3151

26/Nov	0.838	570	684	2277	2733	2953	3543
27/Nov	0.906	616	739	2462	2954	3192	3830
28/Nov	0.987	671	805	2681	3218	3477	4172
29/Nov	1.000	680	816	2717	3260	3523	4227
30/Nov	0.914	621	746	2483	2979	3219	3863
01/Dec	0.827	563	675	2248	2698	2915	3498
02/Dec	0.961	653	784	2611	3133	3385	4062
03/Dec	0.747	508	610	2030	2436	2633	3159
04/Dec	0.702	477	573	1907	2289	2473	2968
05/Dec	0.730	496	596	1983	2380	2572	3086
06/Dec	0.772	525	630	2097	2517	2719	3263
07/Dec	0.782	532	638	2125	2550	2755	3306
08/Dec	0.751	511	613	2040	2448	2645	3175
09/Dec	0.693	471	565	1881	2258	2440	2928
10/Dec	0.638	434	520	1733	2079	2247	2696
11/Dec	0.602	410	492	1637	1964	2122	2547
12/Dec	0.567	385	462	1539	1847	1996	2395
13/Dec	0.513	349	419	1394	1673	1807	2169
14/Dec	0.493	335	402	1339	1607	1736	2083
15/Dec	0.476	323	388	1292	1551	1676	2011
16/Dec	0.464	315	378	1260	1511	1633	1960
17/Dec	0.448	305	366	1218	1462	1580	1896
18/Dec	0.433	294	353	1177	1412	1526	1831
19/Dec	0.412	280	337	1121	1345	1453	1744
20/Dec	0.388	264	317	1054	1265	1367	1641

21/Dec	0.350	238	285	950	1139	1231	1477
22/Dec	0.335	228	273	910	1092	1179	1415
23/Dec	0.322	219	263	876	1051	1136	1363
24/Dec	0.304	207	248	826	991	1070	1285
25/Dec	0.270	184	220	734	880	951	1141
26/Dec	0.230	156	188	625	750	810	972
27/Dec	0.220	150	179	598	717	775	930
28/Dec	0.200	136	163	543	652	705	845
29/Dec	0.170	116	139	462	554	599	719
30/Dec	0.150	102	122	408	489	528	634
31/Dec	0.100	68	82	272	326	352	423

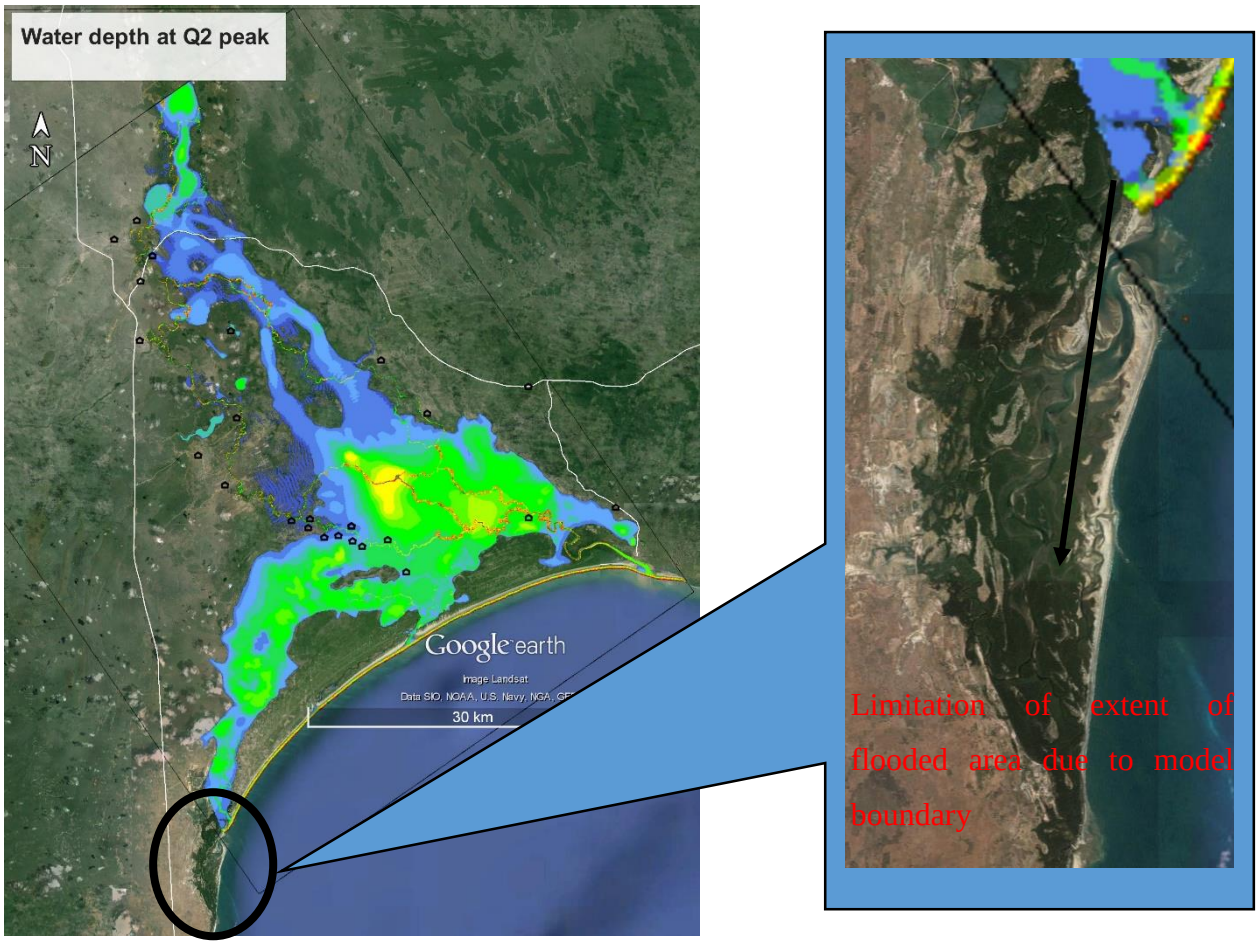

Appendix 7: Pictorial representation of model boundary limitation on extent of flooding